IDŐJÁRÁS

QUARTERLY JOURNAL
OF THE HUNGARIAN METEOROLOGICAL SERVICE

Special compilation: Environmental challenges – Smart solutions

Guest Editor: Kálmán Kovács

* * * * *

Regular papers

VOL. 123 * NO. 3 * JULY – SEPTEMBER 2019

IDŐJÁRÁS

Quarterly Journal of the Hungarian Meteorological Service

Editorial Office: Kitaibel P.u. 1, H-1024 Budapest, Hungary
P.O. Box 38, H-1525 Budapest, Hungary
E-mail: journal.idojaras@met.hu
Fax: (36-1) 346-4669

Indexed and abstracted in Science Citation Index Expanded™ and Journal Citation Reports/Science Edition
Covered in the abstract and citation database SCOPUS®
Included in EBSCO's databases

Subscription by mail:
IDŐJÁRÁS, P.O. Box 38, H-1525 Budapest, Hungary
E-mail: journal.idojaras@met.hu

Editorial

Special compilation: Environmental challenges – Smart solutions

Environmental changes, especially increasing weather variability pose a growing challenge for numerous social and economic areas from agriculture to city operation. Digital sensors and other info-communication tools and technologies play very significant roles in impact assessments and researching the adequate responses. This extremely fast developing digital technological background provides an opportunity to find sustainable and effective solutions for environmental challenges. In this volume we publish four papers from these new researches.

In the first paper, authors, *Adrienn Széles et al.* present an example in the precision agriculture research area where massive amounts of data collected by digital sensors providing more accurate testing than before. Extreme variations in temperature and precipitation amount, as well as the increase of atmospheric CO_2 concentration cause a major challenge to crop production. Atmospheric CO_2 concentration, for example, can increase crop productivity through carbon dioxide fertilization, but may even reduce it, depending on temperature, precipitation, and nutrient levels. The experiments presented in the paper were carried out in a small plot long-term field experiment at the Látókép Crop Production Experiment Site of the University of Debrecen on loess-based calcareous chernozem soil with deep humus layer with a split-strip-plot design and two replications. The main plots were the examined hybrids, while the subplots represent the different irrigation treatments (irrigated and non-irrigated), and the sub-subplots represented the different fertilizer doses. The study focused on the evaluation of the experiment in two crop years (2016 and 2017) under natural precipitation supply, involving hybrids Armagnac (FAO 490) and Renfor (FAO 320). Weather was evaluated based on the data measured and logged by the automatic weather station installed on the experiment site.

The second paper is about the urban microclimate research by *Zsófia Kugler et al*. The authors explain why microclimatic analysis of an urban scenario has always been an interesting but complicated challenge. The available remote sensing equipment ensure multi- or hyperspectral imagery ready to extract excellent land cover information, but the obtained data have lower spatial resolution limiting the efficiency of such analyses. In order to increase the geometric resolution in microclimatic studies, an exercise was executed with an Unmanned Aerial System (UAS). The applied UAS was a DJI

Phantom 4 system. The study area was the northern and middle campus of BME. There were six ground control points (GCPs), and the center of the GCPs was measured by a Leica CS10 GNSS receiver. The measurement was done in RTK mode supported by the Hungarian RTK network. Based on their research, the authors found that UAS technology is capable of creating high-resolution models for microclimatic analysis and simulations.

Direct and indirect effects of weather conditions on road traffic is presented in the third paper from *Mátyás Szántó* and *László Vajta.* Meteorological fronts – through their physiological effects – may cause the deterioration of human reaction times, and therefore, increase the risk of accident occurrence in unexpected and hazardous traffic situations that would require the quick intervention of drivers. In this article, the authors present their research of the relation between weather fronts and traffic accidents as well as between local meteorological parameters and weather fronts. Also, based on the results of their analyses, a crowdsourcing-based approach is presented for road database production that could be the foundation of a driver aiding system ultimately beneficial for increasing road safety.

Millions of people around the world run for various reasons like recreation, professionalism, mental balance, or fun. That is why long-distance running competitions are organized very often. The organizers have to know the expected meteorological conditions and several specific parameters and pieces of information about the performance of the runners retroactively to effectively support them as well as adapt to the running attitude and main goals. The purpose of this study reported in the fourth paper by *Dávid Berke*, was on the one hand to develop a data analysis tool with flexible and multifunctional analytical capabilities to identify which specific – especially meteorological – attributes of long-distance running competitions have relevant impact on the performance of the competitors, and on the other hand, to compare competitions with each other, identify different environmental and social properties in terms of running pace and age. A main result of the study is that distance and elevation attributes of running environment impair running speed mostly, otherwise outside temperature and humidity have less effect on recreational long-distance running pace.

Kálmán Kovács
Guest Editor

DOI:10.28974/idojaras.2019.3.1

IDŐJÁRÁS

Quarterly Journal of the Hungarian Meteorological Service
Vol. 123, No. 3, July – September, 2019, pp. 265–278

The effect of crop years and nitrogen basal and top dressing on the yield of different maize genotypes and marginal revenue

Adrienn Széles[*,1], **Kálmán Kovács**[2], and **Sándor Ferencsik**[3]

[1]*University of Debrecen, Faculty of Agricultural and Food Sciences and Environmental Management, Institute for Land Utilisation, Regional Developmentand Technology*
Böszörményi út 138, H-4032 Debrecen, Hungary

[2]*Budapest University of Technology and Economics, Federated Innovation and Knowledge Centre*
Egry József utca 18, H-1111 Budapest, Hungary

[3]*Agrárgazdaság Kft.*
35-ös útfél 0212/6. hrsz, H-4002 Debrecen, Hungary

**Corresponding Author E-mail:szelesa@agr.unideb.hu*

(Manuscript received in final form June 3, 2019)

Abstract— The effect of the amount and application date of nitrogen fertilizer on maize productivity and profitability was examined in a field experiment established on calcareous chernozem soil at the University of Debrecen in Hungary (47° 33' N, 21° 26' E, 111 m) under different environmental conditions in the wet crop year of 2016 and the average crop year of 2017. In addition to the non-fertilized treatment, N fertilizer doses were applied in the form of basal and top dressing. The 60 and 120 kg N ha^{-1} treatments applied as spring basal dressing were followed by two occasions of 30 kg N ha^{-1} top dressing at the V6 and V12 phenophases each. The longer maturity hybrid Armagnac (FAO 490) had a better conversion ratio concerning the precipitation during the growing season of 2016 (which was higher than the 30-year average), as well as the basal and top dressing (averaged over the different treatments) in comparison with the shorter maturity hybrid Renfor (FAO 320). In the wet crop year, the yield of Armagnac was 21.7% higher, while that of Renfor was 10.4% higher. The 60 kg N ha^{-1} basal dressing and the +30 kg N ha^{-1} top dressing at the V6 phenophase ($V6_{90}$) resulted in more efficient uptake and better conversion rate in the rainy crop year (2016) in the case of both examined hybrids. In the average crop year (2017), a difference was observed in the successfulness of top dressing. In the case of the Armagnac hybrid (FAO 490), top dressing did not cause any significant yield surplus and the 120 kg N ha^{-1} basal dressing was shown to be successful. In the case

of the Renfor hybrid (FAO 320), the early top dressing ($V6_{150}$) applied on the basal dressing of 120 kg N ha^{-1} was favorable. The most favorable income of nutrient management (N) was provided by the basal dressing of 120 kg N ha^{-1} and the +30 kg N ha^{-1} ($V6_{150}$) top dressing applied at the early V6 phenophase, averaged over the examined hybrids and years. In the case of the Renfor hybrid (FAO 320), the highest profitability was reached with the $V6_{150}$ treatment, independently of the prevailing environmental factors. However, as regards the Armagnac (FAO 490) hybrid, the top dressing applied at the V12 phenophase provided the highest profitability, which could be achieved with the lowest dose of $V12_{120}$ treatment in the wet year (2016) and the highest dose of $V12_{180}$ in the average crop year (2017). Altogether, based on the results of yield and marginal revenue analysis, the recommended fertilization technology is basal dressing of 120 kg N ha^{-1} and basal dressing of +30 kg N ha^{-1} ($V6_{150}$) applied at the early V6 phenophase. The obtained findings also show that the effect of N is greatly affected by crop year, genotype, and other elements of the applied technology. Also, marginal efficiency has to be defined for each hybrid, considering the given crop year, too.

Key-words: maize, basal and top dressing, extra revenue

1. Introduction

Climate change, including changes in temperature as well as precipitation and its distribution, and the increase in atmospheric CO_2 concentration - which can increase the productivity of crops through carbon dioxide fertilization, but it may even reduce it, depending on temperature, precipitation, and nutrient levels – poses a major challenge to crop production (*Tuba,* 2005; *Wheeler* and *von Braun,* 2013; *Jolánkai et al.,* 2016*)*. Especially the rise in temperature will have a negative effect on yields (*Ottman et al.,* 2012). It is estimated that the increase in global mean temperature for each Celsius degree reduces the global yield of maize by 7.4% on average (*Lobell*, 2007). However, food production should increase by 70% by 2050 in order to keep pace with the growth of the world's population (*FAO*, 2011). To this end, production and production efficiency should be increased with respect to environmental protection (*Fernandez et al.*, 2009; *Nielsen*, 2013).

Fertilizer use plays an important role in increasing the yield of maize (*Árendás*, 2006; *Sárvári* and *Pepó*, 2014; *Pepó*, 2017). In particular, nitrogen fertilizer is a key element (*Evenson* and *Gollin*, 2003; *Szulc et al*., 2016) as it greatly influences the biomass and grain yield due to the development and durability of the leaf area (*Muchow*, 1998; *Miao et al*., 2006). In the course of maize production, the efficiency of nitrogen fertilization can be enhanced in the proper form, in the required dose, and with a timely application (*Fageria* and *Baligar*, 2005; *Fernandez et al*., 2009; *Wortmann et al*., 2011). This makes it possible to maximize the profitability of maize, but it is/may be modified by the nitrogen demand of the production site and the current hybrid (*Rashid et al.*, 2004; *Nagy*, 2008).

Nitrogen uptake is the lowest at the time of maize germination and it becomes intensive from the 6-7-leaf stage reaching its peak during silking

(*Ciampitti* and *Vyn*, 2013). Nitrogen uptake and incorporation are significant also during the grain filling process (*Blackmer* and *Schepers*, 1996; *Ciampitti* and *Vyn* 2013). 60% of the total nitrogen uptake is incorporated into the grain (*Berzsenyi*, 2013).

Optimally, basal nitrogen dressing is performed in the spring (*Timmons* and *Cruse*, 1990), but some of the active substances of N applied before sowing may evaporate or leach into groundwater. The reason for this phenomenon is that in the early stages of plant development, poorly developed root systems are less able to access reserves in the soil (*Alley* et al., 2009). Applying the proper amount of spring basal and top dressing reduces nitrogen deficiency, increases the efficiency of nitrogen supply, improves the economicalness of nutrient supply, yield and production efficiency as a whole (*Tóth*, 2002; *Csathó*, 2003; *Muthukumar et al.*, 2007; *Sitthaphanit et al.*, 2010).

The uptake and accessibility of nitrogen are greatly influenced by climatic conditions (*Bragagnolo et al.*, 2013). The warmed soil ensures more intense nutrient dissolution, higher nutrient concentration in the soil solution, and better nutrition uptake through the root system.

N farming poses a challenge in maize production for agronomic, environmental, and economic reasons (*Guo et al.*, 2010; *Ma* and *Biswas*, 2016). For this reason, it is necessary to develop a N fertilization strategy for the growing season (*Singh et al.*, 2006). This study intends to contribute to this effort.

2. Materials and methods

Our experiments were carried out in a small plot long-term field experiment at the Látókép Crop Production Experiment Site of the University of Debrecen on loess-based calcareous chernozem soil with deep humus layer with a split-strip-plot design and two replications. The main plots are the examined hybrids, while the subplots represent the different irrigation treatments (irrigated and non-irrigated), and the sub-subplots represent the different fertilizer doses. This study focuses on the evaluation of the above described experiment in two different crop years (2016 and 2017) under natural precipitation supply, involving hybrids Armagnac (FAO 490) and Renfor (FAO 320).

2.1. Soil properties

Based on the soil analysis results of 2012, the average pH_{KCl} of the soil is 6.6 (slightly acidic), which is optimal from the aspect of crops' nutrient uptake. In the upper (20 cm) layer of the soil, the Arany's plasticity index is 39, the total amount of water-soluble salts (anions and cations) is 0.04%, i.e., the soil is salt deficient. The calcareous chalk content is around 0% in the upper 80 cm of the soil (i.e., chalk deficient), but it is 12% from 100 cm down (moderately

calcareous). The organic matter content in the upper 20 cm layer of the soil does not exceed 2.3%, while it does not exceed 1.0% at the 120 cm depth. The potassium supply of the soil is appropriate, and its P supply is moderate.

2.2. Characteristics of the experiment site

In the field experiment, in addition to the non-fertilized (control) treatment, different fertilizer doses were applied in the form of basal and top dressing as follows:

- Basal dressing: $A_{(0)}$ = non-fertilised control, A_{60} = 60 kg N ha^{-1}; A_{120} = 120 kg N ha^{-1};
- Top dressing at the V6 phenophase: $V6_{90} = A_{60}$+30 kg N ha^{-1}, $V6_{150} = A_{120}$+30 kg N ha^{-1};
- Top dressing at the V12 phenophase: $V12_{120} = V6_{90}$+30 kg N ha^{-1}, $V12_{180} = V6_{150}$+30 kg N ha^{-1}.

In each crop year, the applied fertilizer was 27% CAN (Genezis Pétisó). Crop density was 73 thousand crops per ha and the previous crop was maize in both years. Maize was sown on April 19, 2016 and April 25, 2017 and it was harvested on October12, 2016 and October18, 2017. The harvested grain yield was corrected to a moisture content of 14%.

2.3. Climatic parameters of the examined crop years

Weather was evaluated based on the data measured and logged by the automatic weather station installed on the experiment site. The obtained values were compared to the means of the period between 1985 and 2015 (30-year average). The method of *Szász* (1973) was used, as it provides a highly accurate estimation:

$$PET = \beta\,[0.0095(T-21)^2(1-R)^{2/3} f(v)], \quad (1)$$

where *PET* is the potential evapotranspiration [mm day^{-1}], *T* is the daily mean temperature [°C], *R* is the relative humidity, $f(v)$ is the effect function wind speed, and β is a factor of expressing the oasis effect. The oasis effect is the ratio of environment and evaporating water.

The growing season of 2016 was rich in precipitation (*Fig. 1*). The sum of precipitation (450 mm) was 110 mm higher than the 30-year average (340 mm). April was dry, less than 15 mm of rain fell, well below the multiple-year average of 45 mm. In May, 69 mm of precipitation fell, which was 17% higher than the average for many years. The amount of rainfall in June (146 mm) was more than twice as high as the average precipitation sum (69 mm). Unfortunately, more

than a third (45 mm) of this amount came in a single day. Significant rainfall was seen in July, August and September. Compared to the average, precipitation was 39% higher in July, 20% higher in August, and 37% higher in September. In August and September, more than half of the total rainfall arrived in one day – on August 21 and September 21. The potential evapotranspiration (*PET*) was 140 mm higher than the amount of precipitation. The average temperature of the growing season was 16.5 °C, which was only a few tenths (+ 0.3 °C) above the multiple-year average. The month of sowing was significantly warmer than the average (+ 1.8 °C), while May was colder by 0.9 °C. June was more than 1 °C warmer than the 30-year average, while the temperature in July was average. In August, the average temperature decrease was 0.5 °C, while September was warmer than the average by 1.3 °C.

In the first month of the 2017 growing season, the amount of rainfall was 18% higher than the average, however, the precipitation in May was 85% lower and that of June was 11% lower than the average (*Fig. 1*). In July, the amount of precipitation was 11 mm higher, while in August, there was 13 mm less rain compared to the average. August was significantly drier (26%) than the average, while in September, the amount of rain was nearly twice as much (79.8%) as the multiple-year average. 63.4% of the precipitation in August and 39.9% of rain in September arrived in only one day. The growing season ended with a total precipitation of 349 mm. The *PET* value was significantly higher (+325 mm) than the amount of precipitation. The temperature of April, May, July, and September was only a few tenths lower than the average, but June and August were 1.7–1.8 °C above the average. The amount of precipitation and average temperature of the growing season were in accordance with the average.

2.4. Economic data and statistical evaluation

In 2016, the buying-in price of maize was 40 400 HUF per ton, while in 2017 it was 43 500 HUF per ton. The purchase price of fertilizer (CAN) was 74 600 HUF in 2016, while it was significantly lower (66 200 HUF per ton) in 2017. Cultivator use showed differences between the V6 and V12 phenophase in terms of the number of turns taken on the field. As a consequence, the cost of cultivator use was 3 650 HUF per ha in 2016 and 3720 HUF per ha in 2017. Additional revenue resulted from fertilization was represented by the amount of production value (yield x unit price) reduced by the cost of fertilization and machine work. The marginal revenue of fertilization was determined on the basis of the amount of applied fertilizer and revenue.

The relationship between the dependent variable (yield) and the production factor (fertilizer) was evaluated using a general linear model (GLM). Yield and its mean values were compared to each other using the Duncan's test. Evaluation was performed with SPSS for Windows 21.0.

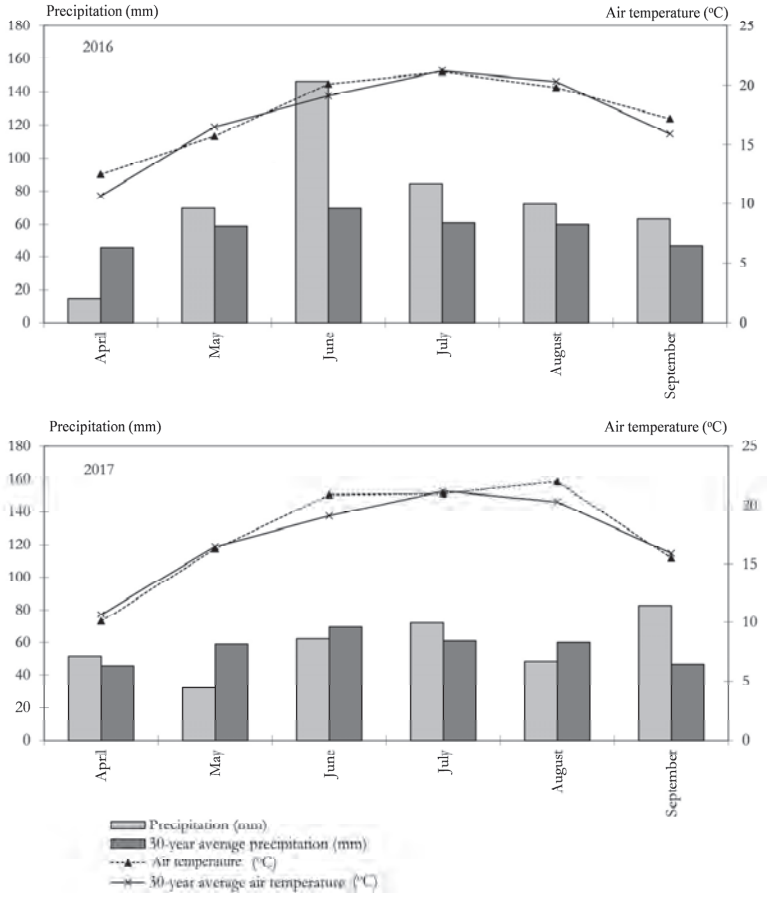

Fig.1. Precipitation and air temperature changes of the experimental space in the growing period (Debrecen, 2016 and 2017).

3. Results and conclusions

3.1. The effect of basal and top dressing on the yield of maize hybrids

In the wet year of 2016, both hybrids reached outstanding yield. The yield of the Armagnac (FAO 490) hybrid was 11.652 t ha^{-1} without fertilization. Compared to the control treatment, the lowest basal dressing of 60 kg N ha^{-1} (A_{60}) increased yield by 16.2% significantly, at the significance level of $P<0.05$. The 0.970 t ha^{-1} increase between basal dressing treatments A_{60} and A_{120} was not significant. The basal dressing of 60 kg N ha^{-1} was further

increased by applying 30 kg N ha^{-1} at the V6 phenophase, resulting in a yield increase of 4.042 t ha^{-1} ($P<0.05$). Compared to the $V6_{90}$ treatment, the effect of the $V12_{120}$ treatment was 1.030 t ha^{-1}, but this difference was not significant. There was a notable increase as a result of the $V6_{150}$ treatment (3.787 t/ha; $P<0.05$) in comparison with the 120 kg N ha^{-1} basal dressing (A_{120}), but the extra 30 kg N ha^{-1} applied at the V12 phenophase resulted in a decrease of 2.313 t ha^{-1}. The highest yield was provided by the $V12_{120}$ treatment (18.611 t ha^{-1}). However, based on the Duncan's test, the 17.581 t ha^{-1} result of the $V6_{90}$ treatment was shown to be the most favorable.

The yield of the Renfor (FAO 320) maize hybrid without fertilization (control) (10.469 t/ha) showed the outstanding nutrient conversion ability of the hybrid. Despite this fact, the yield of Renfor was 11.3% below ($P<0.05$) the yield of Armagnac (FAO 490) obtained without fertilization. In the case of Renfor (FAO 320), compared to the control treatment, the basal dressing of 60 kg N ha^{-1} (A_{60}) increased yield by 1.489 t ha^{-1}, but this increase was not significant. The difference between basal dressings A_{60} and A_{120} was 543 kg ha^{-1}, and the higher basal dressing dose did not result in any significant increase. However, a significant difference was observed as a result of applying 30 kg N ha^{-1} as top dressing at the V6 phenophase in addition to the A_{60} basal dressing, with the increase being 2.552 t/ha ($P<0.05$). However, the extra 30 kg N ha^{-1} applied at the V12 phenophase resulted in a decrease of 2.649 t ha^{-1}. There was a significant difference between the yields of A_{120} and $V6_{150}$, i.e., the combination of the 120 kg N ha^{-1} basal dressing and 30 kg N ha^{-1} top dressing provided a yield increase of 2.598 t ha^{-1} ($P<0.05$). When further increasing the fertilizer dose by 30 kg N ha^{-1} at the 12-leaf stage ($V12_{180}$), the yield increased in comparison with the $V6_{150}$ treatment. However, the extent of this increase was not significant. Again, the highest yield and the highest significant yield was not the same in this case either. The $V12_{180}$ treatment (15.225 t ha^{-1}) provided the highest yield, but it did not significantly differ from the yield resulting from the $V6_{90}$ treatment (*Table 1*).

In the average crop year of 2017, the yield obtained in the case of the Armagnac (FAO 490) maize hybrid as a result of the 60 kg N ha^{-1} basal dressing showed a 19.4% increase in comparison with the non-fertilized treatment ($P<0.05$). There was a significant yield difference (2.932; $P<0.05$) between the 60 and 120 kg N ha^{-1} basal dressing treatments. The Armagnac (FAO 490) hybrid responded well to the extra 30 kg N ha^{-1} applied at the V6 phenophase ($V6_{90}$) in addition to the basal dressing of 60 kg N ha^{-1}, resulting in a yield increase of 2.073 t ha^{-1} ($P<0.05$). Applying an extra dose of 30 kg N ha^{-1} at the V12 phenophase resulted in more yield increase (1.635 t ha^{-1}; $P<0.05$). Compared to the A_{120} basal treatment, the top dressing treatments applied either at the V6 or the V12 phenophase did not result in any significant difference. The highest yield increase was provided by the $V12_{180}$ treatment, but the A_{120} treatment showed the highest significance.

Table 1. Effect of the N basal and top dressing on the yield of maize hybrids (t ha^{-1}) (Debrecen, 2016)

Hybrids	Treatments						
	Non-fertilised	**A_{60}**	**A_{120}**	**$V6_{90}$**	**$V6_{150}$**	**$V12_{120}$**	**$V12_{180}$**
Armagnac (FAO 490)	11.652a *	13.538b ns	14.509b c ***	17.581d e ***	18.296e ***	18.611e ***	15.982cd ns
Renfor (FAO 320)	10.469a	11.958a b	12.501b	14.510c	15.099c	11.861a b	15.225c

Note: based on the Duncan's test, yields indicated with different letters (b, c, e) show significant differences from each other at the significance level of P≤0.05; ***: P=0.001%, *: P=0.05%, ns: the difference between hybrids is not significant, based on the paired t-test.

The yield of the Renfor (FAO 320) hybrid without fertilization (8.174 t ha^{-1}) was increased by the 60 kg N ha fertilizer treatment by 34.8% (P<0.05). There was no significant difference between treatments A_{60} and A_{120}. The increase of the 60 kg N ha^{-1} basal dressing resulted in a yield increase with two top dressings. Increasing the 120 kg N ha^{-1} basal treatment by 30 kg N ha^{-1} at the V6 phenophase was shown to be efficient, resulting in a yield increase of 2.621 t ha^{-1} (P<0.05). However, the second occasion of top dressing ($V12_{180}$) did not increase yield (*Table 2*).

Table 2. Effect of the N basal and top dressing on the yield of maize hybrids (t ha^{-1}) (Debrecen, 2017)

Hybrids	Treatments						
	Non-fertilised	**A_{60}**	**A_{120}**	**$V6_{90}$**	**$V6_{150}$**	**$V12_{120}$**	**$V12_{180}$**
Armagnac (FAO 490)	8.988a ns	10.730b ns	13.662c d *	12.803c ns	14.389d ns	14.438d ***	14.922d **
Renfor (FAO 320)	8.174a	11.017b	11.133b	11.479b c	13.754d	12.454c	13.648d

Note: based on the Duncan's test, yields indicated with different letters show significant differences from each other at the probability level of P≤0.05; ***P=0.001%, *P=0.05%, ns=the difference between hybrids is not significant, based on the paired t-test

In 2016, no significant difference was observed between the yields of the Armagnac (FAO 490) and Renfor (FAO 320) hybrids in terms of the 60 kg N ha^{-1} basal dressing (A_{60}) and the $V12_{180}$ treatment. The Armagnac (FAO 490) hybrid had a better yield than Renfor (FAO 320) in all other treatments at the significance level of 0.1. The smallest difference (11.3%, $P<0.05$) was observed in the non-fertilized treatment, while the biggest difference (56.9%, $P<0.001$) was shown in the case of the $V12_{120}$ treatment. In 2017, a smaller difference was observed between the examined hybrids. Armagnac (FAO 490) provided higher yields in the case of the 120 kg N ha^{-1} basal dressing (22.7%; $P<0.05$), as well as the $V12_{120}$ (15.9%; $P<0.001$) and in the case of $V12_{180}$ (9.3%; $P<0.01$) treatments (*Tables 1* and *2*).

3.2. The effect of climatic factors on the yield of maize hybrids

2016 was rich in precipitation and the mean temperature was in accordance with the multiple-year average, while the temperature in 2017 was also in accordance with the average. These two years provided different conditions in the growing season for the production of the long maturity hybrid Armagnac (FAO 490) and the short maturity hybrid Renfor (FAO 320).

The natural nutrient conversion ability of the Armagnac (FAO 490) hybrid was 29.6% better ($P<0.001$) and that of the Renfor (FAO 320) hybrid was 28.1% better ($P<0.001$) in the wet year of 2016 than in the average crop year of 2017. Averaged over the different fertilizer treatments, both hybrids had higher yields in 2016. In the case of the Armagnac (FAO 490) hybrid, the difference between the two examined years was more significant (2.891 t ha^{-1}), this index was 1.424 t ha^{-1} in the case of the Renfor (FAO 320) hybrid.

The modifying effect of crop year was not significant in the case of the Armagnac (FAO 490) hybrid as a result of the 120 kg N ha^{-1} basal dressing and the $V12_{180}$ treatment. The weather of 2016 had a significant positive effect in the case of all other treatments – at a significance level of 0.1 in all cases –, especially in the $V6_{90}$ treatment, which resulted in a yield increase of 37.3%. In the case of the Renfor (FAO 320) hybrid, no significant difference was found between the examined crop years in the A_{60} and $V12_{120}$ treatments. As a result of the growing season of the wet crop year of 2016, the $V6_{90}$ treatment resulted in the biggest yield surplus (3.032 t ha^{-1}; $P<0.001$) compared to 2017.

3.3. Revenue analysis of nitrogen supply

In 2017, due to the decrease in fertilizer prices, nutrient replenishment could be achieved at a lower cost level than in 2016. In all examined cases, fertilization at all cost levels resulted in extra yields and additional revenue compared to the non-fertilized control plot. The highest surplus revenue for the longer maturity hybrid Armagnac (FAO 490) in the rainy year (2016) was provided by the

60 kg N ha^{-1} basal dressing + 30 + 30 kg N ha^{-1} ($V12_{120}$) top dressing combination, while in 2017, the maximum yield compared to the control treatment was observed at the highest fertilizer level (120 kg N ha^{-1} basal dressing + 30 + 30 kg N ha^{-1} top dressing) (*Table 3*). The difference between these treatments was 34 048 HUF per ha in 2016.

Table 3. Marginal revenue analysis of the N level of basal and top dressing – Armagnac (FAO 490) maize hybrid (Debrecen, 2016–2017)

	2016			
	Fertilizer (kg)	**Total cost (HUF ha^{-1})**	**Additional revenue (HUF ha^{-1})**	**Marginal revenue (HUF kg ha^{-1})**
Non-fertilised	0	0	-	-
A_{60}	222	16 561	59 633	2 120
A_{120}	444	33 122	82 300	1 232
$V6_{90}$	333	24 842	211 040	1 760
$V6_{150}$	556	41 478	223 290	1 277
$V12_{120}$	444	33 122	240 721	1 693
$V12_{180}$	667	49 758	117 874	968
	2017			
	Fertilizer (kg)	**Total cost (HUF ha^{-1})**	**Additional revenue (HUF ha^{-1})**	**Marginal revenue (HUF kg ha^{-1})**
Non-fertilised	0	0	-	-
A_{60}	222	14 696	61 081	1 761
A_{120}	444	29 393	173 926	1 051
$V6_{90}$	333	22 045	140 258	1 785
$V6_{150}$	556	36 807	194 486	1 002
$V12_{120}$	444	29 393	200 382	1 415
$V12_{180}$	667	44 155	206 674	973

In the case of the Renfor (FAO 300) hybrid, the highest revenue could be reached by applying 120 kg N ha^{-1} basal dressing and 30 kg N ha^{-1} top dressing ($V6_{150}$) in both the rainy year (141 924 HUF per ha) and the average crop year (202 273 HUF per ha). The 60 348 HUF per ha difference in surplus revenue between the two years is significant (*Table 4*).

Table 4. Marginal revenue analysis of the N level of basal and top dressing – Renfor (FAO 320) maize hybrid (Debrecen, 2016–2017)

2016				
	Fertilizer (kg)	**Total cost (HUF ha^{-1})**	**Additional revenue (HUF ha^{-1})**	**Marginal revenue (HUF kg ha^{-1})**
Non-fertilised	0	0	-	-
A_{60}	222	16 561	43 594	1 905
A_{120}	444	33 122	48 970	1 088
$V6_{90}$	333	24 842	134 765	1 517
$V6_{150}$	556	41 478	141 924	1 054
$V12_{120}$	444	33 122	15 814	1 079
$V12_{180}$	667	49 758	135 084	922
2017				
	Fertilizer (kg)	**Total cost (HUF ha^{-1})**	**Additional revenue (HUF ha^{-1})**	**Marginal revenue (HUF kg ha^{-1})**
Non-fertilised	0	0	-	-
A_{60}	222	14 696	108 974	1 602
A_{120}	444	29 393	99 324	1 079
$V6_{90}$	333	22 045	118 073	1 454
$V6_{150}$	556	36 807	202 273	898
$V12_{120}$	444	29 393	149 487	1 220
$V12_{180}$	667	44 155	186 664	890

The marginal revenue was the lowest at the highest nutrient supply level in the case of both hybrids in the examined years, i.e., the unit revenue increase resulting from the supplementary fertilizer active substance was the lowest at these levels.

4. Summary

Based on a multivariate analysis of variance (ANOVA), the effect of the main factors (crop year, N fertilization, date of application, genotype) on yield is significant at the level of 0.1. Based on the MQ value, the crop year had a significant yield modifying effect, followed by genotype and fertilization. The date of application had the smallest effect on yield. The interactions between year and genotype ($P<0.001$), year and fertilization ($P<0.001$) and genotype and fertilization ($P<0.05$) were significant.

In the rainy year of 2016, the top dressing applied at the V6 and V12 phenophases in addition to the 60 kg N ha^{-1} basal dressing had a significant effect in the case of the Armagnac (FAO 490) hybrid, exceeding the yield resulting from the 120 kg N ha basal dressing. The application of an extra dose of 30 kg N ha^{-1} as top dressing at the V6 phenophase in addition to the 120 kg N ha^{-1} basal dressing increased yield. However, the second occasion of applying 30 kg N ha^{-1} resulted in yield decrease. Significant yield surplus was observed in the case of the Renfor (FAO 320) hybrid, when applying an extra dose of 30 kg N ha^{-1} at the V6 phenophase in addition to the 120 kg N ha^{-1} basal dressing. However, any further top dressing treatment applied at the 12-leaf stage, i.e., treatments $V12_{120}$ ($P<0.05$) and $V12_{180}$ resulted in (non-significant) decrease.

In the average crop year of 2017, significant yield increase was observed in the case of the Armagnac (FAO 490) maize hybrid as a result of the extra 30-30 kg N ha^{-1} applied both at the 6- and 12-leaf stages as top dressing in addition to the 60 kg N ha^{-1} basal dressing. The 120 kg N ha^{-1} basal dressing was not efficient even when two doses of top dressing were applied. No favorable effect was observed on the yield of the Renfor (FAO 320) hybrid when applying further N fertilizer doses at the V6 and V12 phenophases in addition to the 60 kg N ha^{-1} basal dressing. However, significant yield increase ($P<0.05$) was shown as a result of the first 30 kg N ha^{-1} as top dressing (V6) in addition to the basal dressing of 120 kg N ha^{-1}.

In the case of the Armagnac (FAO 490) hybrid, the yield modifying effect of crop year was shown, with the exception of treatments A_{120} and $V12_{180}$. The yield increasing effect of the rainy year (2016) ranged between 26.2–37.3% (A_{60}-$V6_{90}$). As for the Renfor (FAO 320) hybrid, climatic factors did not affect yield in the case of treatments A_{60} and $V12_{120}$. The higher amount of rainfall in 2016 had a yield modifying effect ranging between 9.8–28.1% ($V6_{150}$-control).

Compared to the control plot, the additional nutrients applied to all fertilized plots resulted in an increase in revenue. The obtained results confirmed the principle of diminishing returns, according to which, if the resources used were increased, the revenue that could be realized with one kilogram of fertilizer would also increase to a given value, followed by a decreasing tendency, i.e., an additional unit of fertilizer expenditure would cause smaller and smaller increase of revenue.

Altogether, the top dressing technology applied at the early V6 phenophase in addition to the basal dressing applied in the spring provided the maximum yield at the most favorable fertilizer application costs, averaged over the different crop years and hybrids.

Acknowledgement: The research was financed by the Higher Education Institutional Excellence Programme of the Ministry of Human Capacities in Hungary, within the framework of the 4th thematic programme of the University of Debrecen, and the projects "GINOP-2.2.1-15-2016-00001 - Developing a scale-independent complex precision consultancy system" and "EFOP-3.6.3-VEKOP-16-2017-00008".

References

Alley, M.M., Martz, Jr., Marvin, E., Davis Paul, H., and *Hammons, J. L.*, 2009: Nitrogen and Phosphorous Fertilization of Corn, Virginia Cooperative Extension, Virginia Tech, and Virginia State University. http://pubs.ext.vt.edu/ 424/424-027/424-027.html

Árendás, T., 2006: Növénytáplálás új szemlélettel. *Agrofórum 17*, 12: 8–10. (In Hungarian)

Berzsenyi, Z., 2013: Növénytermesztés. Agroinform Kiadó, Budapest. (In Hungarian)

Blackmer, T.M. and *Schepers, J.S.,* 1996: Aerial Photography to Detect Nitrogen Stress in Corn. *J. Plant Physiol. 148,* 440–444. https://doi.org/10.1016/S0176-1617(96)80277-X

Bragagnolo, J., Amado, T.J.C., Nicoloso, R.S., Jasper, J., Kunz, J., and *Teixeira, T.G.*, 2013: Optical crop sensor for variable-rate nitrogen fertilizaton in corn: I. Plant nutritien and dry matter production. *R. Bras. Ci. Solo. 37,* 1288–1298. https://doi.org/10.1590/S0100-06832013000500018

Ciampitti I.A. and *Vyn, T.J.,* 2013: Grain nitrogen source changes over time in maize: a review. *Crop Sci 53,* 366–377. https://doi.org/10.2135/cropsci2012.07.0439

Csathó, P., 2003: Kukorica N–hatásokat befolyásoló tényezők vizsgálata az 1960–2000 között publikált hazai szabadföldi kísérletek adatbázisán. *Agrokémia és Talajtan 52,* 169–184. (In Hungarian) https://doi.org/10.1556/Agrokem.52.2003.1-2.14

Evenson, R.E. and *Gollin, D.*, 2003: Assessing the impact of the green revolution, 1960 to 2000. *Science 300,* 758–762. https://doi.org/10.1126/science.1078710

Fageria, N.K. and *Baligar, V.C.*, 2005: Enhancing nitrogen use efficiency in crop plants. *Adv. Agronomy 88,* 97–185. https://doi.org/10.1016/S0065-2113(05)88004-6

FAO, 2011: www.theguardian.com/environment/2011/nov/28/un-farmers-produce-food-population

Fernandez, F.G., Nafziger, E.D., Ebelhar, S.A., and *Hoeft, R.G.*, 2009: Managing nitrogen in. Illinois agronomy handbook. Univ. Illinois Coop. Ext. Serv., Urbana-Champaign. 113–132.

Guo, J., Liu, X., Zhang, Y., Shen, J., Han, W., Zhang, W., and *Zhang, F.*, 2010: Significant acidification in major Chinese croplands. *Science 327,* 1008–1010. https://doi.org/10.1126/science.1182570

Jolánkai, M., Tarnawa, Á., Horváth, Cs., Nyárai, H.F., and *Kassai, M.K.,* 2016: Impact of climaticfactors on yield quantity and quality of grain crops. *Időjárás 120,* 1: 73–84.

Lobell, D.B., 2007: Changes in diurnal temperature range and national cereal yields. *Agric. Forest Meteorol. 145,* 229–238. https://doi.org/10.1016/j.agrformet.2007.05.002

Ma, B.L. and *Biswas, D.K.*, 2016: Field-level comparison of nitrogen rates and application methods on maize yield, grain quality and nitrogen use efficiency in a humid environment. *J. Plant Nutr. 39,* 727–741. https://doi.org/10.1080/01904167.2015.1106556

Miao, Y., Mulla, D.J., Robert, P.C., and *Hernandez, J.A.,* 2006: Within-field variation in corn yield and grain quality responses to nitrogen fertilization and hybrid selection. *Agron. J. 98*, 129–140. https://doi.org/10.2134/agronj2005.0120

Muchow, R.C., 1998: Nitrogen utilization efficiency in maize and grain sorghum. *Field Crops Res. 56,* 209–216. https://doi.org/10.1016/S0378-4290(97)00132-9

Muthukumar,V.B., Velayudham, K., and *Thavaprakaash, N.*, 2007: Plant growth regulators and split application of nitrogen improves the quality parameters and green cob yield of baby corn (*Zea mays* L.). *J. Agron. 6,* 208–211. https://doi.org/10.3923/ja.2007.208.211

Nagy, J., 2008: Maize production: Food, bioenergy, forage. Akadémiai Kiadó, Budapest.

Nielsen, R.B., 2013: Root Development in Young Corn, in, Purdue University Department of Agronomy. http://www.kingcorn.org/news/timeless/Roots.html

Ottman, M.J., Kimball, B.A. White, J.W., and *Wall, G.W.*, 2012: Wheat growth response to increased temperature from varied planting dates and supplemental infrared heating. *Agron J. 104,* 7–16. https://doi.org/10.2134/agronj2011.0212

Pepó, P., 2017: Role of agrotechnical elements in sustainable wheat and maize production. *Columella J. Agric. Environ. 4,* 59–64.

Rashid, M.T., Voroney, P., and *Parkin, G.*, 2004: Predicting nitrogen fertilizer requirements for corn by chlorophyll meter under different N availability conditions. *Can. J. Soil Sci. 85,* 149–159. https://doi.org/10.4141/S04-005

Sárvári, M. and *Pepó, P.,* 2014: Effect of production factors on maize yield and yield stability. *Cereal Res. Commun. 42,* 4: 710–720. https://doi.org/10.1556/CRC.2014.0009

Singh, I., Srivastava, I.A., Chandna, P., and *Gupta, R.,* 2006: Crop sensors for efficient nitrogen management in sugarcane: Potential and constraints. *Sugar Technol. 8,* 299–302. https://doi.org/10.1007/BF02943572

Sitthaphanit, S., Limpinuntana, V., Toomsan, B., Panchaban, S. W., and *Bell, R.*, 2010: Growth and yield responses in maize to split and delayed fertilizer applications on sandy soils under high rainfall regimes. *Kasetsart J. Nat. Sci. 44,* 991–1003.

Szász G., 1973: A potenciális párolgás meghatározásának új módszere. *Hidrológiai Közl. 53,* 435-442.

Szulc, P.,Waligóra, H., Michalski, T., Rybus-Zając, M., and *Olejarski, P.,* 2016: Efficiency of nitrogen fertilization based on the fertilizer application method and type of maize cultivar (*Zea mays* L.). *Plant Soil Environ. 62,* 135–142. https://doi.org/10.17221/654/2015-PSE

Tuba, Z., 2005: Az emelkedő légköri CO2-koncentráció hatása a növényközösségek összetételére, szerkezetére és produktivitására. *Bot. Közlem. 92,* 1–2: 189–206. (In Hungarian)

Timmons, D.R. and *Cruse, R.M.,* 1990: Effect of fertilization method and tillage on nitrogen – 15 recovery by corn. *Agron. J. 82,* 777–784. https://doi.org/10.2134/agronj1990.00021962008200040025x

Tóth, Z., 2002: *A* fejtrágyázás jelentősége*. Agro Napló 6,* 3: 55–56. (In Hungarian)

Wheeler, T. and *von Braun, J.*, 2013: Climate change impacts on global food security. *Science 341,* 508–513. https://doi.org/10.1126/science.1239402

Wortmann, C.S., Tarkalson, D.D., Shapiro, C.A., Dobermann, A.R., Ferguson, R.B., Hergert, G.W., and *Walters, D*., 2011: Nitrogen use efficiency of irrigated corn for three cropping system in Nebraska. *Agron. J. 103,* 76–84. https://doi.org/10.2134/agronj2010.0189

DOI:10.28974/idojaras.2019.3.2

IDŐJÁRÁS

Quarterly Journal of the Hungarian Meteorological Service
Vol. 123, No. 3, July – September, 2019, pp. 279–294

Supporting microclimate modeling with 3D UAS data acquisition

Zsófia Kugler [1], **Zoltán Tóth** [2], **Zsuzsa Szalay** [3], **Dóra Szagri** [3], and **Árpád Barsi** [*,1]

[1] *Department of Photogrammetry and Geoinformatics*
Budapest University of Technology and Economics
Műegyetem rkp. 3, H-1111, Budapest, Hungary

[2] *Institute of Geoinformatics, Óbuda University*
Bécsi út 96/B, 1034 Budapest, Hungary

[3] *Department of Construction Materials and Technologies*
Budapest University of Technology and Economics
Műegyetem rkp. 3, H-1111, Budapest, Hungary

**Corresponding author E-mail:barsi.arpad@epito.bme.hu*

(Manuscript received in final form June 3, 2019)

Abstract— Microclimatic analysis of an urban scenario has always been an interesting but complicated challenge. The available remote sensing equipments ensure multi- or hyperspectral imagery being ready to extract excellent land cover information, but the obtained data have lower spatial resolution limiting the efficiency of such analyses. In order to increase the geometric resolution in microclimatic studies, an exercise was executed with an Unmanned Aerial System. The calibration of the imaging camera on a dedicated test field was followed by the data capture flight over the campus of the Budapest University of Technology and Economics. The evaluation of the acquired images has resulted a point cloud containing millions of points. The high density point cloud was able to be transformed into 3D mesh representation and could be fed into a geographic information system for further analysis steps. Based on the color and height information of all individual points, the obtained geometric base was easily to be converted into land cover model representing man-made and natural objects, like buildings or trees. The segmentation of the model is a suitable input for climatic analyses and simulation software packages, where extreme high geometric resolution is required.

Key-words: urban microclimate, building heat balance, UAS, camera calibration, 3D surface model, canopy structure

1. Introduction

A microclimate is the distinctive climate of a small area, such as a garden, park, valley, or part of a city. The weather variables in a microclimate may be subtly different to the conditions prevailing over the area as a whole. While a particular climate is representative for a large area over long periods of time, microclimate refers to a climate over a very small area. Local conditions can alter climate, for example the presence of vegetation causes cooler and wetter microclimate in its surroundings. Typical microclimate environments are urban regions, where the presence of anthropogenic activity and build-up environment may alter weather conditions compared to its surroundings. Since urban expansion has been facing an exponential rise during the last century, urban microclimate is a target of investigations for decades.

It has been observed that urban areas are generally warmer than its surrounding rural environment (*Barry et al.*, 2016). This phenomenon is called the Urban Heat Island (UHI) effect. Multiple factors like change in surface materials, lack of evapotranspiration, urban canyon effect, and anthropogenic heat release may cause the formation of UHIs (*Liang et al.,* 2012). According to the Met Office Factsheet (MOF, 2019), in the UK, temperature contrast of urban (London) and rural areas was found to be up to 5 °C on in mid-May during clear sky conditions. Climate change is expected to exacerbate the UHI effect, increasing the cooling energy consumption and also severely affecting human health. Understanding and analyzing urban microclimate, evaluating UHI effect and heatwave vulnerability is particularly important for urban public planning measures.

For this reason, urban planning, urban landscape design, and emergency services should obtain a clear understanding of the phenomenon in order to plan sustainable measure and mitigation strategies for the current and future situations.

Urban microclimate characteristics are difficult to measure, since the sampling density of in-situ meteorological stations are usually not dense enough to reveal spatial distribution of local weather parameters. To set an example in Budapest (Hungary) which is a capital of almost 2 million inhabitants on 525 km^2, only 4 meteorological observation stations are in operation and not all situated in standard measuring environment. Hence to study urban effects on local climate, asses risk, and resilience of urban population related to heatwaves, microclimate has to be expressed using simulations, modeling supported by indirect measures.

2. Remote sensing to support microclimate models

Thermal remote sensing technology has been successfully applied in microclimate observations of urban temperature patterns. The first satellite-based analysis of an urban heat island was performed by *P. K. Rao* (*Rao*, 1972), which was followed by numerous studies in the past decades. Both satellite and aerial platforms were

applied to perform observations on Land Surface Temperature (LST) to map UHI. Thermal infrared (TIR) satellite sensors of MODIS, Landsat, AVHRR, ASTER, ATSR, SEVIRI, HCMM were extensively used in LST retrieval (*Zhou et al*., 2019). Besides, airborne data also offers numerous advantages and has been used in urban thermal heat mapping. Yet both acquisition platforms are not necessarily following the spatial, temporal, and spectral resolution needs of the application.

In order to analyze urban climate, Unmanned Aerial Systems (UAS) with high resolution imaging capabilities offer a good solution. Due to the local scale characteristic of local urban climate, the small scale acquisition techniques of UAS remote sensing can better meets the objectives than satellite or aerial remote sensing. Compared to satellite images, the advantage of using UAS is in the temporal frequency or high repetition rate of the recordings. Using thermal UAS sensors, daily dynamics of small scale thermal variations can be easily measured by repeated flights during a given day. UAS is appropriate to estimate surface microclimate indicators by low cost acquisition and processing compared to aerial data capturing (*Kotchi et al*., 2016). UAS not only has the advantage of local scale data acquisition but also the repetition cycle is not limiting factor in temporal density of observations. What is more, image capturing is not limited to cloud-free weather conditions.

Therefore, a study has been carried out how optical UAS sensors can collect valuable information to support urban microclimate modeling and building energy simulations. Besides 3D surface modeling, different types of local scale characteristics of urban land cover were derived too. The study has been dedicated to understand what type of parameters can be derived particularly on urban vegetation cover not only from nadir looking but from oblique UAS acquisition techniques to support microclimate modeling. Future plan is to analyze the outdoor building heat conditions by thermal UAS measures captured during summer season to better understand and simulate in-door thermal conditions during heatwaves.

Microclimate is primarily depending on the surface albedo of a given object, which expresses the ratio of reflected sunlight to irradiance. Several field and laboratory measurements are able to determine albedo (*Chen et al.*, 2019). With the latest technology, an accurate and high resolution albedo can be derived using a combination of a digital camera, broadband pyranometers, and UAS platform (*Ryan et al*., 2017). With this technique, the effect of large trees on microclimate can be evaluated properly (*Eckmann et al.*, 2018), which could lead to better decisions in urban planning. According to the latest research, the changes in surface temperature depend on the albedo and apparent thermal inertia (*Gaitani et al*., 2017a).

Vegetation cover is very important for reducing the ambient air temperature. Based on measurements, the temperature difference between a dense green area and a built-up university campus residence may reach 4 °C on a summer day (*Wong et al.,* 2007). By combining on-site measurements and numerical

simulations, we can get accurate results showing how to improve the microclimate of a given area using green surfaces (*Srivanit* and *Hokao,* 2013). In the case of community spaces (campuses, playgrounds, town squares etc.), it is important to assist decision makers, since large population are exposed to thermal stress, which is mainly influenced by the design of the landscape zone (*Égerházi et al*., 2013).

To map vegetation activity of a given area, NDVI (Normalized Difference Vegetation Index) can be derived from near infrared (NIR) images (*Gaitani et al.*, 2017b). This value quantifies the vegetation by measuring the difference between near infrared (NIR) and visible red (RED) bands, and the results can be used when making microclimatic design decisions. 3D oblique viewing UAS data acquisition can derive information beyond this. Vegetation surveys together with 3D canopy surface can be efficiently conducted, even over moderately large areas (*Cruzan et al.*, 2016).

The use of UAS in microclimate analysis can be a useful tool even without special sensors, as image processing can deliver input data for building heights and vegetation in several simulation models.

In the future, urban land use will change along with the population's age and structure patterns. By examining different future scenarios, development of new urban areas was projected in Hungary to be mainly around the capital and regional centers (*Li et al.*, 2017), therefore, the analysis of urban environment and microclimate needs to be at the forefront of research.

2.1. UAS-based imaging technology

Vehicles of the Unmanned Aerial Systems can be grouped into two main clusters: the fix wing and the rotary wing systems. Fix wing vehicles have high similarity with airplanes, while rotary wing vehicles with the helicopters. In our research we have conducted all field works with a rotary wing system. Depending on the number of rotating wings (the rotors), one can speak about quadrocopters (with 4 rotors), hexacopters (with 6 rotors), or octocopters (with 8 rotors). There are high variety of rotor configurations.

The system consists of the flying vehicle (Unmanned Aerial Vehicle – UAV), a ground based controller, and a communication system. The vehicle is a platform carrying the navigation and control, as well as the imaging equipment. Navigation system is responsible for serving information about the current position of the vehicle and specifying the commands for the motors. Control component affects the behavior of the vehicle's engines by increasing or decreasing the revolution rate individually. The imaging system is the most important payload component: it is for capturing the data, in this case the images.

The ground based part of the system is a device, where the pilot can control the flight of the vehicle, start or stop the image streams, and receives all data coming from the vehicle. Therefore, UAS is also called as Remotely Piloted Aerial System (RPAS). Communication solution is for transferring data and

commands between the ground and the flying component. Both the ground controller and the vehicle are equipped with suitable power supply.

UAS has different degrees of autonomy: pilots have to react for all circumstances (wind, vibrations, etc.), there is a functionality to stabilize the vehicles, it gets prior the flying and image capturing instructions and executes them. This last option is a kind of automated flight, which is very advantageous in field survey tasks.

The workflow (*Fig. 1*) starts with mission planning, where the boundary of area to be surveyed must be exactly set, then a flying plan has to be elaborated considering the features of the aerial vehicle. There is a bunch of commercial and freely available software tools to support the mission planning.

Fig. 1. The general UAS workflow.

The planned flying trajectory and commands must be transferred onto the vehicle, and after take-off, it can be instructed to go alone. Under continuous human control the flying vehicle executes the image capture task and obtains the required data set. GNSS measurements (like GPS with e.g., Real Time Kinematic measurement modus, RTK) can define ground control points (GCPs), which have mapping coordinates and can be identified in the obtained imagery. Prior point marking with colored plates can increase the available computational accuracy.

The data processing starts with downloading the images and entering a photogrammetric evaluation software. The image processing software of nowadays have a strong base on computer vision principles; the driving methodology is mostly the Structure-from-Motion (SfM) technique. The algorithm defines well-identifiable points in all images; this is the interest operator phase. Thousands of image observations have to be paired in all combinations, but only those are kept, which exceed a preliminary limit of correspondence. By the use of corresponding points, the projection centers and orientation angles are calculated for each captured image. A sophisticated bundle block adjustment can minimalize the overall matching errors and creates a basic geometric model.

Having all images oriented, the multi-view stereo (MVS) algorithms evaluate the images. This step will result a dense point cloud of the interest area. This phase requires the most computation power. After getting millions or even billions of object points, the obtained point cloud must be complemented with regular topology, like a triangle network, so a mesh model can be achieved. Mesh

triangles can be extended by the color information of the original images. A colored point mesh is the base of all photorealistic visualizations. In Geographic Information System (GIS) applications, the obtained point clouds and mesh models are used as Digital Surface Models (DSM) and Digital Elevation Models (DEM), as filtering and similar techniques can differentiate between the bare Earth height information and covered natural (typically the vegetation) and human objects (buildings, roads, etc.). DSMs and DEMs can be later used in form of terrain sections. The work is usually finished by deriving an orthoimage mosaic.

2.2. Calibration of UAV cameras

An important processing step in both the aerial photogrammetry (used for mapping purposes) and close range photogrammetry (used mostly for object reconstruction) is to determine the internal and external orientation parameters. The internal orientation data consists of the principal point coordinates and the focal length. The image coordinate system is determined by the array of pixels.

Another parameter having significant impact on the metric quality of an image is the lens distortion. In general, low cost lenses are expected to have significantly higher distortions compared to lenses of professional metric cameras. There are many software packages available for deriving the interior orientation parameters (including the lens distortion). Usually, the calibration procedure has been done automatically using imagery of black-and-white (B&W) checkerboard targets (*Fig. 2*).

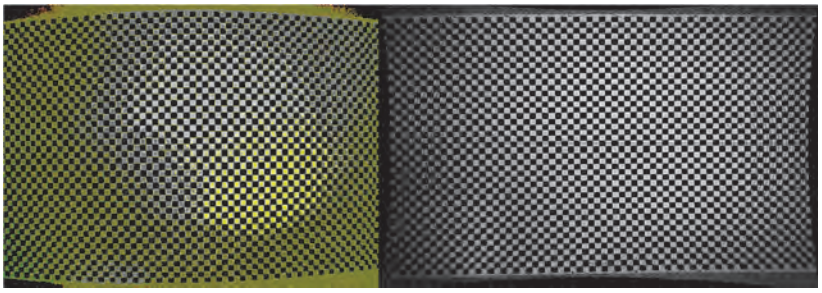

Fig. 2. B&W checkerboard calibration target before and after applying the calibration.

The exterior orientation parameters ensure the transformation between the image coordinate system and the mapping (or object reconstruction) coordinate system: three parameters for translation (x, y, z) and three for Eulerian rotation angles (omega, fi, kappa). It is possible to measure (usually preliminary) exterior orientation parameters with GNSS and IMU sensors. Final parameters are usually computed by using aerial triangulation (AT) process based on ground control points (GCP) with known mapping coordinates. For more efficient workflow and

more accurate results it is very common to combine these two methods, involving GNSS and IMU observations together with GCPs in an AT process. It is very common in today's practice, that the interior and exterior orientation parameters are determined in one single processing session. Due to the highly automated processing workflow, many software packages give the users very limited freedom of control over the calculation parameters. These black-box-like solutions are getting more common thanks to the growing popularity of UAS based mapping systems.

Since the spatial accuracy of many mapping projects must meet a certain threshold given by governmental standards, by the customer, or simply by the nature of the project, the quality of the end product must be proven and well documented. A black-box-like processing workflow is not able to meet this requirement. To address this issue, the Alba Regia Faculty of Óbuda University created a test and calibration site for UAS based mapping systems. The high quality, high accuracy test site has been created for system calibration, reliability investigations, and performance analyses.

Fig. 3 shows this 200 m × 200 m sized test field on a hilly terrain. The 7 × 7 array of GCPs is roughly oriented to North. The terrain consists of relatively even areas as well steep hillsides. The maximum difference in elevation is approximately 20 meters.

Prior to our investigation on the BME campus, the applied UAS camera has been calibrated in the test field, and the obtained parameters are kept for the later computations.

Fig. 3. Calibration test field near Székesfehérvár.

2.3. UAS survey on BME campus

The applied UAS was a DJI Phantom 4 system. The flying vehicle (*Fig. 4a*) has been equipped with a synchronous image transfer (first person view – FPV) option that forwards the current flying parameters (e.g., height, speed, tilt, power reserve), too.

Our study area is the northern and middle campus of BME. In order to get homogeneous geometric accuracy, we have decided to execute the flight in fully automated mode in double grid formation (*Fig. 4b*). There were six ground control points installed with red and white colored 1 × 1 m size plastic plates (*Fig. 4c*). The center of the GCPs were measured by a Leica CS10 GNSS receiver. The measurement was done in RTK mode supported by the Hungarian RTK network.

The vehicle is equipped with a camera mounted onto a 2 DoF gimbal. The camera has a fix focus lens of 2.77 mm focal length and is capable to acquire image with 3000 × 4000 pixels. The stored image format was sRGB jpg, the sensitivity was set to ISO 100. The aperture was also fixed for 2.8, while the shutter speed was varied to adjust the exposure adequately. Generally, the shutter speed was set to 1/400 s.

The mission was executed in the morning between 9:00 and 12:00, on April 1, 2017, the flying time was about 32 minutes for the northern and about 28 minutes for the middle campus. The overall flying time was 1 hour. There were 489 images taken in the northern and 429 in the middle campus. The total number of images is 918. The required storage capacity was 2.75 GB. The compression rate is better than 1:10 in average.

The photogrammetric image processing was done with the Pix4D Mapper software, which is available also as cloud service. The available performance is scalable, after uploading the image and GNSS data into the cloud, the following computing power was given: Intel Xeon CPU E5-2666 v3 @ 2.90GHz CPU with 59GB RAM and Cirrus Logic GD 5446 GPU. The operating system behind the computations was Linux 3.13.0-91-generic x86_64.

The applied software has used SfM based technology also. The parameters from the test field calibration were also uploaded. The bundle block adjustment was initiated by 7 125 323 points, then the results of the orientation can be summarized in *Table 1*.

a) The DJI Phantom 4 drone in work

b) The planned mission with the double grid imaging

c) Installation of a ground control point

Fig. 4. The image caption technology with DJI system

Table 1. Relative and absolute camera positions and orientation parameters with accuracy measures after bundle block adjustment

	X [m]	Y [m]	Z [m]	Omega [degree]	Phi [degree]	Kappa [degree]
Relative camera positions and orientation	0.047 ± 0.011	0.046 ± 0.010	0.122 ± 0.059	0.065 ± 0.030	0.051 ± 0.023	0.016 ± 0.004
Absolute camera positions and orientation	0.425 ± 0.088	0.425 ± 0.088	1.035 ± 0.245	0.271 ± 0.047	0.362 ± 0.035	0.085 ± 0.001

The computation time for the complete orientation with bundle block adjustment was 1 hour 19 minutes.

These more than 7 million points are only a sparse representation of the interest area. The higher quality dense point cloud has been achieved after 44 minutes computation. The dense point cloud contains 55 797 678 points with RGB color information, which means a spatial point density of 71.98 points/m^3. Based on the point cloud, a mesh model was also derived after 23 minutes run. The obtained mesh model has been built with 1 million triangle elements. The point cloud can be visualized with sophisticated GIS tools, like QGIS as in *Fig. 5*. Mesh means a photorealistic visualization, see *Fig. 6*.

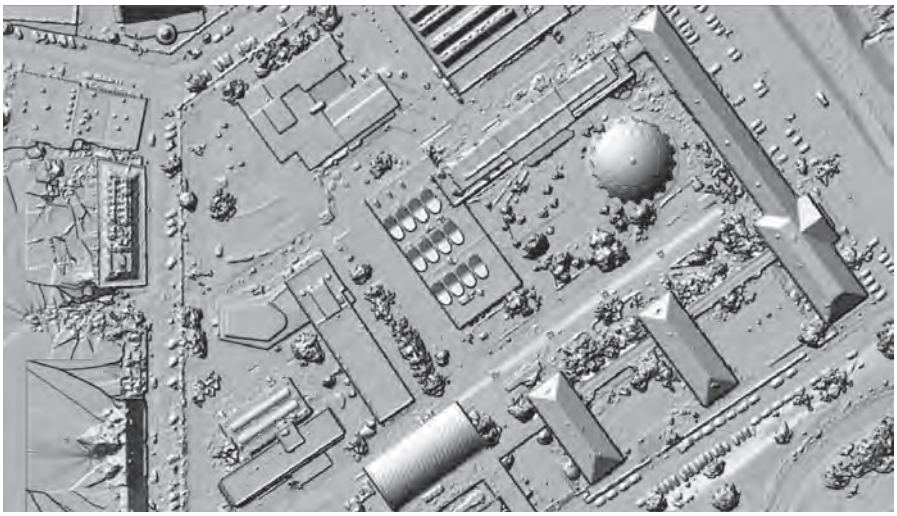

Fig. 5. Plastic visualization of point cloud in QGIS.

Fig. 6. Perspective view of mesh model (it is a composite view of 1 million colored triangles).

The point cloud serves as a base for computing regular Digital Surface Model (DSM) and an orthoimage mosaic (*Fig. 7*). Our interest area of the university campus has an extent 600.5, 871.3, and 79.1 m in X, Y, and Z directions, respectively. The suggested ground sampling distance was 3.27 cm, whereas the total covered area took 28.53 ha. The production of DSM and orthomosaic took further 13 and 30 minutes computation.

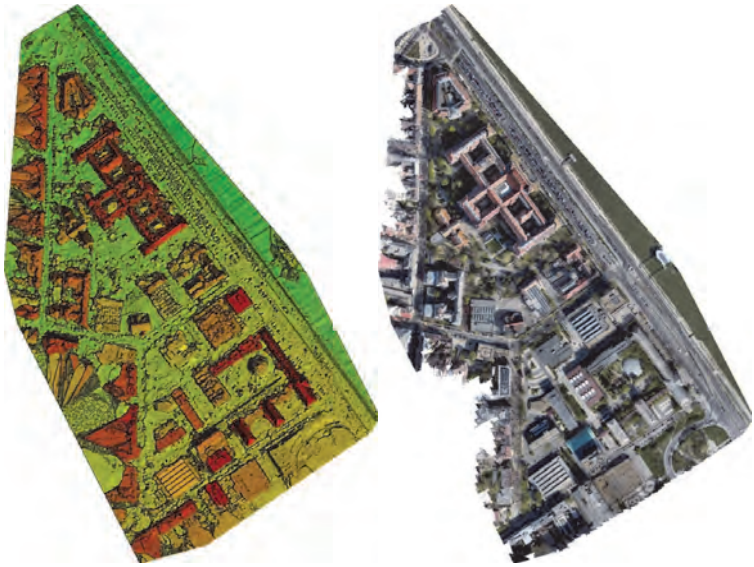

Fig. 7. False-color Digital Surface Model and orthophoto mosaic for the covered area.

2.4. Vegetation mapping from UAV imagery

Having a closer look on the DSM, one can realize that the building and tree heights can be differentiated by some threshold operations (*Fig. 8*). Trees are typically irregular circular blobs having less heights than the regularly built buildings.

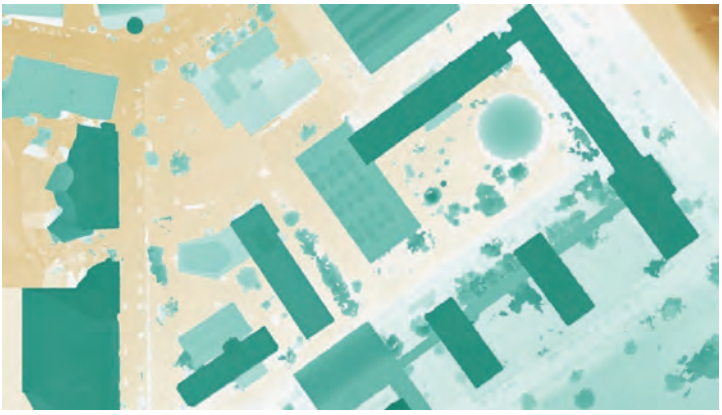

Fig. 8. False-color visualization of the heights of the DSM (same detail as in Fig. 5)

The land cover categories (building, road, grass, tree) can be estimated by the pixel color of the orthoimage, still some manual inspection and fixing is required.

After some manual correction of the differentiation, the vegetation map has been achieved (*Fig. 9*).

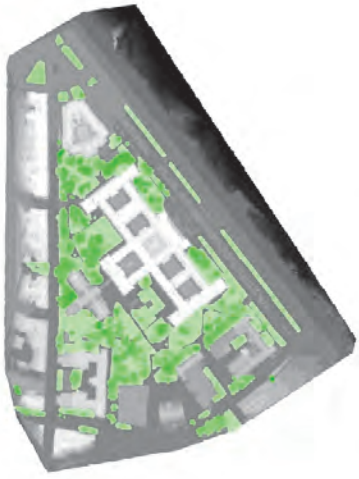

Fig. 9. Vegetation map for the northern campus.

3. Climatic analyses

Urban microclimate is controlled by many parameters, not only by the albedo of the surface. Both natural and man-made elements in the urban landscape interact resulting in a complex response to solar energy gain. Microclimate is not only controlled by building materials and outdoor surface materials of the built-up environment but the presence of vegetation is principally influencing radiation fluxes. Building energy exchange is not only influenced by air temperature but a major impact is dedicated to outdoor vegetation cover.

The effect of vegetation cover on microclimate is enormous. Not only evapotranspiration but also shading plays a key role in influencing urban heat transfer. The cooling effect of vegetation presence is important. Besides, air quality can also be influenced by trees altering the distribution of pollutants in field. For this reason, the detailed mapping of large scale vegetation cover and vegetation structure like canopy distribution can improve the urban microclimate models.

Nadir viewing optical remote sensing sensors can only obtain information like vegetation cover, type or leaf area index (LAI) in general. Only the latter responds to the demand to deduct information over canopy structure. On the contrary, oblique viewing UAS optical data can gather information on the canopy surface resulting in more detailed information on vegetation pattern. Parameters of canopy volume and structure can support urban microclimate models like ENVI_met or building heat balance-based energy simulation like Energy Plus**.**

From nadir viewing UAS images, it is possible to capture and derive vegetation extent maps (*Fig. 9*). However, using the oblique viewing capability of UAS acquisition, the vertical surface of vegetation around the buildings was captured during the study. Therefore, vegetation extent information can be extended with data on canopy structure. In a first step, vegetation was derived from DSM data by histogram thresholding (*Fig. 10*). A clear distinguish could be achieved by defining grassland below 40 m, trees between 40 and 58 m, and roof was established for all points above 58 m. This segmentation process leads to a clear difference between trees and grassland of the campus land cover classes.

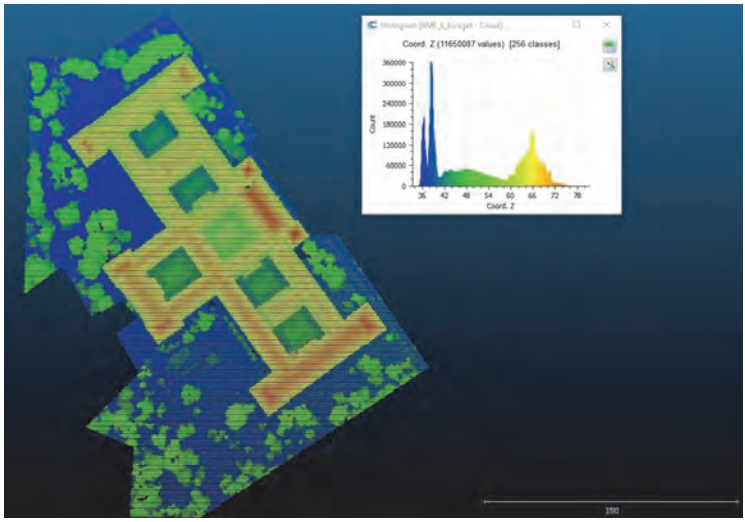

Fig. 10. Vegetation map for the northern campus by DSM histogram thresholding.

In a next step, DSM data over area covered by trees on grassland was studied in more details to support microclimate simulations (*Fig. 11*). The height of individual trees can be deducted from its surface model. Furthermore, the canopy is clearly distinguishable from tree-trunk, thus a ratio of these two characteristic geometric parameters can be derived from the DSM model. Canopy geometry can help to estimate canopy volume which can be highly correlated to LAI for a given tree type. Geometric properties of tree canopy surface can support both shading calculations and tree evapotranspiration estimates to calculate local cooling effects. Once tree types are derived, predefined phenologic annual lifecycles of plants can be simulated in microclimate models too.

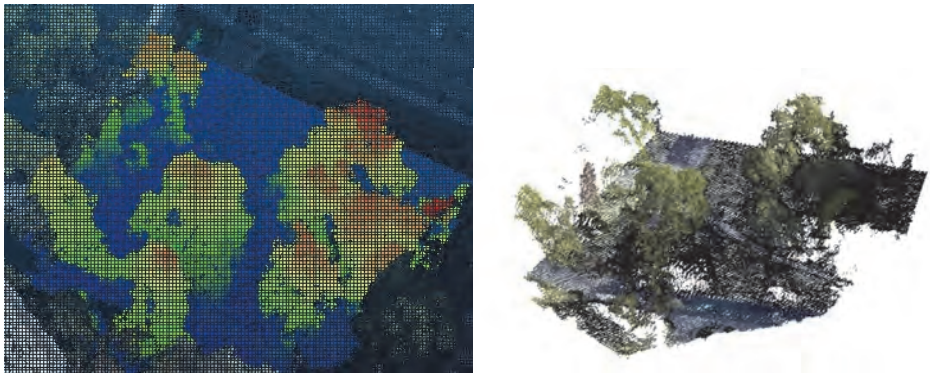

Fig. 11. Tree canopy surface model as height shading (left) and perspective true-color view (right).

Another major influence of urban microclimate is geometric parameters from built-up environment like building height. DSM can help to measure on building height, roof structure, window size, or even shading elements on the building facade. All these parameters influence in-door thermal conditions in a building and can support calculations of building energy balance.

4. Conclusion

The Unmanned Aerial Systems are flexible, easy-to-use image data capture technique, which has already been proven in several technical aspects. Its capability to create high resolution geometric models of urban scenarios enables it to be involved also in microclimatic analyses and simulations. The freely adjustable flying height considering the camera resolution allows to obtain geometric models with prior designed information content. Beyond the pure geometry of the focus area (with building blocks, road surfaces, etc.), such elements can also be described which affect the microclimatic circumstances as the vegetation. Trees, bushes, and grass surfaces can be identified by manual to (semi)automatic techniques based on color and height information. After the segmentation the parameters of the vegetation like tree heights, types, canopy volumes, etc., can be extracted, being able to transfer them into sophisticated climatic modeling software environment. Thanks to the mobility of the UAS technique and the corresponding data processing workflow, the data acquisition demand of microclimatic research has got a new powerful aid.

***Acknowledgement*:** The research reported in this paper was supported by the Higher Education Excellence Program of the Ministry of Human Capacities in the frame of the Artificial Intelligence Smart City (BME FIKP-MI/SC) and Water sciences & Disaster Prevention (BME FIKP-VÍZ) research areas of BME.

References

Barry, R.G. and *Blanken, P.D*., 2016: Microclimate and Local Climate. Cambridge University Press. https://doi.org/10.1017/CBO9781316535981

Chen, J., Zhou, Z., Wu, J., Hou, S., and *Liu, M.,* 2019: Field and laboratory measurement of albedo and heat transfer for pavement materials, *Constr. Build. Materials 202*, 46–57. https://doi.org/10.1016/j.conbuildmat.2019.01.028

Cruzan, M.B., *Weinstein, B.G., Grasty, M.R., Kohrn, B.F., Hendrickson, E.C., Arredondo, T.M., and Thompson, P.G.* 2016: Small Unmanned Aerial Vehicles (Micro-Uavs, Drones) in Plant Ecology, *Appl. Plant Sci.* 4(9). https://doi.org/10.3732/apps.1600041

Eckmann, T., Morach, A., Hamilton, M., Walker, J., Simpson, L., Lower, S., McNamee, A., Haripriyan, A., Castillo, D., Grandy, S., and Kessi, A. 2018: Measuring and modeling microclimate impacts of Sequoiadendron giganteum, *Sust. Cities Soc. 38*, 509–525. https://doi.org/10.1016/j.scs.2017.12.028

Égerházi, L.A., Kovács, A., and *Unger, J.*, 2013: Application of microclimate modelling and onsite survey in planning practice related to an urban micro-environment, *Adv. Meteorol. 2013*, Article ID 251586. https://doi.org/10.1155/2013/251586

Gaitani, N., Burud, I., Thiis, T., and *Santamouris, M.*, 2017a: High-resolution spectral mapping of urban thermal properties with Unmanned Aerial Vehicles. *Build. Environ. 121*, 215–224. https://doi.org/10.1016/j.buildenv.2017.05.027

Gaitani, N., Burud, I., Thiis, T., and *Santamouris, M.*, 2017b: Aerial Survey and In-situ Measurements of Materials and Vegetation in the Urban Fabric. *Proc. Engineer. 180*, 1335–1344. https://doi.org/10.1016/j.proeng.2017.04.296

Kotchi, S.O., Barrette, N., Viau, A.A., Jang, J., and *Gond, V.,* 2016: Estimation and Uncertainty Assessment of Surface Microclimate Indicators at Local Scale Using Airborne Infrared Thermography and Multispectral Imagery. In (Eds. I*mperatore, P.* and *Pepe, A.*) Geospatial Technology - Environmental and Social Applications. IntechOpen, 574–643. https://doi.org/10.5772/64527

Li, S., Juhász-Horváth, L., Pedde, S., Pintér, L., Rounsevell, M.D.A., and *Harrison, P.A.*, 2017: Integrated modelling of urban spatial development under uncertain climate futures: A case study in Hungary. *Environ. Modell. Software 96*, 251–264. https://doi.org/10.1016/j.envsoft.2017.07.005

Liang, S., Li, X., and *Wang, J.,* 2012: Advanced Remote Sensing: Terrestrial Information Extraction and Applications, Academic Press.

Met Office Factsheet, 2019: https://www.metoffice.gov.uk/research/collaboration/ukcp/factsheets, Last access: 2019-02-22.

Rao, P.K., 1972: Remote sensing of urban heat islands from an environmental satellite. *Bull. Amer. Meteorol. Soc. 53*, 647–648.

Ryan, J.C., Hubbard, A., Box, J.E., Brough, S., Cameron, K., Cook, J.M., Cooper, M., Doyle, S.H., Edwards, A., Holt, T., Irvine-Fynn, T., Jones, C., Pitcher, L.H., Rennermalm, A.K., Smith, L.C., Stibal, M., and *Snooke, N.*, 2017: Derivation of High Spatial Resolution Albedo from UAV Digital Imagery: Application over the Greenland Ice Sheet. *Front. Earth Sci. 5*, 40. https://doi.org/10.3389/feart.2017.00040

Srivanit, M. and *Hokao, K.,* 2013: Evaluating the cooling effects of greening for improving the outdoor thermal environment at an institutional campus in the summer. *Build. Environ. 66*, 158–172. https://doi.org/10.1016/j.buildenv.2013.04.012

Wong, N.H., Kardinal, S.J., La Win, A.A., Kyaw Thu, W., Syatia Negara, T., and *Xuchao, W.*, 2007: Environmental study of the impact of greenery in an institutional campus in the tropics. *Build. Environ. 42*, 2949–2970. https://doi.org/10.1016/j.buildenv.2006.06.004

Zhou, D., Xiao, J., Bonafoni, S., Berger, C., Deilami, K., Zhou, Y., Frolking, S., Yao, R., Qiao, Z., and *Sobrino, J.A.*, 2019: Satellite Remote Sensing of Surface Urban Heat Islands: Progress, Challenges, and Perspectives. *Remote Sensing 11*, 48. https://doi.org/10.3390/rs11010048

DOI:10.28974/idojaras.2019.3.3

IDŐJÁRÁS

Quarterly Journal of the Hungarian Meteorological Service
Vol. 123, No. 3, July – September, 2019, pp. 295–312

Towards an intelligent traffic control system using crowdsourcing, based on combined evaluation of weather information and accident statistics

Mátyás Szántó* and **László Vajta**

Department of Control Engineering and Information Technology,
Faculty of Electrical Engineering and Informatics
Budapest University of Technology and Economics
Műegyetem rkp. 3, H-1111, Budapest, Hungary

**Corresponding author E-mail:mszanto@iit.bme.hu*

(Manuscript received in final form May 13, 2019)

Abstract— Weather conditions have both direct and indirect effects on road traffic. On the one hand, precipitation heavily influences road traction as well as vehicle visibility, and on the other hand, medical meteorology phenomena – for example weather fronts – have a great effect on the driving ability and accuracy of drivers. Weather fronts – through their physiological effects – may cause the deterioration of human reaction times, and therefore increase the risk of accidents' occurrence in unexpected and hazardous traffic situations that would require quick intervention of drivers. In this article, our research regarding the relation between weather fronts and traffic accidents as well as between local meteorological parameters and weather fronts is presented.

In this article, a crowdsourcing-based methodology is presented, that is supported by a database, which is assembled using data that is far more heterogeneous with regard to acquisition frequency and quality, than those available previously. Using such a database, a driver aiding system can be created for use in cars currently supporting lower levels of autonomy. Such driver assistance systems would be capable of informing or, in a given situation, indirectly decrease the likelihood of the development of an emergency by warning the driver.

Key-words: weather fronts, traffic accidents, accident statistics, local weather and weather fronts, crowdsourcing, road safety, Hungary

1. Introduction

Weather conditions and their effects on humans have been studied thoroughly in the past century by biometeorologists and medical meteorologists (*Everett*, 1879; *Örményi*, 1975). According to the research of Örményi, the most significant atmospheric change, which has the most considerable effect on the human body, is the transition of weather fronts. Numerous researchers have conducted investigations ever since in order to understand the physiological consequences that these phenomena might have on the population and especially on individuals with certain conditions – e.g. rheumatic diseases –, that make them more weather sensitive than others (*Dúll*, 2014). In a study, conducted using data collected from individuals across two countries, Germany and Canada (*von Mackensen et al.,* 2005) concluded that more than half of the population of these countries consider themselves weather sensitive – 54.5% in Germany and 61% in Canada.

Most of the studies in the field of medical meteorology are considered longitudinal studies, since their main aim is to identify the statistical correlations between time series of meteorological and medical records (*Bucher* and *Haase*; 1993). Consequently, these studies focus on the direct medical effect of weather conditions on humans. *Von Mackensen et al.* (2005) listed symptoms, such as headache/migrane, lethargy, fatigue, and irritation in their survey: their results show that many individuals are affected by these conditions as a result of their weather-sensitiveness.

Such symptoms and health conditions may have considerable indirect impact on road safety as well. *Brown* (1994) suggests that as much as 25% of single-vehicle road accidents may be traced back to issues regarding driver fatigue: weariness could deteriorate individual's performance in tasks that require sustained vigilance, selective attention, and complex decision-making.

The influence of local weather conditions, e.g., temperature, precipitation, wind, on traffic accidents has been studied broadly in the past decade for Hungary (*Vécsei* and *Kovács,* 2014) and for other countries (*Jaroszweski* and *McNamara,* 2014; *Shahid* and *Minhans,* 2016; *Darzi et al.*, 2018) as well. *Darzi et al.* (2018) studied the effect of local meteorological phenomena as well as fatigue, achieved through sleep deprivation, on the driver vigilance using a purpose-built driving simulation.

This article, however, presents a different approach: in Section 2, using data available over a time span of 10 years (within 2001 and 2010), road accident statistics are assessed in a longitudinal fashion, in order to identify some trends present between weather front transitions and variation in the distributions of number of traffic accidents. Secondly, another statistical study is presented whose aim is to identify trends in front type transitions by comparing and selecting locally obtainable weather data, e.g., local temperature values, with the use of a detailed database. Then, on the basis of the results of these two analyses, a crowdsourcing-based approach is presented for road database production that

could be the foundation of a driver aiding system ultimately beneficial for increasing road safety.

2. The effect of weather conditions on road safety

2.1. Original and modified databases

For conducting the study presented in this article, the same database was used as in *Vécsei* and *Kovács* (2014). That is, the database consisted of hourly statistics of domestic – i.e., Hungarian – road traffic accidents (source: KSH data collection, data provider: police OSAP1009) and the extensive local weather data recorded at selected meteorological observatory sites (Budapest, Pécs, Szeged, Debrecen, Szombathely, Győr, Nagykanizsa, and Siófok) of the Hungarian Meteorological Service for the same time-period. The database was initially created by acquiring and assembling data collected on an hourly basis between January 1, 1990 and December 31, 2010. However, the data used in this article were summed or averaged over individual days – that is, summed in case of accident statistics and averaged for weather related data. The database was also cropped for the ten-year time-period of January 1, 2001 and December 31, 2010. The reason for this data reduction was the database containing the front types registered for Hungary.

Records of front types in this latter database has been made available for the purpose of this study on a daily basis between January 1, 2001 and December 31, 2010, courtesy of the Data Supply Department of the Hungarian Meteorological Service. The main front types can be found in *Table 1.*

Table 1. Front types and their codes in the used database

Front type	No front	Stable warm front	Unstable warm front	Unstable cold front	Stable cold front
Code in database	1	2	3	4	5

For days, when two different front types have been recorded in Hungary, two separate codes were given in the database – e.g., 3,4 or 1,5. However, in the study presented in this paper, only those front codes have been used which were unambiguous – i.e., only one type of weather front was indicated for a certain day for the whole country. This measure, while reducing the amount of data, enables a more precise statistical evaluation of the available records.

The thus assembled and cropped database has been used for carrying out the study presented below. Every record contains hourly data over the above specified 10-year time-period for traffic accident, local and medical meteorology related data information, including[1]:

- Front type for the given day;
- Front type for the previous day;
- Temperature and temperature difference (for the selected cities);
- Cumulative precipitation and cumulative precipitation difference;
- Wind and wind difference;
- Absolute number of traffic accidents within city limits;
- Absolute number of traffic accidents outside city limits;
- Timestamp.

The above database containing records regarding local weather and traffic accidents, which has been made available for the purpose of this study, is relatively outdated – i.e., some data have been collected almost twenty years prior to the preparation of this paper. Since the database has 3652 records over the assessed years, it is safe to say that it is representative of the chosen time-period.

However, one of the main purposes of this study was to identify possible connections between medical meteorological phenomena and accident statistics. The fact that several studies concerned with this effect written several decades apart (*Everett*, 1879; *Örményi*, 1975) concluded into similar results regarding the effect of meteorological weather data on human behavior suggests that the connection between the two aspects are not subject to change significantly over time. This also suggests that the conclusions of this paper are applicable for the traffic circumstances of present days.

The amount of traffic flow on the roads plays a major role in the number of accidents occurring. Fluctuation for vehicles on the road can be observed on different scales. The daily fluctuation of road usage of Hungarian roads in particular is shown in *Kovács* (2013). *Karacusu et al.* (2011) have studied this relationship in depth for Eskisehir, Turkey for daily, weekly, and seasonal vehicle number fluctuations and have concluded that more vehicles present on the roads means greater probability for accidents. Because of this fluctuation, a normalization step has been introduced for the number of accidents in the database. First, the number of accidents has been averaged between January 1, 2001 and December 31, 2010 for regular days – i.e., working Mondays to Fridays and ordinary weekend Saturdays and Sundays. The mean values for this period are shown in *Table 2.*

[1] Difference is always calculated between the current and the previous record

Table 2. Mean number of accidents for different 'regular' days for the time-period between January 1, 2001 and December31, 2010

Mean number of accidents	Days of the week						
	Monday	**Tuesday**	**Wednesday**	**Thursday**	**Friday**	**Saturday**	**Sunday**
Budapest	11.74	11.53	11.53	11.73	12.67	9.21	7.40
Szeged	0.84	0.81	0.83	0.90	0.91	0.78	0.51
Pécs	0.85	0.86	0.83	0.88	1.00	0.70	0.61
Szombathely	0.51	0.48	0.48	0.49	0.61	0.43	0.31
Total within city limits	37.32	36.17	37.09	37.95	43.50	36.27	27.37
Total outside city limits	14.83	14.29	14.31	15.02	18.53	20.30	16.56

In the case of the database used for this study, the difference of the traffic is also rather significant. After identifying the days, that are possible outliers, meaning the mean accident values are higher and lower than the total mean, a similarity test has been carried out for the number of accidents that occurred within and outside city limits on the identified days (Fridays and Sundays). It was found, that the similarity test of the accident numbers on the given days resulted in significances of under 0.0005 (*Fig. 1*). This showed, that the normalization step was indeed necessary before the accident values were compared.

Hypothesis Test Summary

	Null Hypothesis	Test	Sig.	Decision
1	The distribution of Number of accidents within city limits is the same across categories of Grouping variable.	Independent-Samples Mann-Whitney U Test	.000	Reject the null hypothesis.
2	The distribution of Number of accidents outside city limits is the same across categories of Grouping variable.	Independent-Samples Mann-Whitney U Test	.000	Reject the null hypothesis.

Asymptotic significances are displayed. The significance level is .05.

Fig. 1. Results of similarity tests of accident distributions within and outside city limits for the possible outlier days – rejecting the null hypothesis, i.e., the distributions are considered not similar.

According to the database, there have only been 21 Fridays that were holidays in Hungary during this ten-year interval. However, this fact has a significant effect on the mean values of number of accidents occurring on these days: excluding holidays caused a daily increase from 42.87 to 43.50.

In *Table 2,* a two orders of magnitude difference in daily mean accident occurrences can be observed between different cities. This difference can be traced back to the sheer number of cars owned in the two areas. According to data provided by the Hungarian Central Statistical Office (*KSH,* 2018, 2019), in 2002, 594 246 cars were registered in Budapest, which is almost six times as much as the number of cars registered for the whole of Baranya county (100 611) – the capital of which is the city of Pécs. For perspective: the total population of Baranya county was 404 709, whereas the same figure for Budapest was 1 719 342 at the beginning of 2003.

Because of the big gap between different urban areas, only the total number of accidents outside and within city limits has been used in this study. Using the mean values in *Table 2*, total daily accident numbers have been normalized. The thus calculated variables have been introduced in the database:

- Normalized number of traffic accidents within city limits;
- Normalized number of traffic accidents outside city limits.

The weekly distributions of mean accident numbers are visualized in *Figs. 2* and *3* for within and for outside city limits, respectively. Different trends can be identified for within-city and outside-city traffic flow in these figures.

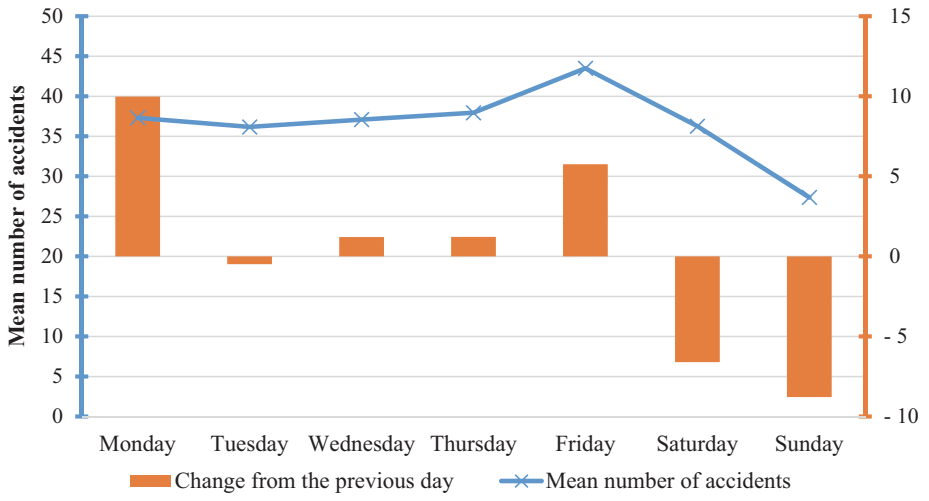

Fig. 2. Mean number of accidents within city limits for different regular days for the time-period between January 1, 2001 and December 31, 2010.

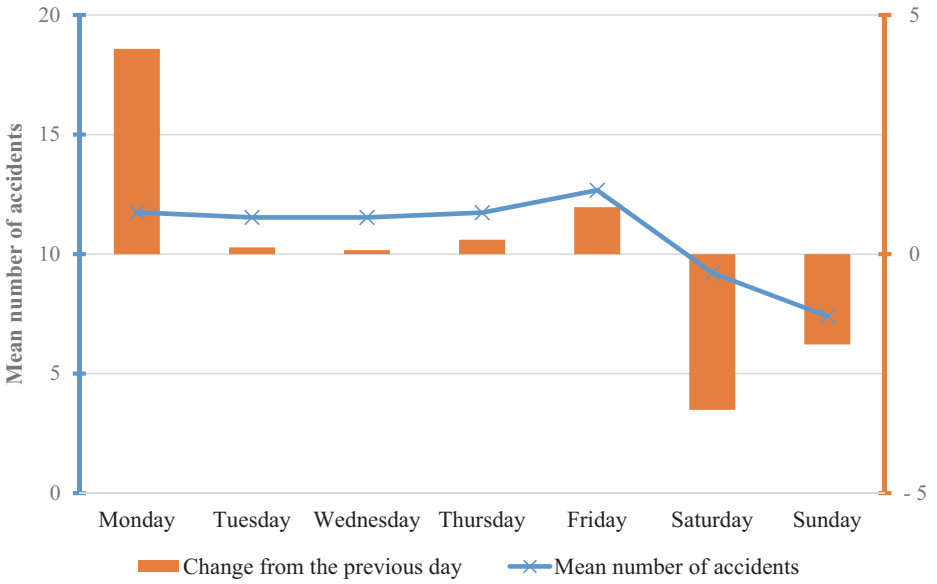

Fig. 3. Mean number of accidents outside city limits for different regular days for the time-period between January 1, 2001 and December 31, 2010.

2.2. *Statistical analysis of the relationship between weather fronts and traffic accidents*

The used environment for the statistical tests and visualization was IBM SPSS Statistics 23 version (*Ketskeméty et al.,* 2011).

Using the above-introduced databases, a three-step statistical test-sequence has been developed in order to identify the possible relationships between weather phenomena and traffic safety. More specifically, an attempt has been made to find trends of weather front transition-related change in the number of accidents that occur on the roads. The test sequence consisted of the following steps:

1) *Normality assessment:* The variables of normalized accident occurrences have been tested using a parametric test. That is, each independent sample has been tested against the null hypothesis, that they were normally distributed around their mean value. For sample sizes smaller than 2000 elements, the Shapiro-Wilk test is used, otherwise, the normality may be tested using the Kolmogorov-Smirnov test. This test step, therefore, has been carried out using the Shapiro-Wilk test at a significance level of 0.05 – or

5%. As a part of the normality assessment, the distributions of the variables have been visualized using their histograms. The results of this step are shown in *Fig. 4.*

2) *Mean value comparison:* This step was introduced in order to manually assess the relation of the mean values of two variables, i.e., normalized accident numbers in case of no front transition versus the case of front transition. It involved the visualization of the two variables overlaid on each other by means of a stacked histogram. Using this step, the preliminary direction of change between the two variables, i.e., increase or decrease, could have been established. The results of this step can be observed in *Fig. 5.*

3) *Similarity test of distributions:* In this step, the hypothesis, that the independent variables were sampled from the same distribution has been tested. The significance level used for the test of this step was also 5%. The results of this step are shown in *Fig. 6.*

For step 3) of the above described test sequence, an independent samples nonparametric test was used, since the normality of the samples' underlying distributions could not be granted in all cases. The selected variables, however, met the requirements for the Mann-Whitney U test in all cases, and considering the arguments made by *Sawilowsky* (2005), this test proved to be the most robust for the testing of the significant similarity of the samples.

The output of the test sequence of the comparison of distributions of normalized accident numbers outside city limits is shown in *Figs. 4, 5,* and *6*. Test case: no front transition from unstable cold front versus transition from no front to unstable cold front.

1) Normality assessment and histogram of distribution of normalized number of accidents outside city limits

a) No front to unstable cold front transition

Tests of normality

	Shapiro-Wilk		
	Stat.	df	Significance
Normalized number of accidents outside city limits	0.976	105	0.055

Accept the null hypothesis
(normally distributed sample)

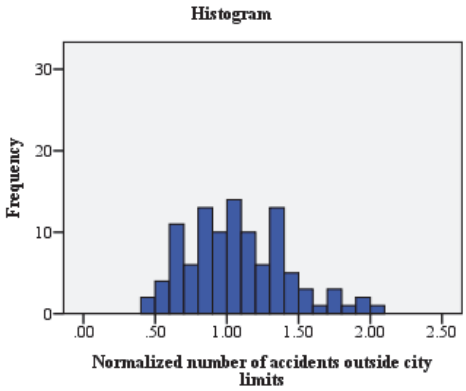

b) No transition from unstable cold front

Tests of normality

	Shapiro-Wilk		
	Stat.	df	Significance
Normalized number of accidents outside city limits	0.972	190	0.001

Reject the null hypothesis
(not normally distributed sample)

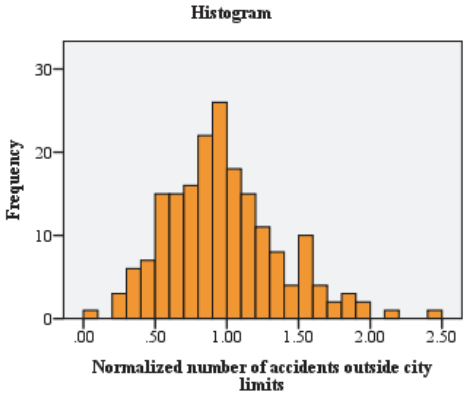

Fig. 4. Output of the normality assessment and histograms step. Test case: outside city limits; no front transition from unstable cold front versus transition from no front to unstable cold front. *df* is the degree of freedom of the sample, which is equal to *N-1*, where *N* is the size of the sample.

2) Mean value comparison

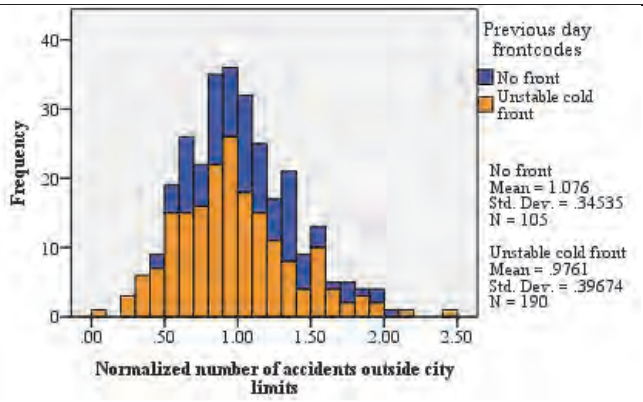

Higher mean value in case of no front to unstable cold front transition - **increase**

Fig. 5. Output of mean value comparison step. Test case: outside city limits; no front transition from unstable cold front versus transition from no front to unstable cold front.

3) Similarity test of distributions

Hypothesis Test Summary

	Null Hypothesis	Test	Sig.	Decision
1	The distribution of normalized number of accidents outside city limits is the same across categories of grouping variable.	Independent-Samples Mann-Whitney U Test	.013	Reject the null hypothesis.

Asymptotic significances are displayed. The significance level is .05.

Reject the null hypothesis – **the difference of the distributions is significant**

Fig. 6. Output of similarity test of distributions step. Test case: outside city limits; no front transition from unstable cold front versus transition from no front to unstable cold front.

The above introduced test sequence has been carried out on several test cases – i.e., no front transition versus front transition pairs. The results of these test sequences are summarized in *Table 3.*

Table 3. Test sequence results for different test cases

Test cases		Difference in normalized number of accidents in case of front transitions		
Front transition types	**No transition front type**	**Outside city limits (significance)**	**Within city limits (significance)**	**Number of cases**
NF to UC	UC	Increase (0.013)	Increase (0.001)	295
NF to SC	SC	Increase (0.075)	Increase (0.041)	74
NF to SW	SW	Decrease (0.167)	Decrease (0.854)	234
NF to UW	UW	Increase (0.529)	Increase (0.457)	174
UC to NF	NF	Increase (0.008)	Decrease (0.180)	878
SW to UC	UC	Increase (0.804)	Increase (0.049)	260
UW to UC	UC	Increase (0.002)	Increase (0.518)	290
SC to UC	UC	Increase (0.191)	Increase (0.698)	214

Legend	
NF	No front
SW	Stable warm front
UW	Unstable warm front
UC	Unstable cold front
SC	Stable cold front
Increase is significant	
Increase is not significant	
Decrease is significant	
Decrease is not significant	
Significance level	0.05 or 5%

As a result of the null hypothesis of the independent samples Mann-Whitney U test, the lower the test result's significance value – shown in brackets in *Table 3* – the smaller the resemblance between the underlying distributions that the two variables are sampled from. With this information in mind, we can observe that the only front transition that is followed by a significant increase in accident numbers both within and outside city limits is the 'no front to unstable cold front' transition. The significance levels in the case of this transition are among the lowest figures yielded by the test sequences.

From the test sequence results listed in *Table 3,* it can be identified that, based on the test data, the strongest relationship between the increasing number of traffic accidents and the transition of weather fronts can be shown in the case of the '*no front to unstable cold front*' transition. These results endorse the cliché, that under the influence of some weather fronts, drivers in general become more precarious and upset.

2.3. Suggesting front types based on local meteorological data

Because the results of the previous section showed that the unstable cold front type might be linked to the most significant increase of traffic accidents, in the following sections of this paper, an effort is made to distinguish this front type – number 4 in *Table 1* – from the others.

The foundation beneath the weather front type-suggestions presented in this section was that based on the comparison and variation of the local meteorological parameters for different parts of the country – or different cities in this case – the current weather front might be presumed. For the case of this study, the temperature measured at 5 Hungarian cities (Szombathely, Pécs, Budapest, Debrecen, and Szeged) was used. In order to monitor the daily mean temperature difference between the 'neighboring' cities amongst these, 7 additional variables have been calculated in the database. The city-pairs, for which the temperature differences have been calculated for, are as follows:

- Budapest – Debrecen
- Budapest – Pécs
- Budapest – Szeged
- Budapest – Szombathely
- Pécs – Szombathely
- Pécs – Szeged
- Szeged – Debrecen

The direction of the subtractions have been decided by the geographical position of the cities. The meteorological processes, especially weather fronts, tend to approach Hungary from the northwest and move along towards the southeast, therefore the sequence of the cities in the subtractions have been selected accordingly. This caused the calculations to yield a negative difference if cold weather was approaching from the northwestern-western part of the country.

Another variable – a flag – has also been introduced for this analysis. If the largest absolute value among the temperature differences was the absolute value of an originally negative temperature difference, then the temperature decrease designator flag was set to true (or equal to 1) for the given day. Besides this, another yearly value had to be calculated in order for the front type suggestions

to be effective, was the top percentile of the maximums of absolute values of temperature differences between cities in that year. Several values were considered during the research, but finally the 80th percentile proved to be the most effective. The percentile value has been calculated for the whole year. The 80th percentile values can be seen in *Table 4* for each year of the research.

Table 4. 80th percentile values of the maximums of absolute values of temperature differences yearly

Year	80th percentile
2001	3.3258
2002	3.1604
2003	3.3850
2004	3.2433
2005	3.1242
2006	3.2575
2007	3.2658
2008	2.8896
2009	3.2208
2010	3.1158

Since in general, each year the two most common front types were no front and unstable cold front – latter is the front type of the greatest interest of this research –, the parameters most useful for filtering were identified as follows:

1) The mean temperature is lower in Szombathely than in Budapest.
2) The temperature decrease designator flag is true.
3) The maximums of absolute values of temperature differences between cities was in the 80th percentile.

Upon filtering the database with the above three parameters, a relatively effective unstable cold front suggestion could be reached. The use of the filtering algorithm on the front types are shown in *Fig. 7*, using the histograms of the yearly front type statistics. The two displayed histograms are displaying the unfiltered and the filtered frequencies of the front types for the year 2009.

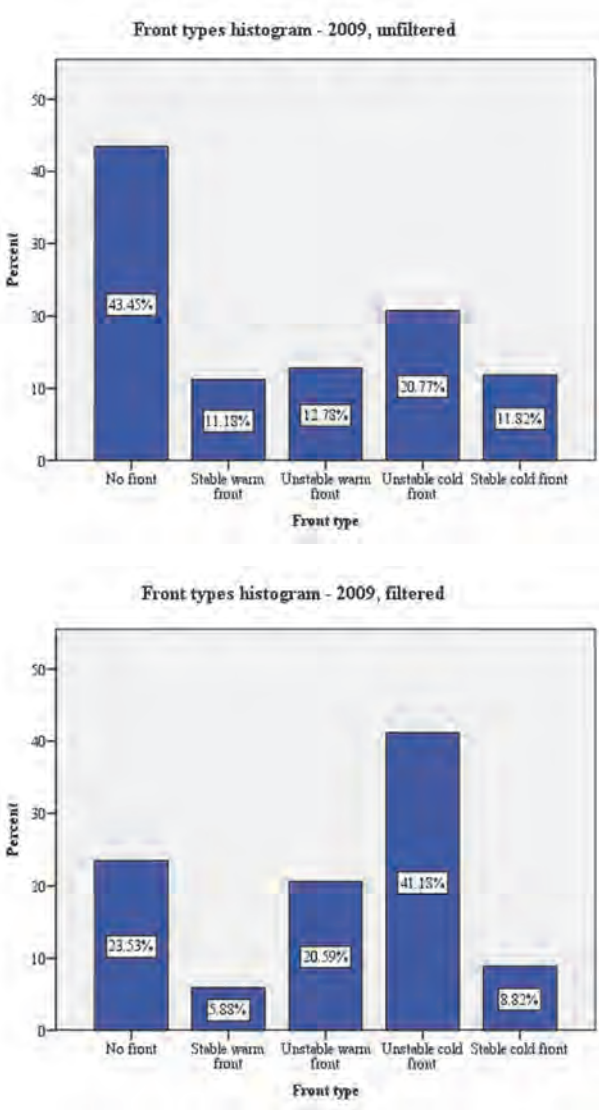

Fig. 7. Percentage histograms of front types in 2009 – unfiltered (above) and filtered (bottom) cases.

The above figure shows that the filtering criteria is fairly efficient for suggesting the front type 'unstable cold front'. The same filtering algorithm has been yearly for the time-period between 2000 and 2010, the results of which are shown in *Table 5*.

Table 5. Yearly results of the front type filtering algorithm

Year	Unfiltered case (percentages)			Filtered case (percentages)			Filtering efficiency (Percentage points)[3]
	No front	Unstable cold front	Part to whole[2]	No front	Unstable cold front	Part to whole[2]	
2001	35.6%	23.1%	39.35%	36.8%	42.1%	53.36%	**14.01%**
2002	34.1%	22.9%	40.18%	34.6%	26.9%	43.74%	**3.56%**
2003	51.9%	17.7%	25.43%	30.4%	17.4%	36.40%	**10.97%**
2004	37.3%	22.5%	37.63%	45.5%	27.3%	37.50%	**-0.13%**
2005	42.1%	21.8%	34.12%	20.0%	24.0%	54.55%	**20.43%**
2006	42.0%	23.1%	35.48%	56.3%	15.6%	21.70%	**-13.79%**
2007	42.3%	22.2%	34.42%	25.0%	32.1%	56.22%	**21.80%**
2008	43.5%	25.5%	36.96%	33.3%	44.4%	57.14%	**20.19%**
2009	43.5%	20.8%	32.35%	23.5%	41.2%		**31.33%**
2010	45.4%	26.3%	36.68%	29.7%	32.4%	52.17%	**15.49%**

The last column in *Table 5* shows the efficiency of the filtering for the given year, using percentage points. The mean efficiency of the above described front suggestion algorithm is *12.39* percentage points, which indicates that it is moderately capable of suggesting the presence of unstable cold weather fronts versus the lack of fronts.

By optimizing the parameters of the filtering algorithm, the fluctuation of the filtering efficiency may be minimized. One of the key reasons for the presence of the outliers is the somewhat chaotic nature of transition of weather phenomena.

[2] Part to whole value is calculated using the following formula:

$$\frac{UC\%}{UC\%+NF\%}, \quad (1)$$

where *UC*% is the percentage of days with unstable cold fronts and *NF*% is the percentage of days with no fronts – i.e., the values in the previous two columns.

[3] Efficiency is the percentage point increase of *part to whole percentage* from the unfiltered case to the filtered case.

Also, when assessing the results shown in the above table, it should be considered, that the input parameters used for the algorithm were chosen heuristically after assessing the input data. In the future, for solving the shortcomings of the front type algorithm, the incorporation of machine learning should be investigated, as a neural network training procedure might result in an algorithm that is capable of producing better results given sufficient training data. Satisfactory training data might be collected using a crowdsourcing-based approach, that is presented in the next section.

3. Development of a crowdsourcing-based adaptive traffic control system

Nowadays, via the increasing importance of smart-city platforms, among other reasons, such real-time traffic control systems are becoming more widespread, whose functionality is based on a sufficiently detailed database, which consists of archive as well as constantly updated data. This database could contain – amongst others – information on the given vehicle's or its driver's transport history, meteorological and medical meteorological factors that might influence the driver's alertness.

A crowdsourcing-based approach is introduced for delivering the increased data-need of such a platform. The idea of including a mass of data acquisition sources is based on the model presented in *Szántó* and *Vajta* (2017). There, the crowd – i.e., the individual road users – help to gather information about the current state of road surfaces, thus creating an up-to-date database containing information on road surface damages.

For the crowdsourcing-based model to be functioning effectively, large amounts of data are required. The data, as it is established in the previous sections of this paper, might be an archive – e.g., meteorological parameters and measurements from preceding days – or up-to-date information that is acquired continuously by rather heterogeneous data sources – e.g., current road usage statistics and driver vigilance indicators. The former type of data are available via precompiled and – in most cases – publicly available databases, such as those, on which the analysis presented in the previous sections were performed. However, the latter type of data may be collected through many different data acquisition points or sources. These may be smart road infrastructure elements (e.g., lamp posts or in-road sensors), connected (or smart) cars, smartphones, or specific internet of things (IoT) devices.

Such crowdsourcing-based databases that could hold information regarding the above specified road safety conditions, may be used as the foundation for an intelligent traffic control system, that, incorporated with driver-specific driver assistance systems (DAS or ADAS for advanced driver assistance systems) could then adapt their parameters and functionality and ultimately improve traffic safety.

The research presented in *Vécsei* and *Kovács* (2014), and the analysis in the previous sections of this paper indicate that local meteorological conditions, as well as medical meteorological phenomena have a statistically significant connection with road accidents. These results, therefore, justify further research to be carried out in the field of crowdsourcing-based meteorological and traffic data acquisition.

4. Conclusion and future work

The purpose of the analysis presented in this article was to assess, at a first reading, whether the endeavor for traffic safety increase based on the detailed investigation of crowdsourced meteorological data is sufficiently founded. The initial inspections presented above were, therefore, carried out using the available databases and utilizing simplified methods. The results introduced above warrant the conduction of further analysis of other traffic safety influencing data, such as:

- accident causes and patterns,
- seasonal and daily variance of accident numbers,
- vehicle type related regulations,
- objective figures for driver vigilance and attention, and
- natural conditions besides weather related data, e.g., pollen concentration.

There are a number of ways that the analysis presented in the previous sections should be improved. Most importantly, the inclusion of the above listed additional data could lead to a more accurate statistical assessment of the relationship between the vehicle driver's objectively perceivable environment and their aptitude for being involved in a traffic accident. Secondly, further investigation of the front type suggestion algorithm may be justified, using monthly or seasonal meteorological parameters rather than yearly data for calculating the temperature variation threshold may lead to higher accuracy. Also, as noted above in Section 2., the utilization of machine learning should be considered for optimizing the parameters of this algorithm. It could also be beneficial for the development of a crowdsourcing-based, real-time traffic control system to develop a probabilistic weather front suggestion system.

Acknowledgements: The authors would like to express their gratitude towards *Dr. László Bozó* for his valuable input on the mechanics of front type transitions. The authors also owe gratitude to *Dr. Kálmán Kovács* and the Data Supply Department of the Hungarian Meteorological Service for sharing the extensive local and medical meteorological and accident databases for the purpose of completion of the authors' research. The research reported in this paper was supported by the BME-Artificial Intelligence FIKP grant of EMMI (BME FIKP-MI/SC), and by the EFOP 3.6.1.-16-2016-00014 program of the Ministry of Human Capacities (Disruptive Technologies).

References

Brown, I.D., 1994: Driver Fatigue. *Human Factors: J Human Fact. Ergonomic. Soc. 36*, 298–314. https://doi.org/10.1177/001872089403600210

Bucher, K. and *Haase C.*, 1993: Meteorotropy and medical-meteorological forecasts. *Experientia 49,* 759–768. https://doi.org/10.1007/BF01923545

Darzi, A., Gaweesh, S.M., Ahmed, M.M., and *Novak, D.*, 2018: Identifying the Causes of Drivers' Hazardous States Using Driver Characteristics, Vehicle Kinematics, and Physiological Measurements. *Front. Neurosci 12,* 568. https://doi.org/10.3389/fnins.2018.00568

Dúll, A., Fülöp, A., and *Mika, J.,* 2014: A Kérdő-féle frontérzékenységi teszt vizsgálata és kísérlet a továbbfejlesztésére. *Légkör 59,* 74–77. (In Hungarian)

Everett, J.T., 1879: Studies in relation to the production of pain by weather. *Chicago Med. J. Exam 38,* 253–260.

Jaroszweski, D. and *McNamara, T.* 2014: The influence of rainfall on road accidents in urban areas: A weather radar approach. *Travel Behav. Soc. 1*, 15–21. https://doi.org/10.1016/j.tbs.2013.10.005

Karacasu, M., Er, A., Bilgiç, Ş.,B. Barut, H., 2011: Variations in Traffic Accidents on Seasonal, Monthly, Daily and Hourly Basis: Eskisehir Case. *Procedia - Social and Behavioral Sciences. 20,* 767–775. https://doi.org/10.1016/j.sbspro.2011.08.085

Ketsketméty, L., Izsó, L., and *Könyves T., E.*, 2011: Bevezetés az IBM SPSS Statistics programrendszerbe. Artéria Stúdió, Budapest. (In Hungarian)

Kovács, Cs., 2013: A lakossági közösségi és egyéni közlekedés jellemzői. *Statisztikai tükör, 2013/47*, 1–5. (In Hungarian)

KSH, 2019: Közúti gépjármű-állomány, december 31. (2000–),*online:* http://www.ksh.hu/docs/hun/xstadat/xstadat_eves/i_ode006b.html (accessed on 05.04.2019.) (In Hungarian)

KSH, 2018: A lakónépesség nem szerint, január 1. (2001–), *online:* www.ksh.hu/docs/hun/xstadat/xstadat_eves/i_wdsd003a.html (accessed on 05.04.2019.) (In Hungarian)

von Mackensen, S., Hoeppe, P., Maarouf, A., Tourigny, P., Nowak, D., 2005: Prevalence of weather sensitivity in Germany and Canada. *Int. J. Biometeorol. 49*, 156–166. https://doi.org/10.1007/s00484-004-0226-2

Örményi, I., 1975: Érzékenyek vagyunk. *Heves Megyei Népújság 26,* 9. (In Hungarian)

Sawilowsky, S.S., 2005: Misconceptions leading to choosing the t test over the Wilcoxon Mann-Whitney U test for shift in location parameter. *J. Modern Appl. Stat. Meth. 4*, 598–600. https://doi.org/10.22237/jmasm/1130804700

Shahid, S. and*, Minhans, A.*, 2016: Climate change and road safety: A review to assess impacts in Malaysia. *Jurnal Teknologi 78(4),* 1–8. https://doi.org/10.11113/jt.v78.7991

Szántó, M. and *Vajta, L.*, 2017: Crowdsourcing Techniques for Environmental Information Using Additional Evaluation of Vision Based Driver Assistant Systems. 2017 International Conference on Control, Artificial Intelligence, Robotics & Optimization (ICCAIRO). Prague, 51–55. https://doi.org/10.1109/ICCAIRO.2017.19

Vécsei, P. and *Kovács, K.,* 2014: Statistical analysis of relationships between road accidents involving personal injury and meteorological variables in Hungary. *Időjárás 118,* 349–378.

DOI:10.28974/idojaras.2019.3.4

IDŐJÁRÁS

Quarterly Journal of the Hungarian Meteorological Service
Vol. 123, No. 3, July – September, 2019, pp. 313–328

Performance comparison of long-distance running competitions in different meteorology and environment based influential conditions

Dávid Berke

Department of Networked Systems and Services,
Faculty of Electrical Engineering and Informatics
Budapest University of Technology and Economics
Műegyetem rkp. 3., H-1111 Budapest, Hungary

Author E-mail: berkedavid89@gmail.com

(Manuscript received in final form May 17, 2019)

Abstract—Long-distance running is one of the most popular daily sports, through which we can keep our health or take care of our body. Millions of people around the world run for different reasons like recreation, professionalism, mental balance, or fun. That is why long-distance running competitions are organized very often. The organizers have to know the expected meteorological conditions and several specific parameters and information about performance of the runners retroactively to support them effectively as well as adapting to the running attitude and main goals.

The purpose of this study was on one side to develop a data analyzing tool with flexible and multifunctional analytical capabilities to identify which specific – especially meteorological – attributes of long-distance running competitions have relevant impact on the performance of the competitors, while on the other side to compare competitions with each other, which have different environmental and social properties in terms of running pace and age.

Starting to design a tool named Running Competition Comparison Tool (RCCT), availability of existing data was discovered, focusing on Hungarian long-distance running competitions. Altogether results and environmental attributes of 28 Hungarian half-marathons and further 7 variable distance competitions were investigated. In all, 146,924 participants were involved and analyzed within this study between 1996 and 2017 within 5 km to 300 km. Specific and unique data classification methods were used to specify age and pace categories for realizing different kinds of statistical analyses. In a final phase, all classified data was represented and visualized by a two-dimensional colored matrix with automatic evaluation capability, combined with column and bar charts.

Numbers of recreational athletes in Budapest national half-marathon have been continuously increased during the last two decades, especially in case of middle pace (5:00-6:59 min/km) runners. Due to a trend prediction of the study, numbers of half-marathon finishers could be reach 20,000 for 2030, which will mean 80–85% additional growth. Extraordinary meteorological conditions like unexpected high air temperature or

humidity and several environmental parameters like ultra-distance and mountain course are able to impair recreational athletes' pace in a similar way as tiredness of well-trained ironman triathletes.

According to this study, running distance and absolute elevation have maximum impact on long-distance running pace and separate age groups mostly. Air temperature and humidity together also have relevant impact on endurance running performance in cases of different distances. Especially high temperature (higher than 25 °C) or high humidity (higher than 70%) could influence long-distance running speed and fluid loss more than lower temperature and humidity. That study highlighted well that the impact of meteorological attributes are relevant in terms of running performance of long-distance running pace, hence organizers have to take meteorological conditions into account during their plan to be done.

Numbers of half-marathon finishers have been continuously increasing since 1996, especially numbers of middle-aged runners. Orientation and main goal of the participants of Hungarian half-marathons have been completely changed from competitive (elite) to recreation and hobby. Because of the athlete separation of multi-distance running events, there are no significant differences between variable distanced (5 km, 10 km, 21 km, 42 km) competitions in terms of running pace.

Key-words: meteorological conditions, environmental dependence, long-distance running, recreational sport, statistical analysis, visual comparison tool

1. Introduction

There is an ongoing debate of the effects of *biological* (gender, age, body mass index, genetics), *environmental* (air temperature, humidity, air pollution, atmospheric pressure, absolute elevation, wind speed), *intellectual* (willpower, tendentiousness, competitive spirit, mental balance), *physical fitness* (endurance, velocity, strength), and real-time *physiological* (heart rate, fluid loss, thirst, body weight loss, blood sugar, body temperature, etc.) attributes on performance of long-distance running athletes. Although, it is commonly believed that most of these attributes are relevant but not at the same degrees.

Popularity of long-distance running events has been growing day by day, especially in cases of half-marathons and marathons. As a result, many physiological and sport science research have been done in the last couple years, not just focusing on elite athletes, but recreational and hobby runners as well, as a part of health maintenance or e-health.

Gaining deeper knowledge about drinking behaviors of long-distance runners is very important. Not a long ago, runners have not had deep understanding of the physiological consequences of hydration, to avoid conditions of dehydrations and over-hydration is not trivial for recreational competitors (*Winger et al*., 2010).

Another research was focusing on effects of fluid intake and thirst sensation on performance of trained half-marathon runners. In that case, rate of fluid intake

above that dictated by their thirst sensation is not able to improve running speed. Based on that, thirst is an efficient identifier to schedule fluid replacement during a race (*Dion et al*., 2013).

During an original marathon, the finishing time and the percentage of body weight loss of the runners are strongly correlated. Competitors, who can complete the whole distance faster, use to lose less percentage of their body weight than slower participants do in an inverse way. The nature of this body loss effect is linear, and statistically independent from gender or age (*Zouhal et al*., 2010).

Environmental parameters like air temperature, humidity, dew point, and atmospheric pressure also can influence running performance. According to several papers, it is not easy to prove the direct effects of the weather conditions even in an obvious area as transport (*Vécsei et al*., 2014). In our case, from all these environmental attributes, obviously, air temperature is the most important factor, because it is significantly correlated with running speed, which describes performance in this case (*El-Helou et al*., 2012). Seemingly, from environmental attributes, air temperature is the only factor, which is linked directly to running speed, but as we can see later in this paper, characterization of a running course, especially ratio of absolute elevation and running distance should be able to generate stronger impact on running speed.

The main goal and purpose to locate refreshment or aid station distributions along long-distance running courses is trying to decrease negative effects of dehydration, fluid loss, and thirst in a human body, to recover fluid, some kind of minerals, salt, and sugar as well. According to public information of long-distance running competitions, it would be possible to estimate and simulate impact of thirst on running performance for optimizing positions of aid stations (*Berke*, 2015, 2017).

Long-distance sports are not consisting of only running, cycling also a relevant and important part of it. Seemingly, dehydration can always influence the endurance sport participants' performance and speed, especially in high temperature environment. According to an environment chamber research for testing well-trained cyclists, the previously mentioned statement is not necessarily true. In some special cases, dehydration does not impair performance in the heat automatically (*Wall et al*., 2013).

Through those research examples, importance and variability of long-distance running performance investigations can be highlighted. Because of diversity of these parameters, which can influence running performance, analyzing all of them has to be not so simple. That is why this research was focusing on modeling, to describe and present an information technological tool, through which additional impact of several hardly comparable factors can be revealed and identified, like athletic habits, course elevation, and running distance.

2. Data and methods

2.1. Data management

In Hungary, specific personal information of the long-distance finishers, like birth year, running time, and gender are mostly available on the official website of the competitions or the organizer company. For this reason, collecting and calculating relevant data of thousands of runners for supporting this research has not been complicated. After the data collection, manual data pre-processing had to be done, like missing data interpolation, false and incorrect data value handling, and different types of data conversion. Finally, all pre-processed data were integrated into an automatic, own designed information technological tool named RCCT, through which different types of statistical analyses could be realized and evaluated, as can be seen hereinafter.

2.2. Running Competition Comparison Tool (RCCT)

Current version of the Running Competition Comparison Tool (RCCT) is a well-structured table sheet, optimized for data storage, automatic data classification, cluster visualization, and specific diagram tracing. Specific parts of a previously referred research (*Berke*, 2017), which focusing on optimization of locations of refreshment stations on half-marathons, gave the basis idea of RCCT.

Competitor classification

This research was describing running performance not just using running pace but age of the competitors as well. Combining both parameters into a two-dimensional classification applied for identifying runner performance categories. Both attributes were separated into seven disjoint clusters independently from each other, considering practical separation techniques of athletics and sport rules and regulations of the Hungarian Athletics Association and IAAF (HAA, 2016; IAAF, 2016).

The first age category represents U20 (under 20), then further categories continuously describe a ten-year-long age interval, lastly the seventh cluster includes runners at least 70. In cases of half-marathon and marathon distance competitions, participating for specified age groups is prohibited for medical and health keeping reasons by several national and international laws. As a result, participating a marathon under 16 and participating a half-marathon under 13 are not allowed in Hungary.

On the other hand, the first pace category represents all those runners, who can reach the finish line performing < 4 min/km average pace. Further categories continuously describe a 1 min/km pace interval, the last one represents ≥ 9 min/km runners. This classification was optimized for recreational endurance running activities, not for elite or professional runners. Performance categories

combine age and pace categories in every possible way, and as a result, 49 performance clusters has been implemented.

Visual representation of running performance

Distribution of percentage of these performance categories is capable of representing importance of all those clusters, which is being analyzed. All of these 49 categories were structured into a 7×7-matrix form to be colored in a logarithmic way, according to the percentage values. The X-axis of that matrix represents pace categories form the slowest (≥9 min/km) to the fastest (<4 min/km). The Y-axis represents age categories from the eldest (≥70) to the youngest (<20). The origin cluster of the matrix can be found on the left bottom corner, which represents all those runners who are not younger than 70 and not faster than 9 min/km in average. Besides that, percentage values of each one-dimensional categories were summarized like border values and visualized into a column or a bar charts next to the original axes. All these visual elements can be seen in *Fig. 1*.

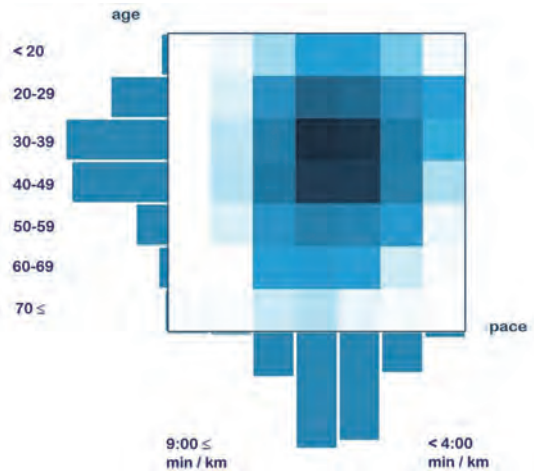

Fig. 1. Two-dimensional matrix representation of running performance according to clusters of age and pace.

2.3. Experimental design

The main concept to identify hidden effects of environmental on running performance (age and pace) was managed to design experimental analyses through which it could be possible to take control over set of attributes. Thus, three independent groups of influencing parameters were specified: *weather conditions*, *running course,* and *event date*. As can be seen, the following

experimental analysis will be able to take control over some of these parameters to reveal impact of the remaining ones on running performance.

Trend analysis

On the first experimental analysis, weather conditions and running course were fastened. To achieve those conditions, such competitions were involved which has been organized on the same place and almost at the same date year by year. This solution was the best to ensure nearly equal weather conditions and equal running environments as well.

The first national Budapest half-marathon was organized more than 30 years ago, however results have been available in public since 1996. Every event was on the first week of September, the running course although was changed sometimes, but the main characteristics of that remained. As a result, the main conditions to fasten weather and course parameters would be guaranteed. Together 22 competitions from 1996 to 2017 through 115,972 finishers' age and pace values were involved into this research. Via these analyses, it has been possible to identify how the nature of running attitude has been changed during these two decades. Besides, calculating and estimating trend functions are also realizable for describing this nature deeper as well as taking predictions for the future.

Half-marathon comparison

This experimental analysis is responsible for fastening event date value and distance of competitions. Alltogether seven Hungarian half-marathon competitions in 2017 through 19,433 finishers were analyzed within this study. All environmental values have been given by the Hungarian Meteorological Service (OMSZ) and reported in *Table 1*.

Table 1. Environment description of examined competitions

Environment characteristics	**Competitions**						
	Siófok (Nov)	**Hortobágy (Jun)**	**Szekszárd (May)**	**Keszthely (May)**	**Budapest (Sept)**	**Budapest (Apr)**	**Budapest (Jan)**
Temperature (°C)	7.0	27.2	18.5	23.2	22.5	19.3	–1.2
Humidity (%)	90	48	51	60	54	52	47
Wind force (m/s)	2.9	3.4	2.5	2.2	2.3	2.1	3.4
Average elevation (m)	10	3	177	29	14	25	11

Distance modification

In this part of the study, a long-distance running event was chosen within which independent competitions has been organized with variable distances. Alltogether 24,550 finishers of five running competitions in 2017 were involved within this study, which were going on in parallel. The available distances were 5 km, 7 km, 10 km, 21 km, and 42 km, from which only one has to be chosen by participants. Based on that, athletes of multi-distance running events always use to be separated and distributed, that nature can be analyzed and characterized through this part of the study.

Extraordinary factors

Extraordinary environmental attributes are able to influence running performance in unexpected ways. In this experimental analysis, three competitions through 2,173 finishers were involved into that part of the study: a mountain race, a marathon phase of an Ironman, and an ultra-marathon running event. Relevant attributes are reported in *Table 2*.

Table 2. Extraordinary environments

Environment characteristics	**Competitions**		
	MT*	**IM†**	**UM‡**
Distance (km)	11,6	42,195	193
Temperature (°C)	22	32	15
Humidity (%)	81	35	50
Average elevation (m/km)	57,84483	0,165896	0,906736

* Uphill running
† Marathon part of an Ironman
‡ Ultra-marathon running

3. Results and discussion

3.1. Trend description of half-marathon running

During the last two decades, nature and performance of runners have been significantly changed in Budapest national half-marathon. In *Fig. 2* differences between 1997 and 2017 can be clearly seen. More than twenty years ago, faster

and younger runners dominated that competition, but now number of middle aged, slower competitors have been indisputably increasing.

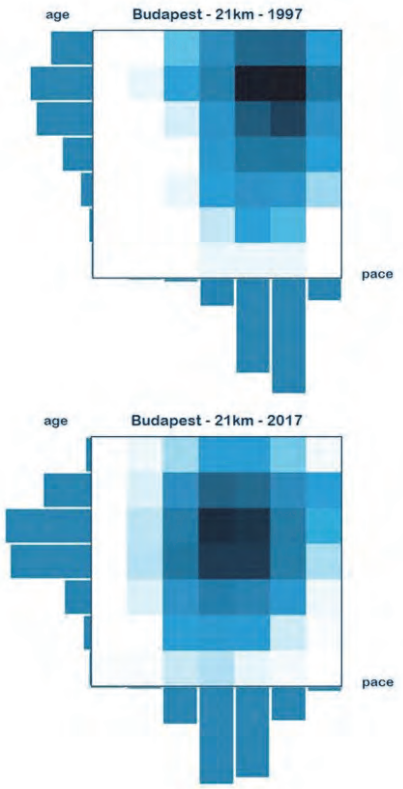

Fig. 2. Visual representation of running performance clusters in the Budapest half-marathon between 1996 and 2017.

The number of runners who have been be able to complete a half-marathon is five times higher this year than twenty years ago. In 1997 the number of finishers could not reach two thousand (1,749), until now this value has been increased around ten thousand (9,054 in 2015). Different trend line estimations have been done for predicting number of finishers in 2020, 2025, and 2030. Estimated numbers, equations, and proper R-square values are reported in table 3 and visualized in *Fig. 8*. Accordingly, the number of participants might be doubled in 2030.

Table 3. Trend line equations and finisher number prediction in 2020, 2025, and 2030

Trend method	2020	2025	2030	equation	R-square
Linear	9232.2	10699.75	12167.3	$y = 293.51x - 583{,}658$	0.9246
Logarithmic	9230.694	10686.48	12138.68	$y = 588{,}865ln(x) - 4E + 06$	0.9244
Exponential	10699.69	14479.22	19593.83	$y = 9E - 50e(0.0605x)$	0.8933
Polynomial (2)	9985.79	12062.64	14329.69	$y = 3.80x^2 - 14{,}971.07x + 14730380.27$	0.9295

Using another, re-categorized version of the results between 1996 and 2017 was able to highlight how the performance changed during this time interval. According to the left diagram in *Fig. 3*, number of elderly runners (50+) has been increasing slowly, number of middle age participants (30–49) has been increasing faster, but number of younger runners (U30) has been stagnating within the examination time interval. Due to the other diagram on the right, similar observations can be done to examine pace: number of slower runners (7:00+) has been increasing in a slowly way, middle speed runners' (5:00–6:59) number has been increasing faster, but number of fast participants (U5:00) has not been statistically changed. A strong correlation between categories of age and pace also can be detected in *Fig. 3*.

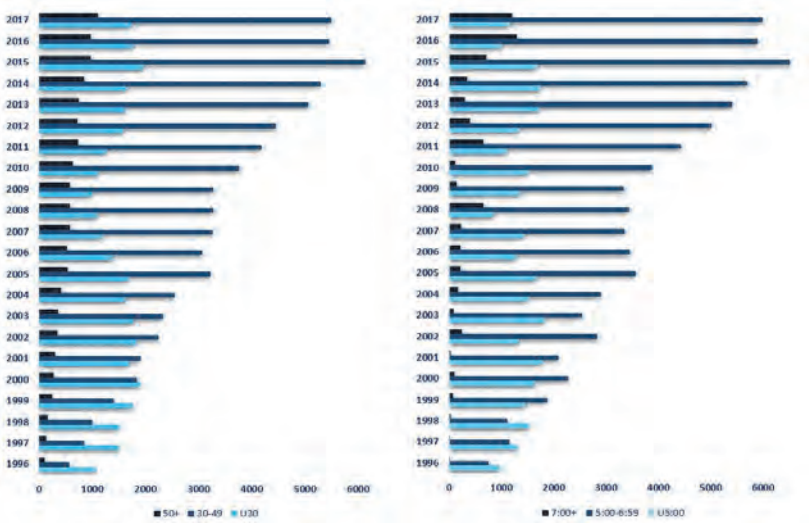

Fig. 3. Age (left) and pace (right) category distributions of individual finishers in the Budapest half-marathon between 1996 and 2017.

3.2. Effect of variable environments on performance

According to *Table 1*, effect of variable environment on age and pace can be examined. As we can see on the left diagram in *Fig. 4*, there is no relevant differences between the analyzed competitions in terms of age categories. On the other hand, distributions of pace categories are much more different due to variable temperature, humidity, and absolute elevation. According to the chart on the right in *Fig. 4*, the average pace of the runners significantly decreased in case of two competitions *Hortobágy(Jun)* and *Szekszárd(May)*. On the first event the temperature was quite high (27.2 °C), in turn, on the second event the absolute elevation (177 m) was higher than in case of any other competitions. Consequently, extremely high temperature or steep running course can impair running pace almost similarly.

As we know, optimal temperature for elite marathon runners is around 5–7 °C, naturally this value should be higher in case of recreational half-marathon competitors. An optimal environment might be included by flat course, tiny wind, and advantageous combination of temperature and humidity. According to the analyzed half-marathon events, another observations, like the best environment including not too high and not too low temperature with standard humidity is justifiable. *Siófok(Nov)* event has got 7 °C with 90% humidity, so temperature was not far from the marathon's optimal, but humidity was very high. The other faster competition was *Budapest(Apr)*, which had 19 °C with 52% humidity, so the temperature was still not too high and humidity was on a normal level in Hungary.

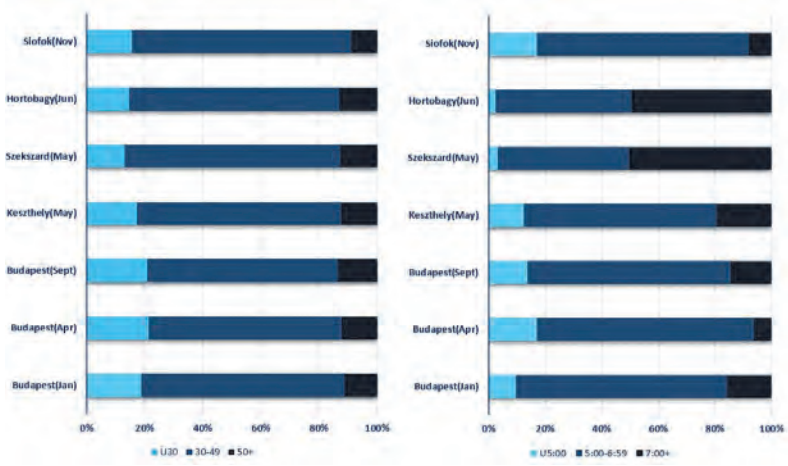

Fig. 4. Age (left) and pace (right) category distributions of individual finishers in Hungarian half-marathons in 2017.

3.3. Effect of variable distance on performance

According to *Fig. 5*, the most popular distance is the half-marathon (21 km), while the popularity of marathon (42 km) and 10 km is almost the same. Better-trained recreational athletes run on as long distance as they can, that is why the number of faster runners (U5:00) is the greatest at half-marathon. Distributions of age groups are able to highlight an expected nature of recreational runners, i.e., that number of younger athletes were higher, who completed shorter distance competitions like 5, 7, 10 km than numbers of marathon and half-marathon runners. As previously mentioned, there are different age limitations to participate a half-marathon and a marathon, this is one reason why children use to attend on shorter distances. Those assumptions can be seen on the left chart of *Fig. 5*.

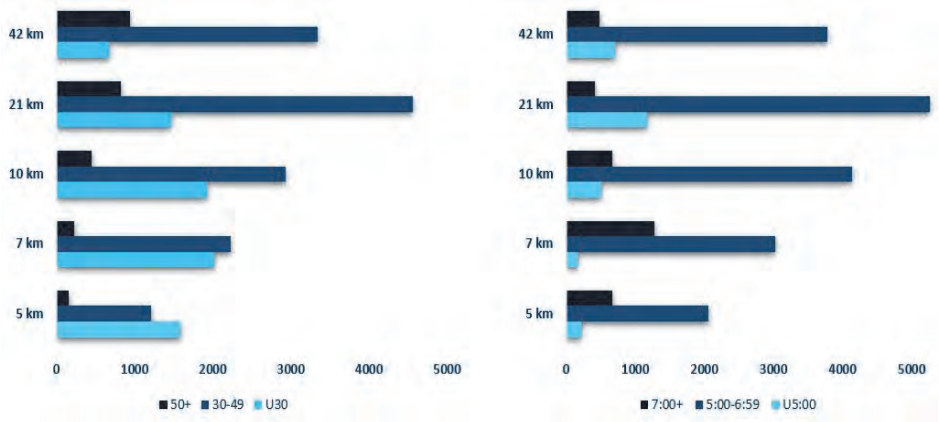

Fig. 5. Distributions of age (left) and pace (right) categories of individual finishers in variable distance competitions in 2017 in Budapest, Hungary without normalization.

In case of long-distance running when runnable distance increases, running pace decreases in a linear way, in general (*Takács et al*., 2004). Variable distance competitions always separate competitors; hence, the aforementioned statement would not be true in that special case. According to *Fig. 6*, it can be clearly seen, that running pace does not follow the hypothesis, as the fastest distance was the half-marathon and the slowest one was the 7 km competition in Budapest, in 2017. Therefore, significant differences between these competitions cannot be identified in terms of pace.

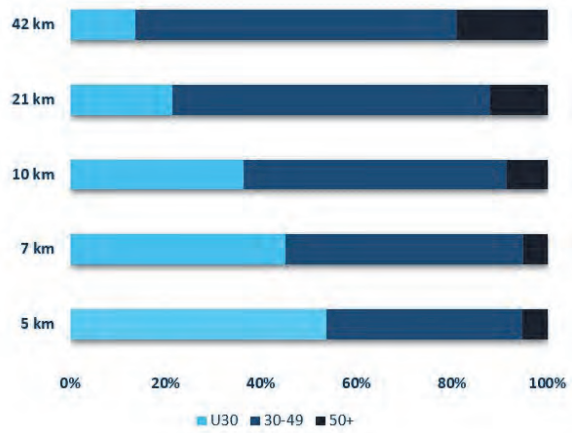

Fig. 6. Normalized version of pace category distributions of individual finishers on variable distances in 2017.

3.4. Effect of extraordinary conditions on performance

Effects of extraordinary environment conditions on running performance can hardly to identify without any investigations. In *Fig. 7*, visual matrix representation of three extraordinary and one standard long-distance competition can be seen. In the left top chart, a fundamental marathon was represented, which disposes standard environment. In the right top matrix, evaluated results of a marathon part of an ironman distance triathlon competition can be seen. There were not any participants under 20 who could be faster than 4:00 min/km in that event. In addition, significant differences can be found between pace distributions, but seemingly, that is not as many as it would be expected. Nevertheless, Ironman is not a recreational sport event; just well-trained athletes can manage to complete it, that might explain the previous observation.

A 11 km long mountain running without any downhill phase represented on the left bottom. Age group distributions are almost similar to those of standard marathons, but relevant differences can be found in terms of pace. Although runnable distance of the mountain event is around four times shorter than on a marathon, values of slower pace clusters are still higher. As a result, extraordinary elevation can impair recreational runners' pace in a similar way as tiredness of ironman triathletes after the cycling phase.

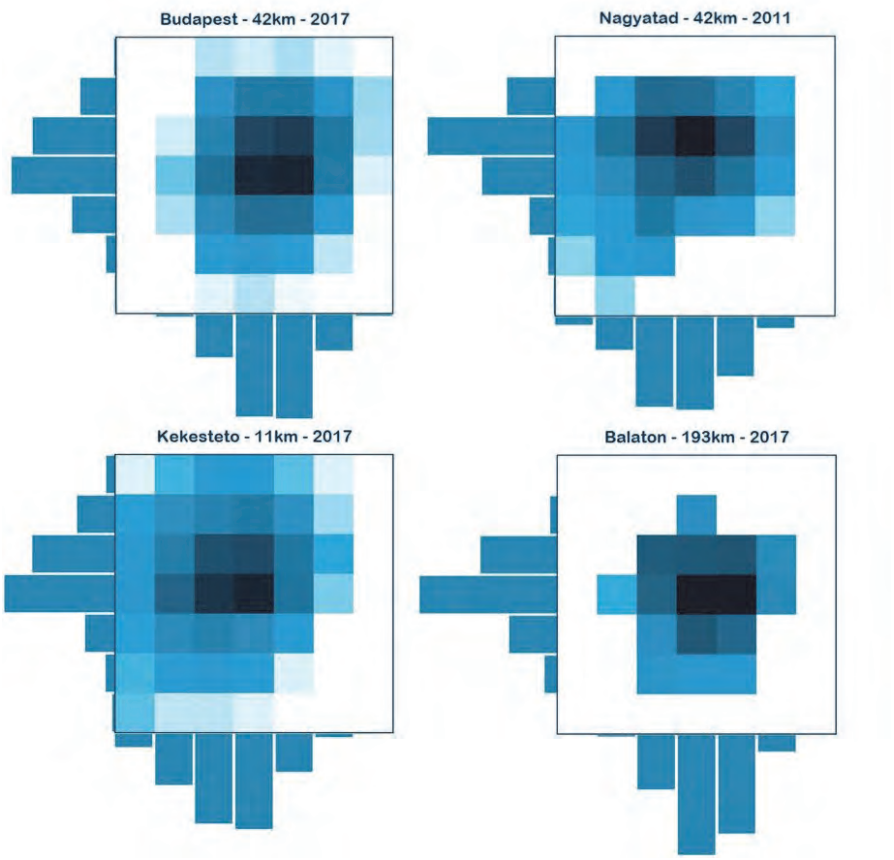

Fig. 7. Visual matrix representation of running performance attributes in extraordinary competitions.

The last chart on the right bottom of *Fig. 7* represents an ultra-distance running competition. That running event is a four-day race, where around 50 km can be done by the participants on every day. Although the final distance is extremely high (193 km), runners have resting and sleeping time between the daily stages. Without extremely endurance and mental stability, there is no chance to manage to complete this competition, that fact can be highlighted in *Fig. 7*. There were not any participants from the fastest and slowest pace cluster, that firstly means distance is too long to complete it with high speed, secondly high training level is essential, that's why extremely slow pace was also not so typical. Besides, clusters of under 30 and above 70 age groups are almost empty, that refers to an expected nature of ultra-distance running regarding keeping health condition.

4. Conclusions

Starting point of this study was to investigate the influence of endurance running performance (age and pace of runners) by taking meteorological and environmental attributes, running distance and course elevation into account. This study was focusing on how those parameters could influence recreational athletes' distribution by age and running pace.

According to the fist analysis, age parameter strongly correlated with running pace, so there is a statistically optimal age for every runner when recreational endurance sport activities can be done in the most efficient way (*Osváth*, 2010). Naturally, age is a fixed, unmodified, so-called independent attribute that cannot be influenced by other parameters, like pace (*Ketskeméty et al.*, 2011). This research was also focusing on those results, through which environmental and other influencing parameters might be identified.

According to the Budapest half-marathon trend analysis, numbers of recreational runners has been continuously increased. Nowadays, the number of participants (*Fig. 8*) almost reached the attendance limit (10,000) which many Hungarian competitions have. Thus, organizers will have to consider how this situation can be handled to find a balance between willingness of athletes and organizing long-distance running events in a proper, securely way.

Fig. 8. Numbers of individual finishers in Budapest half-marathons from 1996–2017.

In Hungary, half-marathon competitions are the most famous running events for recreational athletes. The age groups distributed into the same way, regardless of locations and event dates. In this case, only pace attribute is carrying relevant information about running performance.

Those competitions, which have extraordinary environmental components like extremely long distance or steep running course, are managed to complete by trained athletes having well physical condition, rather than recreational participants. For that reason, such sport events are hardly to complete for young (under 20) and elderly (above 60) persons, that is why range of age categories could be shrunk.

A main result of the study is that the distance and elevation attributes of running environment impair running speed mostly, otherwise outside temperature and humidity have less effect on recreational long-distance running pace. The direct effect of distance can be seen in *Fig. 7*, greater pace than 4 min/km could not be reached, but in all other analyzed distances it could be possible. Uniform elevation without uphill and downhill pats can be run easier than mountain competitions. That can be perfectly highlighted by *Figs. 4* and *7*. At a half-marathon at Szekszárd, distribution of pace categories has been shifted: the number of faster runners (pace below than 5 min/km) was one third, while the number of slow runners (pace greater than 7 min/km) was three times greater than at a flat competition in Keszthely with similar air temperature and humidity.

4.1. Future direction

As can be seen, wide range analyses can be done by using two-dimensional visual matrix representation without any deeper primary data for investigating the influencing parameters. Comparing multi-distance competitions is possible through this model, but different sport events like running, swimming, kayaking, and cycling can be also compared. This tool would be support different types of statistical analyses in variable scientific areas like information technology, sport science, telecommunications, education, and society. In general, age and time is a very important attribute in many human and technological procedures as well, which could be analyzed by some kind of modified version of this Running Competition Comparison Tool model.

Another possible research direction is taking further investigation in terms of effects on meteorological conditions and physiological attributes of endurance running athletes by analyzing primary data collected in an environment chamber in 2017 at the Auckland University of Technology, New Zealand.

Acknowledgements: The authors would like to express their gratitude towards *Dr. László Bozó* for his valuable input on the mechanics of front type transitions. The authors also owe gratitude to *Dr. Kálmán Kovács* and the Data Supply Department of the Hungarian Meteorological Service for sharing the extensive local and medical meteorological and accident databases for the purpose of completion of the authors' research. The research reported in this paper was supported by the BME- Artificial Intelligence FIKP grant of EMMI (BME FIKP-MI/SC), and by the EFOP 3.6.1. -16-2016-00014 program of the Ministry of Human Capacities (Disruptive Technologies).

References

Berke, D., 2015: A given optimization task modelling of fixed route moving units with smart and GIS tools. MSc Thesis in Computer science and engineering, Budapest University of Technology and Economics, Hungary.

Berke, D. 2017. Automatic monitoring system and services for long-distance running competitions. *J. Appl. Multimedia XI.(4)*, 66–71.

Dion, T., Savoie, F.A., Asselin, A., Gariepy, C., and *Goulet, E.D*., 2013: Half-marathon running performance is not improved by a rate of fluid intake above that dictated by thirst sensation in trained distance runners. *Eur. J. Appl. Physiol. 113,* 3011–3020. https://doi.org/10.1007/s00421-013-2730-8

El-Helou, N., Tafflet, M., Berthelot, G., Tolaini, J., Marc, A., Guillaume, M., and *Toussaint, J.-F*.. 2012: Impact of Environmental Parameters on Marathon Running Performance. PloS One, Online. https://doi.org/10.1371/journal.pone.0037407

Hungarian Athletics Association, 2016: Official Sport Rules and Race Regulations in Athletics, http://www.bpatletika.hu/download/szab%C3%A1lyzatok/1_Versenyrend_Utmutato_2016.pdf

International Association of Athletics Federations, 2016: IAAF, Competition Rules 2016-2017, https://www.iaaf.org/about-iaaf/documents/rules-regulations#rules

Ketskeméty, L., Izsó L., and *Könyves, T.E*., 2011: Bevezetés az IBM SPSS. Statistics programrendszerbe. Alinea, Budapest, ISBN 978-963-08-1100-2. (In Hungarian)

Osváth, P., 2010: Sportélettan, sportegészségtan. Budapest, ISBN 978-963-06-8484-2. (In Hungarian)

Takács, L., Kertész, T., Molnár, S., Orosz, F., Vágó, B., Eckschmiedt, S., Szécsényi, J., Schulek, Á., Zarándi, L., Szalma, L., Gyimes, Zs., Kovács, E., and *Radák, Zs.,* 2004: Athletics technique, education, training, Semmelweis University, Department of Sport Science, Budapest, Hungary

Vécsei, P. and *Kovács , K.,* 2014: Statistical analysis of relationships between road accidents involving personal injury and meteorological variables in Hungary. *Időjárás 118*, 349–378.

Wall, B.A., Watson, G., Peiffer, J.J., Abbiss, C.R., Siegel, R., and *Laursen, P.B*., 2015: Current hydration guidelines are erroneous: dehydration does not impair exercise performance in the heat. *British J. Sports Medic. 49*, 1077–1085. https://doi.org/10.1136/bjsports-2013-092417

Winger, J.M., Dugas, J.P., and *Dugas, L.R*., 2010: Beliefs about hydration and physiology drive drinking behaviours in runners. *British J. Sports Medic. 45*, 646–649. https://doi.org/10.1136/bjsm.2010.075275

Zouhal, H., Groussard, C., Minter, G., Vincent, S., Cretual, A., Gratas-Delamarche, A., Noakes, T.D., 2010: Inverse relationship between percentage body weight change and finishing time in 643 forty-two-kilometre marathon runners. *British J. Sports Medic. 45*, 1101–1105. https://doi.org/10.1136/bjsm.2010.074641

DOI:10.28974/idojaras.2019.3.5

IDŐJÁRÁS

Quarterly Journal of the Hungarian Meteorological Service
Vol. 123, No. 3, July – September, 2019, pp. 329–349

Approximation of wind speed distributions with theoretical distributions of meteorological stations located in different orographic conditions

István Hadnagy[*,1,2] and **Károly Tar** [1,3]

[1]*Department of Meteorology, University of Debrecen,*
Egyetem Square 1, H-4010 Debrecen, Hungary

[2]*Department of Biology and Chemistry*
Ferenc Rákóczi II. Transcarpathian Hungarian Institute
Kossuth Square 6, UA-90202 Berehove, Ukraine

[3]*Institute of Tourism and Geography, College of Nyíregyháza,*
Sóstói Road 31/B, H-4400 Nyíregyháza, Hungary

**Corresponding author E-mail: hadistvan@gmail.com*

(Manuscript received in final form June 13, 2018)

Abstract— This research analyses the daily average wind speed time series of ten Transcarpathian meteorological stations in the period from 2011 to 2015 with the help of statistical methods. We approximated the empirical frequency distribution of measured daily average wind speeds by means of theoretical distributions. The results of the fitting test showed that among the applied theoretical distributions, irrespective of orographic conditions, the Weibull distribution is proved to be the most suitable. However, fitting the Weibull distribution depends on the methods of determining parameters *k* and *c*. By means of the best fitting parameters, the distribution density function and some of its indices at the altitude of 80 m were worked out contrary to the anemometer altitude that is often the hub height of industrial wind turbines, thus estimating the wind conditions of the area from wind energy utilization point of view.

Key-words: wind speed, wind speed distribution, distribution analysis, Weibull distribution, Transcarpathia

1. Introduction

In the process of characterization of wind power resources, the average annual wind speed is often given regarding a particular area. Figures showing wind conditions mostly display averages of long-term. However, a single data is not enough for characterization of wind power resources as far as power output is proportional to the third power of wind speed (*Patay*, 2003). This kind of negligence, or rather averaging, can cause significant deviation in the process of estimating annual energy potentials. Considering energy utilization point of view, it is much more essential to know the frequency of those wind speeds that are suitable for energy production. This can be demonstrated by processing statistical data and the figure showing the frequency of wind speed. By approximation of the empirical frequency distribution of wind observations, we can obtain numerous statistical and energy indices. The statistical distribution functions potentially suitable for this purpose include: Weibull distribution, Rayleigh-distribution, normal distribution, log-normal distribution, square-root normal distribution, and gamma distribution. In wind climatology, the above-mentioned distributions are most frequently applied (*Bonfils*, 2011; *Tar*, 2008; *Kravchyshyn et al.*, 2016). Among these, the advantage of applying double-parameter Weibull distribution lies in the fact that the distribution parameters are determined at anemometer altitude, and as a result, the values of this measurement level can be used to calculate the values of other altitudes, i.e., wind speed distribution can be described for other altitudes as well. This is used in determining wind potential. Therefore, theoretical distribution fitting plays central role in the wind energy studies. This method has been widely applied in such analyses (*Dévényi* and *Gulyás*, 1988; *Bartholy* and *Radics*, 2000; *Patay*, 2003; *Radics*, 2004; *Hunyár et al.*, 2004; *Liubimov et al.*, 2011; *Morgan et al.*, 2011; *Hou et al*., 2012; *Sobchenko* and *Khomenko*, 2015; *Kravchyshyn et al.*, 2016). Weibull distribution has two parameters (k and c) due to asymmetrical distribution, where k stands for shape parameter (a dimensionless number) and c stands for scale parameter (m/s), these can be calculated based on the available database. Parameters k and c valid at anemometer altitude can be determined in several ways (*Justus et al.*, 1978; *Tar*, 2008; *Costa Rocha et al.*, 2012; *Kidmo et al.*, 2015; *Kravchyshyn et al.*, 2016). Weibull distribution is related to several other probability distributions. Depending on k values, the distribution density function significantly changes, while c takes values typical for local wind conditions. When $k=1$ exponential distribution is obtained, while if $k=2$, Rayleigh-distribution is resulted, while when the value is close to $k=3.5$, the distribution is almost symmetric, thus being very close to normal distribution (*Troen* and *Petersen*, 1989). At 13 measurement points in Hungary, the average value of k is 1.44 (*Bartholy* and *Radics*, 2000). In Ukraine, *Sobchenko* and *Khomenko* (2015) analyzed the wind data of Lviv, Kyiv, Odesa, Kryvyi Rih, Simferopol, Dnipro, Donetsk in 2001–2008 and came to the conclusion that parameter k of the Weibull distribution has the following values: 1.36 in Lviv and 1.7 in Odesa, while parameter c changes from 2.74 in Lviv to 4.81 in Simferopol.

The aim of our research is to determine the parameters of statistical distribution functions on the basis of a daily average wind speed data series, to approximate and describe the empirical wind speed distributions of measuring stations in various orographic conditions. This is the most important in wind climatology. Knowing the characteristics of theoretical distribution, we can conclude the structure of empirical distribution and estimate wind potential at a particular measurement point.

2. Data and methods

The data series used come from 10 Transcarpathian (Ukraine) operating meteorological stations. The geographical locations of the stations are shown in *Fig. 1* and *Table 1* showing these stations' exact geographical coordinates, their altitude above sea level, as well as the altitude of the wind-gauge above ground level. The period under analysis lasted from January 1, 2011 to December 31, 2015. In our research, we used the daily average wind speed of the meteorological observatories. The data series were given us by the Transcarpathian Hydrometeorological Center (THMC). During the examined period there were no changes in the stations' geographical position and in the anemometer's altitude above ground level, thus wind measurement conditions did not change.

The observation stations in *Fig. 1* are situated in various orographic environment. The relative difference in altitude between the stations situated at the lowest (Uzhhorod, 112 m) and highest (Pozhyzhevs′ka, 1451 m) altitudes is 1339 m.

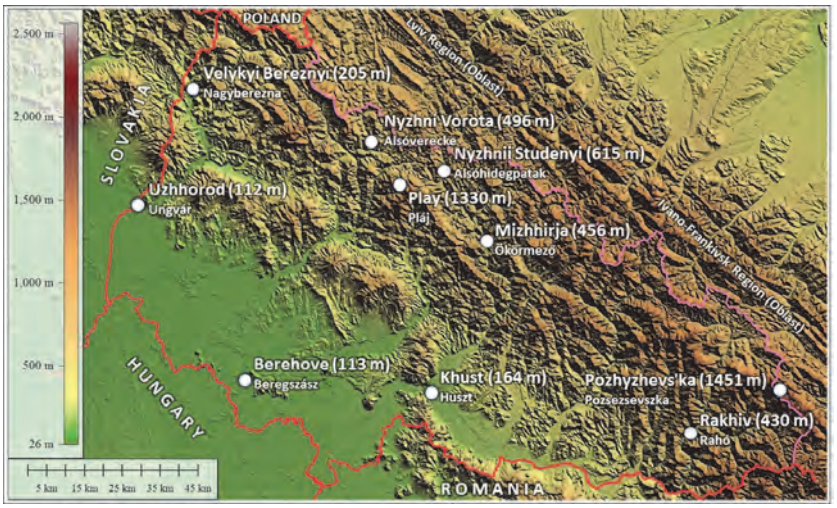

Fig. 1. Geographical locations and altitudes above sea level (m) of the meteorological stations comprising the database.

Table 1. Exact geographical coordinates of the meteorological stations and anemometer altitudes (φ: latitude, λ: longitude, h: elevation, h_a: anemometer altitude above ground level)

Meteorological station		**Geographical coordinates**		**h (m)**	**h_a (m)**
WMO index	Station name	φ (north)	λ (east)	Jan 2011. – Dec 2015.	
33631	Uzhhorod	48°38'	22°16'	112	14
33634	Berehove	48°12'	22°39'	113	10
33638	Khust	48°11'	23°18'	164	16
33514	Velykyi Bereznyi	48°54'	22°28'	205	10
33647	Rakhiv	48°03'	24°12'	430	10
33633	Mizhhirja	48°31'	23°30'	456	10
33517	Nyzhni Vorota	48°46'	23°06'	496	10
33518	Nyzhnii Studenyi	48°42'	23°22'	615	10
33515	Play	48°40'	23°12'	1330	8
33646	Pozhyzhevs′ka	48°09'	24°32'	1451	11

As a first step, a histogram was made from the wind speed data series, similarly to previous studies classifying wind speeds using $\Delta x = 1\ m/s$ (*Khan et al.*, 2014; *Costa Rocha et al.*, 2012; *Xydis*, 2012; *Kravchyshyn et al.*, 2016). Following this, several theoretical distributions were tested in order to approximate the empirical frequency distribution of wind data. The distribution densities and parameters of their determination are as follows:

- *Weibull distribution*. The distribution density of the Weilbull distribution can be presented simplest in the following form (*Justus et al.*, 1978; *Tar*, 2008; *Kartashov*, 2008):

$$f(x;k;c) = \frac{k}{c}\left(\frac{x}{c}\right)^{k-1} e^{-\left(\frac{x}{c}\right)^{k}}. \qquad (1)$$

The following three methods were applied to determine the k and c parameters of the distribution:

The first method is in fact a linear regression made on the transformed values of the center of speed intervals (v_i) and the corresponding cumulated frequency (p_i). Transformations are as follows (*Şahini* and *Aksakal*, 1999; *Tar*, 2008):

$$x_i = \ln(v_i) \qquad \text{and} \qquad y_i = ln[-\ln(1-p_i)]\,. \qquad (2)$$

From $y = a + bx$ the regression equation constants c and k can be determined in the following way:

$$c = \exp\left(-\frac{\mathrm{a}}{\mathrm{b}}\right) \qquad \text{and} \qquad \mathrm{k} = \mathrm{b}. \tag{3}$$

The second method is based on the lower and upper quartiles (*q1* and *q3*), as well as median (*q2*) of wind speed. Thus, the *k* and *c* parameters can be determined in the following way (*Tar*, 2008):

$$k = ln\frac{\left(\frac{\ln 0{,}25}{\ln 0{,}75}\right)}{\ln\left(\frac{q_3}{q_1}\right)} = \frac{1{,}573}{\ln\left(\frac{q_3}{q_1}\right)}, \tag{4}$$

$$c = \frac{q_2}{(\ln 2)^{\frac{1}{k}}}. \tag{5}$$

The third method can be traced back to the estimation of momentum (*Tar*, 2008; *Costa Rocha et al.*, 2012; *Maklad* and *Glencross-Grant*, 2014; *Kravchyshyn et al.*, 2016). If the average wind speed (v_m) and the standard deviation (s_n) are known, then

$$k = \left(\frac{s_n}{v_m}\right)^{-1{,}086}, \tag{6}$$

$$c = \frac{v_m}{\Gamma\left(1+\frac{1}{k}\right)}. \tag{7}$$

where s_n/v_m is the coefficient of variation, while $\Gamma(x)$ is the gamma function.

By means of the three different methods mentioned above the Weibull parameters can be determined at the anemometer altitude. However, if we proceed from this and want to give distributions at different altitudes, then we have to use the above-mentioned characteristics of Weibull distribution, i.e., the distribution parameters for other altitudes can be calculated on the basis of the values related to the measurement level. If the value of parameters at the altitude of anemometer z_a are c_a and k_a, then at a $z \neq z_a$ level (*Tar*, 2008; *Kidmo et al.*, 2015):

$$c_z = c_a\left(\frac{z}{z_a}\right)^n \text{ and} \tag{8}$$

$$k_z = \frac{k_a\left[1-0{,}088\ ln\left(\frac{z_a}{10}\right)\right]}{\left[1-0{,}088\ ln\left(\frac{z}{10}\right)\right]}. \tag{9}$$

Exponent *n* is:

$$n = \frac{[0{,}37 - 0{,}088 \ln c_a]}{\left[1 - 0{,}088\, ln\left(\frac{z_a}{10}\right)\right]}. \quad (10)$$

By working out daily average wind speed distribution at a level different from the anemometer altitude, knowing the scale- and shape parameter at this altitude, average wind speed, standard deviation, mode, and coefficient of variation can be calculated.

The average v_m sample taken from the probability variable of the Weibull distribution can be determined in the following way (*Troen* and *Petersen*, 1989):

$$v_m = c\Gamma\left(1 + \frac{1}{k}\right), \quad (11)$$

where c and k are parameters of the distribution at a given altitude.

Its standard deviation is the following (*Azad et al.*, 2014):

$$\sigma = c\left[\Gamma\left(1 + \frac{1}{k}\right) - \Gamma^2\left(1 + \frac{1}{k}\right)\right]^{\frac{1}{2}}, \quad (12)$$

and its distribution mode is characterized by Eq. (13) (*Dokur* and *Kurban*, 2015):

$$M_0 = c\left(1 - \frac{1}{k}\right)^{\frac{1}{k}}. \quad (13)$$

- *Rayleigh distribution*. If $k=2$, then a special case of the Weibull distribution, the distribution density of the Rayleigh distribution is obtained (*Tar*, 2008; *Kartashov*, 2008; *Schönwiese*, 2013). The distribution density of Rayleigh distribution can be described in the following way:

$$f(x; c) = \frac{2x}{c^2} e^{-\left(\frac{x}{c}\right)^2}. \quad (14)$$

The expected value of the probability variable of such a distribution is:

$$\mu = \frac{c\sqrt{\pi}}{2}, \quad (15)$$

i.e., the estimated value of the c parameter is proportional to the average.

- *Normal distribution.* The distribution function of the normal distribution is:

$$f(x; \mu; c) = \frac{1}{\sigma\sqrt{2\pi}} e^{-\frac{(x-\mu)^2}{2\sigma^2}}. \quad (16)$$

Its parameters are the μ expected value and the σ standard deviation of the ξ probability variable.

- *Log-normal distribution.* The distribution density of the log-normal distribution is:

$$f(x;\mu;\sigma) = \frac{1}{\sigma x\sqrt{2\pi}} e^{-\frac{(\ln x-\mu)^2}{2\sigma^2}} \tag{17}$$

Its parameters are the μ expected value and the σ standard deviation of the $\ln\xi$ probability variable *(ξ >0)*.

- *Gamma distribution.* The distribution density of the gamma distribution is:

$$f(x;\lambda;p) = \frac{\lambda^p}{\Gamma(p)} x^{p-1} e^{-\lambda x}, \text{ if } x>0$$
$$f(x;\lambda;p) = 0, \qquad \text{if } x\leq 0\,, \tag{18}$$

where Γ(*p*) is a gamma-function. The μ expected value and the σ^2 squared standard deviation of a probability variable with such a distribution are:

$$\mu = \frac{p}{\lambda} \text{ and} \tag{19}$$

$$\sigma^2 = \frac{p}{\lambda^2}\,, \tag{20}$$

where parameters *p* and *λ* are easy to estimate (*Dévényi* and *Gulyás*, 1988, *Matyasovszky*, 2002; *Tar*, 2008; *Kravchyshyn et al.*, 2016).

We performed the χ^2 goodness of fit test at significance levels of 10%, 5%, and 1%. The results are summarized in *Table 2,* in which the cases where the approximation proved to be good at least at one of the above significance levels are marked. Finally, having determined the linear correlation coefficient (*r*), significant statistical relations between the altitude above sea level of the measurement point and the scale parameter of the Weibull distribution were looked for. To test our H_0*:* $\rho=0$ hypothesis with the aim of studying the significance of the connection between the two variables, the F-test used in variance analyses was applied (ANOVA). The total sum of squares (*TSS*) has two components: the regression sum of squares (*RSS*) and the error sum of squares (ESS). By means of the sum of squares determined from the samples the existence of the null hypothesis was analyzed (*Huzsvai* and *Vincze*, 2012):

$$F = \frac{\frac{RSS}{\rho}}{\frac{ESS}{n-\rho-1}}, \tag{21}$$

where the numerator's degree of freedom is $szf_1 = m$, and the denominator's degree of freedom is $szf_2 = n\text{-}\rho\text{-}1$.

3. Results

3.1. Frequency distribution of wind speeds at the studied stations

To show the assumed orographic differences, concrete distribution analyses were performed regarding the altitude of the measurement level in the case of each particular station. Histograms of wind speed, Δx=1 m/s, subdivided into classes and formed on the basis of data series referring to the entire period (*Fig. 2*) yield a different picture at various stations according to local wind peculiarities. At the stations situated on plains or in mountainous narrow river valleys, maximum 5 (Nyzhnii Studenyi), 8 (Velykyi Bereznyi, Mizhhirja, Nyzhni Vorota), or 9 (Uzhhorod, Rakhiv) wind speed classes can be singled out. The frequency distribution of stations on high mountain ridges or near the mountain peak can be described by means of more wind speed classes, in Pozhyzhevs′ka by 17, while in Play by approximately 20 classes. Due to slow wind speed, 94.3% of the data in Berehove belong to the 0–1 m/s class. In Khust this class includes 73.7% of the data. For this reason, approximation of the daily average wind speed at these two stations did not yield positive results (*Table 2*).

Table 2. Summarizing table of the empirical and theoretical distributions for the entire period, divided into seasons at various probability levels (marked with an * in the case of a significant fitting)

Distribution-type	Time period	Weibull 1st method			Weibull 2nd method			Weibull 3rd method			Normal			Log-normal			Gamma		
Significance level (%)		10	5	1	10	5	1	10	5	1	10	5	1	10	5	1	10	5	1
Uzhhorod (112 m)	entire				*	*	*	*	*	*									
	winter				*	*	*	*	*	*									
	spring							*	*	*									
	summer							*	*	*									
	autumn				*	*	*	*	*	*									
Berehove (113 m)	entire																		
	winter																		
	spring																		
	summer																		
	autumn																		

Table 2. Continue

Distribution-type	Time period	Weibull 1st method			Weibull 2nd method			Weibull 3rd method			Normal			Log-normal			Gamma		
Significance level (%)		10	5	1	10	5	1	10	5	1	10	5	1	10	5	1	10	5	1
Khust (164 m)	entire																		
	winter																		
	spring																		
	summer																		
	autumn																		
Velykyi Bereznyi (205 m)	entire				*	*	*	*	*	*									
	winter				*	*	*	*	*	*							*	*	*
	spring							*	*	*									
	summer							*	*	*									
	autumn				*	*	*	*	*	*							*	*	*
Rakhiv (430 m)	entire							*	*	*							*	*	*
	winter				*	*	*	*	*	*									
	spring							*	*	*									
	summer							*	*	*									
	autumn						*	*	*	*									
Mizhhirja (456 m)	entire				*	*	*	*	*	*									
	winter							*	*	*									
	spring							*	*	*									
	summer				*	*	*	*	*	*									
	autumn							*	*	*									
Nyzhni Vorota (496 m)	entire					*	*	*	*	*									
	winter	*	*	*	*	*	*	*	*	*									
	spring							*	*	*									
	summer				*	*	*	*	*	*									
	autumn				*	*	*	*	*	*									
Nyzhnii Studenyi (615 m)	entire							*	*	*									
	winter				*	*	*	*	*	*	*	*	*						
	spring																		
	summer																		
	autumn				*	*	*	*	*	*									
Play (1330 m)	entire				*	*	*	*	*	*									
	winter				*	*	*	*	*	*									
	spring				*	*	*	*	*	*									
	summer				*	*	*	*	*	*									
	autumn				*	*	*	*	*	*	*	*	*						
Pozhyzhevs′ka (1451 m)	entire				*	*	*	*	*	*							*	*	*
	winter				*	*	*	*	*	*							*	*	*
	spring	*	*	*	*	*	*	*	*	*							*	*	*
	summer				*	*	*	*	*	*									
	autumn	*	*	*	*	*	*	*	*	*							*	*	*

3.2. Analysis of the shape- and scale parameter of Weibull distribution

Table 2 shows that in most cases, the Weibull distribution offers the best approximation among the empirical frequency distribution of daily average wind speed time series. The two input parameters of the Weibull distribution, as it has already been mentioned above, can be determined by numerous methods, see Eqs. (2)–(7). The three selected methods resulted different parameter values. Therefore, the fittings were not the same. Among the three-parameter determining methods, the third method was proved to be the best at Transcarpathian stations, therefore we analyze its results.

In the entire period, the value of the *k* parameter (*Table 3*) varied from station to station: 0.64 in Berehove and 2.71 in Khust. However, the data series of these two stations could not be approximated by Weibull distribution. In the case of the rest of the stations, the *k* value varied from 1.0 in Rakhiv to 2.19 in Nyzhnii Studenyi. With reference to the whole observation plot, the oscillation makes up 2.07. When divided into seasons, the *k* value seems to be different at different stations. Highest values are found in spring (Berehove, Mizhhirja) and in summer (Uzhhorod, Khust, Velykyi Bereznyi, Rakhiv, Nyzhni Vorota, Nyzhnii Studenyi, Play, and Pozhyzhevs′ka). When compared, the highest seasonal values also show significant deviation; the difference between 3.95 in Khust and 0.70 in Berehove is 3.25.

Table 3. Values of *(k)* the shape parameter (a dimensionless number) subdivided into the whole studied period and into seasons (*italics* – a value showing no significant fitting, but offering the best approximation; bold – the highest value)

Period	**Uzhhorod (112 m)**	**Berehove (113 m)**	**Khust (164 m)**	**Velykyi Bereznyi (205 m)**	**Rakhiv (430 m)**	**Mizhhirja (456 m)**	**Nyzhni Vorota (496 m)**	**Nyzhnii Studenyi (615 m)**	**Play (1330 m)**	**Pozhyzhevs′ka (1451 m)**
entire	1.82	*0.64*	***2.71***	1.32	1.0	1.48	1.59	2.19	1.65	1.15
winter	1.68	*0.65*	*2.24*	1.21	0.79	1.43	1.56	2.07	1.65	1.18
spring	2.12	***0.70***	*2.79*	1.50	1.36	**1.84**	1.82	2.64	1.76	1.23
summer	**2.20**	*0.64*	***3.95***	**1.78**	**1.38**	1.79	**2.04**	**2.66**	**1.81**	**1.44**
autumn	1.61	*0.23*	*2.74*	1.13	0.87	1.31	1.46	2.04	1.58	1.17

Where the average wind speed is the highest and the shape parameter of Weibull distribution is the lowest, the specific wind power is the greatest (*Henessey*, 1977). In Transcarpathia, the *k* values are relatively low, they are not combined with significant average wind speed (*Table 5*), thus the specific wind power is surely not high except for the Play station. High *k* values can mean low variability of the wind power.

With reference to the whole period, the value of the *c* parameter (*Table 4*) shows greater variability at different stations. For a five-year-long period the value was 5 m/s. The highest value was found at Play station (5.23), while the lowest one was detected at Berehove station (0.23). The occurrence of the two extremes was expected for the scale parameter values closely followed the average wind speed values of the stations (Table 5). Side by side with the spread, the standard deviation values support the differences arising from the wind at two measurement points, since at Berehove station the standard deviation value is 0.38 m/s, while at Play station it is 0.66. At Pozhyzhevs′ka station the standard deviation is 0.82 m/s, however, it is not here that the *c* value is the highest as the average wind speed is not the highest here, only the standard deviation of data is significant. This indicates that wind differs in various parts of the observation plot.

Table 4. Values of the scale parameter *c* (m/s) subdivided into the whole studied period and into seasons (italics – a value showing no significant fitting, but offering the best approximation; bold – the highest value)

Period	Uzhhorod (112 m)	Berehove (113 m)	Khust (164 m)	Velykyi Bereznyi (205 m)	Rakhiv (430 m)	Mizhhirja (456 m)	Nyzhni Vorota (496 m)	Nyzhnii Studenyi (615 m)	Play (1330 m)	Pozhyzhevs′ka (1451 m)
entire	2.30	*0.23*	*1.03*	1.42	1.44	1.30	2.02	1.66	**5.23**	3.59
winter	2.25	*0.24*	*0.94*	1.30	1.22	1.47	**2.40**	**1.93**	**5.91**	**4.73**
spring	**2.82**	***0.35***	***1.18***	**1.92**	**2.15**	**1.66**	2.32	1.76	5.54	3.47
summer	2.21	*0.18*	*1.03*	1.43	1.31	0.86	1.71	1.44	4.36	2.74
autumn	1.92	*0.00*	*0.95*	1.02	1.12	1.03	1.69	1.50	5.16	3.65

The maximum value of the *c* parameter at stations in Uzhhorod, Berehove, Khust, Velykyi Bereznyi, Rakhiv, and Mizhhirja occurs in spring, while at Nyzhni Vorota, Nyzhnii Studenyi, Play, and Pozhyzhevs′ka stations it occurs in winter. This can be explained by that the primary wind maximum at the stations is generally observed at this time of the year.

3.3. Frequency distribution of the daily average wind speed at 80 m above ground level

By means of the Weibull distribution parameters, the distribution density function, some of its statistical parameters, the average value of the probability variable, its standard deviation, mode, and coefficient of variation were worked out at an altitude z=80 m differing from the anemometer altitude (z_a). There is a significant fitting between the stations in *Tables 3* and *4*, in Berehove and Khust. Significant fitting was not used, but the parameters determined using the third Weibull method that showed the best approximation was applied. First of all, by means of Eqs. (8), (9), and (10) the n exponent, then the c_z and k_z parameters were determined. The obtained distribution at z=80 m is presented in *Fig. 2*.

By comparing the statistical parameters of wind conditions at two levels, the average values of wind speed at 10 measurement stations in the period between 2011 and 2015 at anemometer altitude vary between 0.32 m/s in Berehove and 4.68 in Play. Average wind speed at stations does not exceed 3 m/s except for Play and Pozhyzhevs′ka (3.41 m/s), as they have higher altitude above sea level. The same spatial distribution can be observed, however, with higher values regarding the 80 m level at the stations, i.e., Berehove has the lowest (0.74 m/s), while the station at Play has the highest (7.32 m/s) average value. Among the stations not situated in highlands or on mountain ridges, Uzhhorod and Nyzhni Vorota could be highlighted where average wind speed at 80 m reaches 3.85 m/s and 3.40 m/s, respectively. Regarding the most frequent value in the data series, i.e., the mode, again the station at Play had the maximum value (2.13 m/s). Conversely, in Pozhyzhevs′ka, which is also situated in a highland, the mode value is 0.50 m/s compared to the relatively high average (3.41 m/s). This is likely to be caused by the fact that side by side with predominantly low wind speeds and longer windless periods at the station, there are wind storms with wind speeds exceeding 15 m/s (*Lavnyi* and *Lässig*, 2009) as well. The mode of wind speed values in Pozhyzhevs′ka at 80 m is only 2.51 m/s. Higher values at 80 m can be detected at the stations in Nyzhnii Studenyi (2.74 m/s), Uzhhorod (3.26 m/s), and Play (5.98 m/s). Having analyzed the coefficient of variation as the index-number of dispersion, it can be stated that the most changeable station with reference to wind at both levels is Berehove (1.50 and 1.30), while the least changeable is Khust (0.40 and 0.34). However, these two stations have the lowest average wind speed. Uzhhorod (0.49) and Play (0.51) stations are interesting as at both studied altitudes compared to other measurement points, low coefficient of variation accompanies a relatively higher average and mode, thus the occurrence of higher wind speed is more balanced, wind is more even, which is favorable from wind energy utilization point of view.

Analyzing the frequency distributions of the daily average wind speed of stations it was observed, that with wind turbines, the cumulated frequency (v_{mean}≥3 m/s (%)) of starting (3 m/s) and stronger wind speeds at anemometer

altitude remained below 10% at half of the stations. However, at the altitude of 80 m it exceeds 50%: at Nyzhni Vorota (53.8%), Uzhhorod (63.9%), Pozhyzhevs′ka (65.1%), and Play (83.2%).

Table 5. Weibull distribution parameters and basic statistics describing daily average wind speed distribution at anemometer (z_a) altitude and at 80 m above ground level in the period between 2011 and 2015

Height	Parameter	Uzhhorod (112 m)	Berehove (113 m)	Khust (164 m)	Velykyi Bereznyi (285 m)	Rakhiv (430 m)	Mizhhirja (456 m)	Nyzhni Vorota (496 m)	Nyzhnii Studenyi (1145 m)	Play (1330 m)	Pozhyzhevs′ka (1451 m)
	z_a	**14**	**10**	**16**	**10**	**10**	**10**	**10**	**10**	**8**	**11**
z_a m	k_a	1.82	0.64	2.71	1.32	1.0	1.48	1.59	2.19	1.65	1.15
	c_a (m/s)	2.30	0.23	1.03	1.42	1.44	1.30	2.02	1.66	5.23	3.59
	mean (m/s)	2.05	0.32	0.92	1.30	1.44	1.18	1.82	1.47	4.68	3.41
	st. dev. (m/s)	1.18	0.48	0.37	1.01	1.44	0.82	1.18	0.71	2.96	2.99
	mode (m/s)	1.13	0.00	0.88	0.75	0.75	1.00	1.01	1.25	2.13	0.50
	var. coeff.	0.58	1.50	0.40	0.80	1.00	0.70	0.65	0.49	0.63	0.88
	v_{mean}≥3 m/s (%)	17.8	0.5	0.1	6.3	12.5	2.4	14.0	2.6	62.5	42.6
z=80 m	k_z	2.16	0.78	3.18	1.61	1.23	1.82	1.95	2.68	2.06	1.40
	c_z (m/s)	4.35	0.64	2.29	2.87	2.91	2.68	3.84	3.26	8.27	6.15
	mean (m/s)	3.85	0.74	2.05	2.57	2.72	2.38	3.40	2.90	7.32	5.61
	st. dev. (m/s)	1.88	0.96	0.71	1.63	2.23	1.36	1.82	1.17	3.74	4.06
	mode (m/s)	3.26	0.00	2.03	1.57	0.73	1.73	2.65	2.74	5.98	2.51
	var. coeff.	0.49	1.30	0.34	0.64	0.82	0.57	0.54	0.40	0.51	0.72
	v_{mean}≥3 m/s (%)	63.9	3.4	7.5	33.8	35.0	28.9	53.8	44.9	83.2	65.1

In wind energy examinations, the vertical wind profile is often determined by means of the so-called Hellmann's power law (*Patay,* 2003):

$$\frac{v_z}{v_a} = \left(\frac{z}{z_a}\right)^{\alpha}, \tag{22}$$

where v_z is z, while v_a is the average wind speed, z_a is measured at anemometer altitude, exponent α depends on the surface raggedness and the stability of the air; it changes, according to the latter, in time (e.g., daily) (*Tar*, 2008). Long-term, two-level wind speed measurements are necessary to determine it; however, the stations under analysis do not have them. Thus, without knowing the value of α, the Hellmann-equation cannot be applied. However, scale c parameter according to Eq. (7), is proportionate to average wind speeds, therefore, Eq. (8) can be interpreted as a kind of approximation of Hellmann-equation, where exponent α is given by Eq. (10).

Thus, only this exponent can be taken into account while applying Hellmann-equation, i.e., the results would most probably coincide with those of Weibull distribution (exponent *n, Table 6*).

Table 6. Values of exponent *n* at the studied stations for the entire period and per season

Time period	Uzhhorod (112 m)	Berehove (113 m)	Khust (164 m)	Velykyi Bereznyi (205 m)	Rakhiv (430 m)	Mizhhirja (456 m)	Nyzhni Vorota (496 m)	Nyzhnii Studenyi (615 m)	Play (1330 m)	Pozhyzhevs'ka (1451 m)
entire	0.31	0.50	0.38	0.34	0.34	0.35	0.31	0.33	0.22	0.26
winter	0.30	0.50	0.38	0.35	0.35	0.34	0.29	0.31	0.21	0.23
spring	0.28	0.46	0.36	0.31	0.30	0.33	0.30	0.32	0.22	0.26
summer	0.30	0.52	0.37	0.34	0.35	0.36	0.32	0.34	0.24	0.28
autumn	0.31	0.52	0.37	0.37	0.36	0.37	0.32	0.33	0.23	0.26

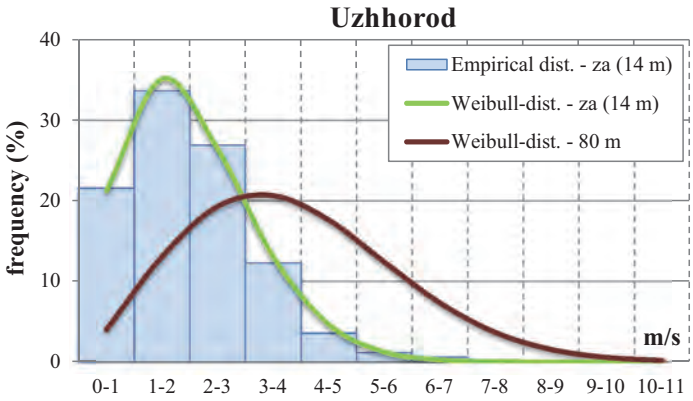
Uzhhorod
frequency (%)
40
30
20
10
0
Empirical dist. - za (14 m)
Weibull-dist. - za (14 m)
Weibull-dist. - 80 m
m/s
0-1
1-2
2-3
3-4
4-5
5-6
6-7
7-8
8-9
9-10
10-11

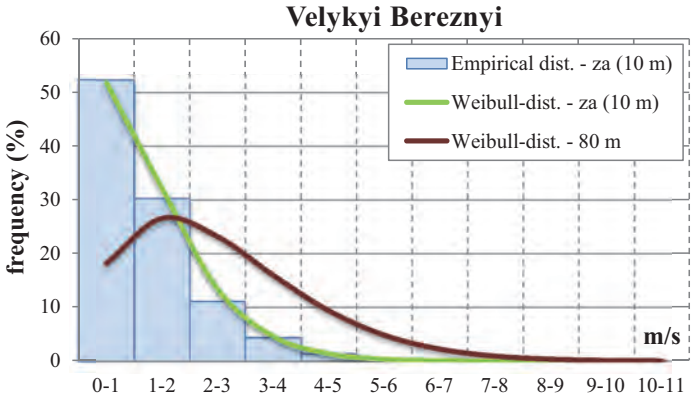
Velykyi Bereznyi
frequency (%)
60
50
40
30
20
10
0
Empirical dist. - za (10 m)
Weibull-dist. - za (10 m)
Weibull-dist. - 80 m
m/s
0-1
1-2
2-3
3-4
4-5
5-6
6-7
7-8
8-9
9-10
10-11

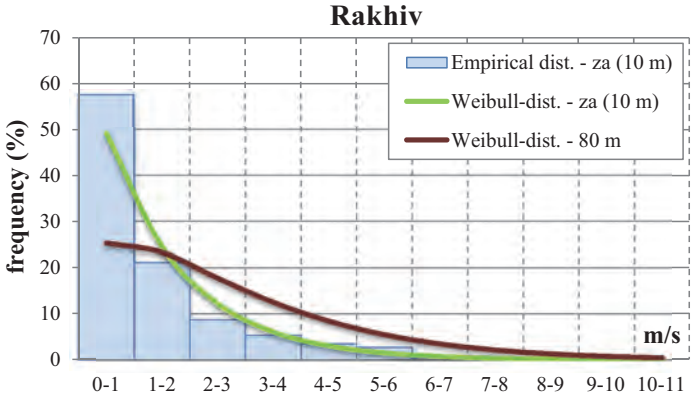
Rakhiv
frequency (%)
70
60
50
40
30
20
10
0
Empirical dist. - za (10 m)
Weibull-dist. - za (10 m)
Weibull-dist. - 80 m
m/s
0-1
1-2
2-3
3-4
4-5
5-6
6-7
7-8
8-9
9-10
10-11

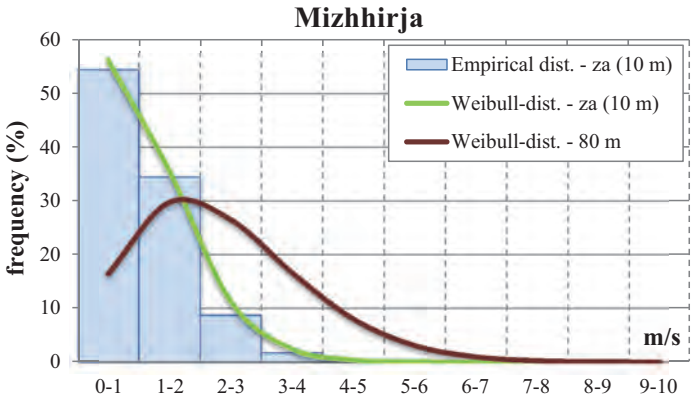
Mizhhirja
frequency (%)
60
50
40
30
20
10
0
Empirical dist. - za (10 m)
Weibull-dist. - za (10 m)
Weibull-dist. - 80 m
m/s
0-1
1-2
2-3
3-4
4-5
5-6
6-7
7-8
8-9
9-10

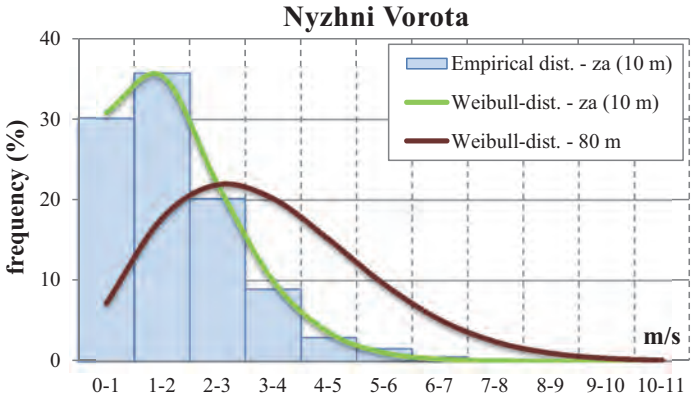
Nyzhni Vorota
frequency (%)
40
30
20
10
0
Empirical dist. - za (10 m)
Weibull-dist. - za (10 m)
Weibull-dist. - 80 m
m/s
0-1
1-2
2-3
3-4
4-5
5-6
6-7
7-8
8-9
9-10
10-11

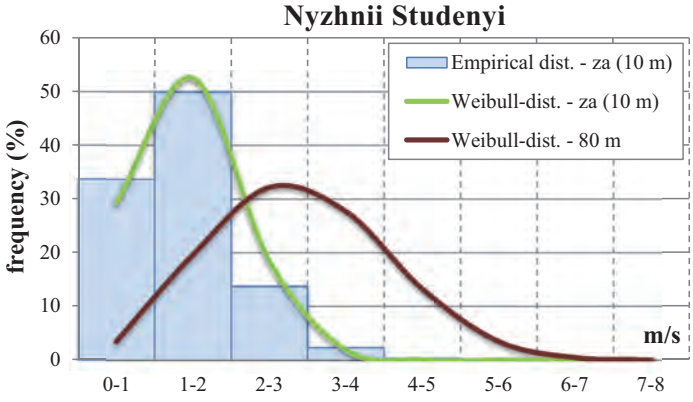
Nyzhnii Studenyi
frequency (%)
60
50
40
30
20
10
0
Empirical dist. - za (10 m)
Weibull-dist. - za (10 m)
Weibull-dist. - 80 m
m/s
0-1
1-2
2-3
3-4
4-5
5-6
6-7
7-8

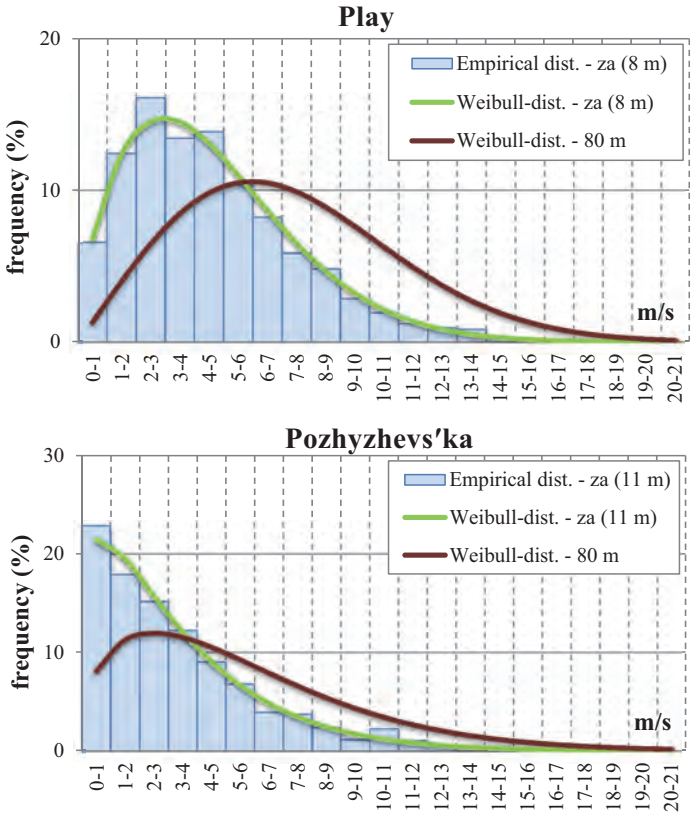

Fig. 2. Distribution of daily average wind speeds at each of the stations at anemometer altitude (z_a) and at 80 m above ground level in the period between 2011 and 2015.

3.4. Analysis of the relationship between the altitude above sea level of the measurement points and the Weibull distribution scale parameter

The scale parameter values of Transcarpathian measurement stations are compared with their altitude above sea level. In *Table 7* the *c* values and correlation coefficients of the three parameters obtained by means of the determining method are summarised.

It seems clear that at the same station the values vary in all the three cases; values determined by means of the first method (Eqs. (2) and (3)) show the greatest difference compared to the other two. The average of absolute differences of the values obtained by means of the second (Eqs. (4) and (5)) and third (Eqs. (6) and (7)) method make up 0.02 m/s, comprising minimal deviation.

Table 7. Comparison of scale parameters *c* (m/s) of the measurement stations with altitude above sea level (m)

Measuring point	Altitude	$c_{w1.\ medhod}$	$c_{w2.\ method}$	$c_{w3.\ method}$
Uzhhorod	112	9.82	2.31	2.30
Berehove	113	10.57	0.53	0.23
Khust	164	12.58	0.96	1.03
Velykyi Bereznyi	205	25.78	1.30	1.42
Rakhiv	430	13.97	1.34	1.44
Mizhhirja	456	11.41	1.29	1.30
Nyzhni Vorota	496	9.72	1.86	2.02
Nyzhnii Studenyi	615	5.43	1.57	1.66
Play	1330	3.56	5.19	5.23
Pozhyzhevs′ka	1451	8.54	3.63	3.59
Correlation coefficient (r)		-0.524	0.856	0.850

Fig. 3 shows that by analyzing the linear correlation between the scale parameter, determined by Eqs. (6) and (7) yielding fitting in most cases and the altitude above sea level, significant connection is found at 95% probability level between the two variables.

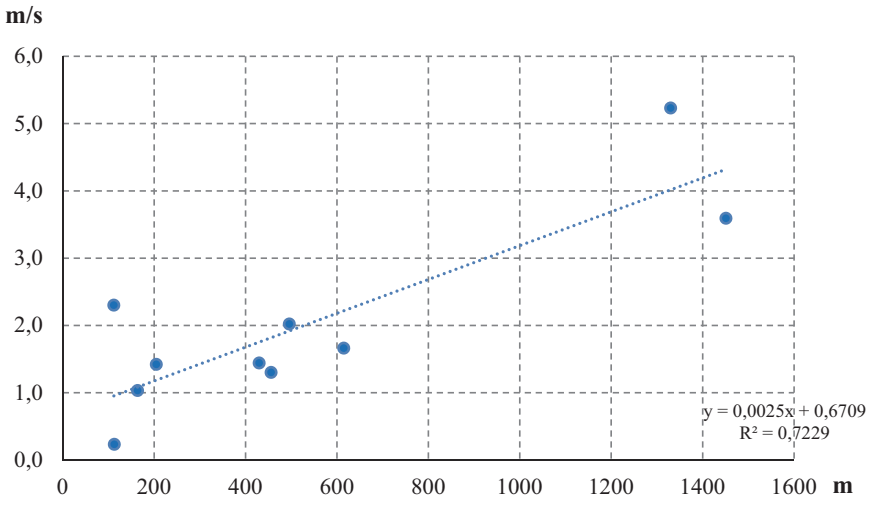

Fig. 3. Relationship between the altitude above sea level and the scale parameter.

4. Conclusions

- The frequency distribution of time series related to the daily average speed of the whole period between 2011 and 2015, irrespective of the orographic environment, can easily be approximated by Weibull distribution. Berehove and Khust stations are exceptions, for no distribution yielded appropriate fitting at any chosen significance level.
- However, fitting of the Weibull distribution depends on the methods of determining the k and c parameters. At 8 out of 10 stations (76% of cases) the best fittings were obtained on the basis of parameters of Eqs. (6) and (7).
- The Weibull parameters determined according to Eqs. (4) and (5) yielded positive fitting in most cases at the significance level of at least 5%. The Weibull distribution parameters calculated in accordance with Eqs. (2) and (3) yielded good fitting only in some seasons at Nyzhni Vorota and Pozhyzhevs′ka stations. Similarly, gamma distribution could only be applied in Velykyi Bereznyi, Rakhiv, and Pozhyzhevs′ka stations in the entire period or in a particular season; normal distribution proved to be good in two cases. Log-normal distribution and a special case of Weibull distribution making it easier to determine parameters, while the Rayleigh distribution cannot be applied for the daily average wind speed time series of the Transcarpathian measurement stations.
- The k and c parameters of the Weibull distribution show significant territorial variability being influenced by orographic conditions as well. In seasonal subdivision k yields the highest value in spring and summer, while c does so in winter and spring.
- There is a connection between the altitude above sea level of the measurement stations and the scale parameter value. 72.3% of the scale parameter's total variance can be explained by its linear connection with the altitude above sea level of the measurement point.
- By analyzing the frequency distribution of daily average wind speed and some of its statistical indices at anemometer altitude and at 80 m determined by means of Weibull distribution parameters, we can say that among the examined stations, the most favorable conditions to utilize wind energy are offered by the Play station situated on the Borzhava snow-covered mountain ridge. In vicinity of the measurement points located on plains and in narrow river valleys of highlands, there are no sufficient wind speeds for industrial utilization even at the altitude of 80 m above ground level.

References

Azad, A.K., Rasul, M.G., and *Yusaf, T.,* 2014: Statistical Diagnosis of the Best Weibull Methods for Wind Power Assessment for Agricultural Applications. *Energies 7*, 3056–3085. https://doi.org/10.3390/en7053056

Bartholy, J. and *Radics, K.* (Eds.), 2000: A szélenergia hasznosítás lehetőségei a Kárpát-medencében. Egyetemi Meteorológiai Füzetek. 14., Budapest. (in Hungarian)

Bonfils, S., 2011: Modeling wind speed and wind power distributions in Rwanda. *Renew. Sustain. Energ. Rev. 15*, 925–935. https://doi.org/10.1016/j.rser.2010.11.001

Costa Rocha, P.A., Coelho de Sousa, R., Freitas de Andrade, C., and *Vieira da Silva, M.E.,* 2012: Comparison of seven numerical methods for determining Weibull parameters for wind energy generation in the northeast region of Brazil. *Appl. Energ. 89*, 395–400. https://doi.org/10.1016/j.apenergy.2011.08.003

Dévényi, D. and *Gulyás, O.,* 1988: Matematikai statisztikai módszerek a meteorológiában. Tankönyvkiadó, Budapest. (in Hungarian)

Dokur, E. and *Kurban, M.,* 2015: Wind Speed Potential Analysis Based on Weibull Distribution. *Balkan J. Elect. Comput. Engin. 3*, 231–235. https://doi.org/10.17694/bajece.72748

Henessey, J.P., 1977: Some aspects of wind power statistics. *J. Appl. Met. 16,* 119–128. https://doi.org/10.1175/1520-0450(1977)016<0119:SAOWPS>2.0.CO;2

Hou, Y., Peng, Y., Johnson, A.L., and *Shi, J.,* 2012: Empirical Analysis of Wind Power Potential at Multiple Heights for North Dakota Wind Observation Sites. *Energ. Sci Technol 4* , 1–9.

Hunyár, M., 2004: A szélenergia potenciál hasznosítását korlátozó tényezők Magyarországon. *Magyar Energetika* 4, 3–10. (in Hungarian)

Huzsvai, L. and *Vincze, Sz*., 2012: SPSS könyv. Seneca Books. (in Hungarian)

Justus, C.G., Hargraves, W.R., Amir, M., and *Graber, D.,* 1978: Method for estimating wind speed frequency distributions. *J. Appl. Meteor. 17*, 350–353. https://doi.org/10.1175/1520-0450(1978)017<0350:MFEWSF>2.0.CO;2

Kartashov, M.V., 2008: Probability, processes, statistics. ВПЦ „Київський університет", Київ. (in Ukrainian)

Khan, P.A., Halder, P.K., and *Rahman, S.,* 2014: Wind energy potential estimation for different regions of Bangladesh. *Intern. J. Renew. Sustain. Energ. 3*, 47–52. https://doi.org/10.11648/j.ijrse.20140303.11

Kidmo, D.K., Danwe, R., Doka, S.Y., and *Djongyang, N.,* 2015: Statistical analysis of wind speed distribution based on six Weibull Methods for wind power evaluation in Garoua, Cameroon. *Rev. Energ. Renouvel. 18*, N1, 105–125.

Kravchyshyn, V.S., Medykovskyi, M.O., and *Halushchak ,M.O.,* 2016: Modelling the energetic potential of a wind power station. *Вісник Національного університету "Львівська політехніка"*. Серія: Інформаційні системи та мережі 854, 80–87. (in Ukrainian)

Lavny,i V. and *Lässig, R.,* 2009: Strong Winds in the Ukrainian Carpathians [Characteristics of Storms in the Ukrainian Carpathians]. *Науковий вісник НЛТУ України*, вип. 19.14., Львів, 239–246. (in Ukrainian)

Liubimov, O.D., Kovalenko V.M., and *Chubenko A.I.,* 2011: Methods of processing statistical data on wind parameters to make the decision to place a wind power station in a specific region. *Електроніка та системи управління*, 2 (28), 116–119. (in Ukrainian)

Maklad, Y. and *Glencross-Grant, R.,* 2014: A Seasonal Analysis of Potential Wind Power for Armidale NSW, Australia. *Int. J. Energ. Econom. Policy 4*, 92–107. https://doi.org/10.9790/3021-04910932

Matyasovszky I., 2002: Statisztikus klimatológia. Idősorok elemzése. ELTE Eötvös Kiadó, Budapest. (in Hungarian)

Morgan, E.C., Lackner, M., Vogel, M.R., and *Baise, G.L.,* 2011: Probability distributions for offshore wind speeds. *Energ. Convers. Manage. 52*, 15–26. https://doi.org/10.1016/j.enconman.2010.06.015

Patay, I., 2003: A szélenergia hasznosítása. Szaktudás Kiadó Ház, Budapest. (in Hungarian)

Radics, K., 2004: A szélenergia hasznosításának lehetőségei Magyarországon: hazánk szélklímája, a rendelkezésre álló szélenergia becslése és modellezése. Doktori értekezés, ELTE, Budapest. (in Hungarian)

Şahini, Z.A. and *Aksakal, A.,* 1999: A Statistical Analysis of Wind Energy Potential at the Eastern Region of Saudi Arabia, *Int. J. Energy Res. 23*, 909–917. https://doi.org/10.1002/(SICI)1099-114X(199908)23:10<909::AID-ER529>3.0.CO;2-1

Schönwiese, C.-D., 2013: Practical Statistics for Meteorologists and Geoscientists. 5. Vollständig überarbeitete und erweiterte Auflage. Gebrüder Borntraeger Verlagsbuchhandlung, Stuttgart.

Sobchenko, A. and *Khomenko, I.,* 2015: Assessment of regional wind energy resources over Ukraine. *Energy Procedia*, 76, 156–163. https://doi.org/10.1016/j.egypro.2015.07.889

Tar, K., 2008: Some statistical characteristics of monthly average wind speed at various heights. *Renew. Sustain. Energ. Rev. 12*, 1712–1724. https://doi.org/10.1016/j.rser.2007.01.014

Troen, I. and *Petersen, L.,* 1989: European Wind Atlas. Risø Nat. Labs, Roskilde, Denmark.

Xydis, G., 2012: Wind-direction analysis in coastal mountainous sites: An experimental study within the Gulf of Corinth, Greece. *Energ. Conver. Manage. 64*, 157–169. https://doi.org/10.1016/j.enconman.2012.05.018

DOI:10.28974/idojaras.2019.3.6

IDŐJÁRÁS

Quarterly Journal of the Hungarian Meteorological Service
Vol. 123, No. 3, July – September, 2019, pp. 351–370

Future climate change impacts on residential heating and cooling degree days in Serbia

Aleksandar Janković[1]*, **Zorica Podraščanin**[2], and **Vladimir Djurdjevic**[3]

[1]*University of Banja Luka, Faculty of Architecture*
Civil Engineering and Geodesy
Bulevar vojvode Petra Bojovića 1A
Banja Luka 78000, Bosnia and Herzegovina

[2]*University of Novi Sad, Faculty of Sciences*
Dr Zorana Đinđića 1, Novi Sad 21000, Serbia;

[3]*University of Belgrade, Faculty of Physics*
Studentski trg 1, Belgrade 11000, Serbia;

**Corresponding author E-mail: aleksandar.jankovic@aggf.unibl.org*

(Manuscript received in final form June 1, 2018)

Abstract— This study analyzes the potential changes of residential heating and cooling degree days (*HDD* and *CDD*) in the 21st century over Serbia with the regional climate model (RCM) EBU-POM under two different forcing scenarios (A1B and A2). The validation of the model shows that the model reproduces the spatial variability, magnitude, and annual cycles of *HDD* and *CDD* for the reference period very well. According to both scenarios, a significant decrease of *HDD* and increase of *CDD* is expected all over Serbia. The simulations show a spatial heterogeneity in the potential changes, with the largest decrease of *HDD* in southern (mountainous) Serbia and largest increase of *CDD* in northern (lowland) Serbia. Results also show that by the end of the 21st century, the existing ratio between populations weighted regional mean *CDD* and *HDD* of 1:7.3 could be reduced to 1:2.3 according to the A1B scenario and 1:2.0 according to the A2 scenario. At the end of the 21st century cooling season length will be for about two times longer than at the reference period, while length of the heating season will be reduced for about 25%. According to both scenarios model projected an increase of the heating and cooling season temperature through 21st century by slightly less than 2 °C. Our study is the first research of future changes in *HDD* and *CDD* over Serbia based on regional climate modeling. Results of the research should help the policy of energy management and planning through provided indications of future spatial and seasonal changes of *HDD* and *CDD* within Serbia.

Key-words: climate change, heating degree days, cooling degree days, regional climate model, building energy demand, Serbia

1. Introduction

The globally averaged surface temperature of the Earth increased 0.85 °C over the 1880 to 2012 period. It is extremely likely that the observed warming of the climate system was caused by the increased anthropogenic emission of greenhouse gases. Due to the further human induced contribution and natural climate variability, it is expected that, according to four different scenarios of greenhouse gases emissions (from scenario of immediate decrease of emissions to scenario of constant increase), global surface temperature will increase from 0.3 to 4.8 °C by the end of the 21st century (2081–2100) relative to the period of 1986–2005 (*IPCC*, 2013). During the period 1960–2012, significant increase of daily mean temperature was observed in Serbia with an average trend of 0.3 °C/decade on annual level. The whole territory of Serbia experienced a significant increase in temperatures from the middle of the previous century, especially during the summer and spring seasons (*Second National Communication of the Republic of Serbia under the United Nations Framework Convention on Climate Change*, 2017). Future changes in climate indices with regional climate models (RCMs) over Serbia were investigated by very few authors (*Krzić et al*., 2011). Recent research shows that relative to the reference period (1961–1990), by the end of the 21st century (2071–2100) it is expected that the surface air temperature will increase for 3.2–3.6 °C and 3.6–4.0 °C (*Second National Communication of the Republic of Serbia under the United Nations Framework Convention on Climate Change*, 2017) according to the A1B and A2 scenarios, respectively.

The predicted increase in temperature due to climate change will significantly affect the energy consumption in the Republic of Serbia (Serbia). Heating and cooling in the building sector of Serbia currently accounts around 45% of gross final energy consumption according to the official data (*National Renewable Energy Action Plan of the Republic of Serbia*, 2013). The expected climate change will significantly alter this balance. In particular, higher temperatures are projected decreasing the energy demand for heating in winter and increasing the electricity demand for cooling in summer. A useful tool for evaluating heating and cooling demands in building sector is the degree day method (*Quayle* and *Diaz*, 1980). Even though this technique is associated with some limitations (*Day* and *Karayiannis*, 1998; *Krese et al.*, 2011), it has been widely used to estimate energy demand for heating and cooling in the climate change studies both at global and regional levels. *Isaac* and *Vuuren* (2009) have shown in their study that regional *HDD* weighted by population will decrease by the 21st century, and that *CDD* will increase for all regions on the Earth. Consequently, the global energy demand for cooling will increase rapidly over the whole 21st century, while global energy demand for heating is expected to increase by 0.8% per year until 2030, and after that it will decrease slowly. A significant decrease of *HDD* is expected through the 21st century over the

European region, especially over Scandinavia and European Russia, while an increase of *CDD* is expected, which peaks over the Mediterranean region and the Balkans (*Spinoni et al.*, 2018). With included population projections over the 21st century it is expected, that despite the persisting warming, the related energy demand expressed as energy degree days (EDD) will result in an overall increase over Europe. According to the author, energy degree days as a measure of total energy demand are obtained by summing heating and cooling degree days. *Christenson et al.* (2006) projected a decrease between 13% and 87% in *HDD* for the period of 1975–2085 for Switzerland and accelerating positive trends for *CDD* through the 21st century, which will lead to significant, seasonally and regionally variable shifts in the energy consumption of Swiss buildings. *Petri* and *Caldeira* (2015) explored future changes in *HDD*/*CDD* in the United Sates and concluded that areas with high *HDD*/*CDD* will suffer relatively large decrease/increase, respectively, while energy degree days (*HDD* + *CDD*) as indicator of total energy demand for heating and cooling will decrease in the middle and northern parts of the United States, while southern parts will suffer an increase of this quantity. *Shi et al.* (2016) predicted the significant decreases in population weighted *HDD* and increases in the *CDD* over China, which will result in a decrease of around 15% in the potential energy demand over China.

The climate change and the consequent necessity for reduction of energy consumption and greenhouse gas emissions motivated us to examine future climate change impacts on indicators of residential heating and cooling energy demand. The objective of the paper is to quantify the impact of expected climate changes on the air temperature on residential heating and cooling degree days over Serbia. It should be emphasized that this research does not quantify future changes in heating or cooling residential energy demand, but gives an overview of projected changes in indicators which point to the sign and trend of changes in energy demand. Climate projections were conducted with the RCM EBU-POM using A1B and A2 scenarios *(Djurdjevic* and *Rajkovic*, 2010). Due to the higher spatial resolution and more precise description of terrain and surface characteristics, RCM can provide more information about the response of heating and cooling degree days (*HDD* and *CDD*) to global warming over some specific region. The first section gives a brief introduction and an overview of the latest research in this area. After that a brief description of the used RCM EBU-POM and calculation methods for *HDD* and *CDD* are presented. The third section covers the results of our research, including validation of the model performance when applied in this impact assessment. Results of the *HDD* and *CDD* calculation from measured and modeled data for the reference period (1971–2000) and for the future periods (2011–2040, 2041–2070, 2071–2100) are shown later in this section. The interpolation of *HDD* and *CDD* data on high resolution over Serbia for the reference period and future period (2071–2100) was done using estimated regression model considering also topography

variability using DEM (Digital Elevation Model) dataset. Temporal evolution and annual cycle of population weighted means of *HDD* and *CDD* over Serbia in the 21st century (2011–2100) were investigated under A1B (medium emissions) and A2 (high emissions) SRES scenarios. Finally, regionally averaged length and temperature of the heating and cooling season of the four considered periods are calculated according to both forcing scenarios. Both quantities are population weighted in order to more accurately reflect on the temperature-related energy demand at the country level. The last section gives a discussion about the importance of our research findings and a basic conclusion with respect to future changes in *HDD* and *CDD* values over Serbia. Results and methodology presented in this study provide the information for assessment of future energy demands and its annual redistribution, and may contribute to the future planning in this sector, which is an important part of the future sustainable development. The results of this study can be very useful for quantifying the future heating and cooling energy demand in the residential sector of Serbia.

2. Material and methods

2.1. Regional climate model

The simulation of future climate conditions are conducted with the RCM EBU-POM (*Djurdjevic* and *Rajković*, 2008) driven by the ECHAM5 coupled atmosphere–ocean general circulation model (*Roeckner et al.*, 2003). EBU-POM is a two-way coupled RCM with an atmospheric domain that covers almost the entire European region with a horizontal resolution of 0.25° over land and 0.2° over ocean. For the Serbian region, model results are validated against the observed data from 17 meteorological stations. The previous analysis showed that an improvement by EBU-POM has been achieved in reproducing the climate variation over a very small region compared to the driving global climate model (*Kržić et al.*, 2012). In this paper, we used bias corrected daily values of temperature for the reference and future periods as it is common for climate impact studies. Bias correction was applied on EBU-POM results (*Ruml et al.*, 2012) using the quantile mapping approach (*Piani et al.,* 2010; *Raisanen* and *Raty*, 2013). A correction function for each month was derived using observed and modeled temperature data over the period 1961–1990 assumpting that the cumulative density functions for observed and modeled values should be equal, also that temperature data follow normal distribution.

2.2. Degree-days

HDD and *CDD* are quantitative indices of required energy for heating and cooling of building. Degree-days are defined as accumulated temperature difference between the daily mean external air temperature and a reference

temperature for a given period of time (*Hitchen*, 1981). In some countries, a threshold temperature different from the reference temperature is used for heating. This threshold temperature determines the beginning, end, and length of the heating season (*EN ISO 15927-6,* 2007). If we introduce the concept of threshold temperature, degree days will indicate the total deficit (°C) relative to the reference temperature and duration of the period (days), when the external air temperature is lower than a determined threshold value, and when a building needs heating to maintain indoor thermal comfort (*Matzarakis* and *Balafoutis*, 2004). The unit for heating and cooling degree days will be labeled with °D as it was labeled in the paper of *Shi et al.* (2016).

Although each building has its own unique reference and threshold temperature depending on the characteristics of the building and the climatic conditions (*Lindelöf*, 2017), in the countries where the government controls the central heating system, the reference and threshold temperature are defined depending on the level of economic development, the average housing insulation properties, and climatic conditions (*Martinaitis*, 1998; *Shen* and *Binhui*, 2016). According to the current policy in the Republic of Serbia (*Rule Book on energy efficiency of buildings*, 2011), the length of the heating season and the number of annual *HDD* is defined by the following equation:

$$HDD = Z \cdot (t_{rh} - t_{ht}) + \sum_{n=1}^{Z} (t_{ht} - t_n) \quad (1)$$

where t_n is the daily temperature normal (it refers to the long-term average of daily mean external air temperautre) and Z is the length of the heating season in days. According to the current policy in the Republic of Serbia, the reference temperature for heating, t_{rh} is equal to 19 °C, and the heating threshold temperature t_{ht} is equal to 12 °C (*Živković* and *Novoselec*, 1998). Defined in this way, *HDD* take into account the accumulated temperature difference only during the heating season, where the length of the heating season is determined on the basis of the daily temperature normals (at least 20-year period of averaging). The heating season officially begins on a first day of autumn with normal daily temperature lower than 12 °C and ends on a first day of spring with normal daily temperature higher than 12 °C.

In order to reflect on the actual energy demand for heating and to avoid a downward bias of *HDD* in transitional months (May, October), we decided not to calculate *HDD* from daily temperature normals and the fixed season length. Instead, we opted to calculate *HDD* from all days of the given year with a daily mean external air temperature less than 12 °C. In this way, it is possible to include the effect of the inter-annual variability of *HDD*, the length of the heating season, and the mean temperature of the heating period. Defined in this way, *HDD* can be calculated according to the following equation:

$$HDD = \sum_{n=1}^{N} hh \cdot (t_{rh} - t_n), \quad (2)$$

where N is the number of days in a year (365 or 366), t_n is the daily mean external air temperature, and t_{rh} is the reference temperature for heating assumed to be equal to 19.0 °C. If a daily mean external air temperature is lower than the threshold temperature (t_n<12 °C), *hh* is equal to 1, otherwise (t_n>12 °C) hh is equal to 0.

However, the methodology for calculating *CDD* is not defined, as the building sector in Serbia on average consumes about 10 times less energy on cooling than on heating on average (*National Renewable Energy Action Plan of the Republic of Serbia*, 2013). There are a number of existing different methods for calculation of *CDD* and different definitions of reference temperatures. The most widely used method is ASHRAE method (*ASHRAE*. 2005; *Al-Hadhrami*, 2013) where the annual *CDD* are defined as:

$$CDD = \sum_{n=1}^{N} cc \cdot (t_n - t_{rc}) \quad (3)$$

where N is the number of days in a year (365 or 366), t_n is daily mean external air temperature and t_{rc} is reference temperature for cooling assumed to be equal to 18.3 °C. If a daily mean external air temperature is higher than the reference temperature, *cc* is equal to 1, otherwise *cc* is equal to 0. According to this method, the cooling threshold temperature is equal to the reference temperature. Since the country in Europe has its own standard computation, the ASHRAE method was accepted as the standard method for calculating *CDD* by the European Insulation Manufacturers Association (EURIMA) in their study on energy performance of European buildings (*Boermans* and *Petersdorff*, 2007).

2.3. Regression analysis

We used the RCM EBU-POM bias corrected daily values of temperature for 30 grid points over Serbia. Thirty output points from the model match the most populated places and the most famous tourist attractions in Serbia. In order to accurately map *HDD*/*CDD* over Serbia andto estimate degree days over the whole territory, the impact of the altitude z [m], longitude θ, and latitude λ [^{0}] on *HDD* or *CDD* values must be taken into account through regression analysis (*Idchabania et al.*, 2013; *Vizi et al.*, 2011). For the information on altitude, longitude, and latitude, we used the Digital Elevation Model (DEM) of Serbia (U.S. Geological Survey, 2017) with resolution of 1-arc-second (approximately 30 m), therefore, final maps of *HDD* and *CDD* for reference and future periods has been drawn on this resolution.

3. Results

3.1. Verification of the regional climate model

The credibility of the RCM to reproduce *HDD* and *CDD* can be assessed by comparing *HDD* and *CDD* calculated using observed daily temperature values with *HDD* and *CDD* calculated using the model daily temperature for the reference period. For that purpose and since we did not have measurements for all of the 30 model points, we used daily temperature observations from 17 stations of meteorological of observing system in Serbia (Republic Hydrometeorological Institute of Serbia). *Table 1* shows the observed and simulated *HDD* and *CDD* values for the period 1971 to 2000, along with the standard deviation (SD) as a measure of the interannual variability and bias. Since the climate of Serbia is moderately continental, much larger values of *HDD* are found than *CDD*. The higher altitude areas, placed between the Pannonian valley and the Adriatic Sea have greater spatial variability of surface temperature and, consequently, *HDD* and *CDD*. The largest values of *HDD* and concurrently the lowest values of *CDD* are found for higher altitude locations (Zlatibor and Požega). Belgrade stands out as the place with the lowest annual *HDD* and the highest annual *CDD*, probably due to the effect of the urban heat island.

Table 1. Observed and simulated *HDD* and *CDD* along with the interannual standard deviation and bias between the modeled and observed values in the reference period (1971–2000) at 17 meteorological stations in Serbia

	Alt. [m]	**Lat. [^{0}]**	**Long. [^{0}]**	**Observed *HDD*±SD [^{o}D]**	**Simulated *HDD*±SD [^{o}D]**	**Bias *HDD* [^{o}D]**	**Observed *CDD*±SD [^{o}D]**	**Simulated *CDD*±SD [^{o}D]**	**Bias *CDD* [^{o}D]**
Sombor	88	45.77	19.15	2,805±223	2,878±192	73.2	285±88	303±78	18.4
Kikinda	81	45.85	20.47	2,777±215	2,843±199	65.4	321±88	342±84	20.9
Loznica	121	44.55	19.23	2,544±230	2,692±195	148.5	330±81	297±69	-33.5
Beograd	132	44.80	20.47	2,410±221	2,507±213	96.6	435±111	432±89	-2.8
Kragujevac	197	44.03	20.93	2,606±192	2,710±208	104.6	307±94	307±72	0.1
S. Palanka	122	44.37	20.95	2,657±190	2,740±205	83.5	306±91	332±77	26.0
Negotin	42	44.23	22.55	2,744±216	2,810±199	66.0	370±100	390±71	19.9
Zlatibor	1028	43.73	19.72	3,765±246	3,896±224	130.9	69±46	77±29	8.3
Pozega	310	43.85	20.03	3,019±176	3,186±169	167.3	194±54	157±44	-37.0
Kraljevo	215	43.70	20.70	2,663±191	2,731±194	68.5	296±87	313±68	16.7
Krusevac	166	43.57	21.35	2,696±180	2,783±200	87.4	287±87	302±65	15.1
Cuprija	123	43.93	21.38	2,738±182	2,822±199	84.2	286±84	300±68	14.0
Nis	201	43.33	21.90	2,553±187	2,657±198	103.9	367±103	372±74	5.0
Zajecar	144	43.88	22.30	2,870±216	2,946±199	76.3	271±91	303±67	32.2
Dimitrovgrad	450	43.02	22.75	2,953±160	3,077±190	124.0	189±64	176±49	-13.2
Vranje	432	42.55	21.92	2,769±175	2,820±190	51.3	263±82	303±65	39.5
Novi Sad	84	45.33	19.85	2,711±222	2,786±203	75.2	315±90	339±82	23.3

The spatial distribution and magnitudes of both *HDD* and *CDD* have been reproduced very well by RCM EBU-POM over Serbia. Spatial correlation coefficients between the modeled and observed data amounts 0.99 for *HDD* and 0.97 for *CDD* (statistically significantly at the 95% confidence level). The model gives slightly higher values of *HDD* all over Serbia. This difference occurs because *HDD* and *CDD* are cumulative values of temperatures for long period of time (heating or cooling period). The small difference in the range of the measurement error of the thermometer (0.2 °C) between the modeled and observed values can cause cumulative error. The relative bias varies from 1.9% for Vranje to 5.8% for Loznica with a spatial average value of 3.4%. Concerning *CDD*, the model gives mainly lower values than those derived from observed temperatures, except for Loznica (–10.2%), Dimitrovgrad (–7.0%), Pozega (–19.0%), and Beograd (–0.6%). The positive relative bias varie from 0.0 % for Kragujevac to 15.0% for Vranje. Observed and simulated SD of *HDD* and *CDD* as a measure of interannual variability were compared. For *HDD,* the model mainly underestimate SD across northern Serbia and overestimate across southern Serbia with the correlation coefficient of 0.56 (statistically significantly at the 95% confidence level). For *CDD,* the model underestimate SD all over Serbia with the correlation coefficient of 0.90 (statistically significantly at the 95% confidence level). The relative difference between the observed and simulated SD of *CDD* varie from –5.0% for Kikinda to –35.4% for Zlatibor with a spatial average value of –20.4%.

The monthly regional averages of *HDD* and *CDD* for the period of 1971–2000 obtained from observations and simulation over Serbia are presented in *Fig. 1*. Both the model and the observations show that the months with the highest regional mean *HDD* and *CDD* are January and July, respectively.The months in which a significant number of *HDD* and *CDD* appear simultaneously are the transitional months of May and September. The observed monthly values have been simulated very well by the RCM EBU-POM with overestimations of *HDD* and *CDD* in most months, mainly due to the overestimation of the mean temperature all over Serbia during summer and the underestimation in southern Serbia during the autumn and spring (*Kržić et al.*, 2011).

The previously presented verification analysis shows that the model reproduces the spatial variability and annual cycles of *HDD* and *CDD* very well (*Table 2*). Biases are present, but at the same time they are smaller than the SD and negligible compared to the magnitude of *HDD* and *CDD*. However, it is important to note that the model underestimated observed the interannual variability of *CDD* to a certain extend all over Serbia.

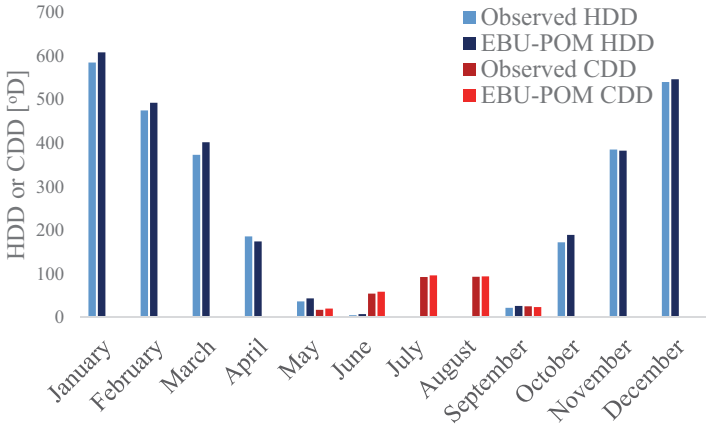

Fig. 1. Annual cycle of the observed and simulated *HDD* and *CDD* average over Serbia in the reference period (1971−2000).

Table 2. Linear regression models of *HDD* and *CDD* for the reference (1971–2000) and future (2071-2100) periods

Period	Equation	Correlation coefficient R []	Coefficient of determination R^2 []	Standard error [°D]
Model (1971-2000)	*HDD*=-4899+1.598·z+149.7·λ+38.13·θ	0.977	0.955	129.5
A1B (2071-2100)	*HDD*=-3907+1.201·z+112.7·λ+34.12·θ	0.966	0.933	119.4
A2 (2071-2100)	*HDD*=-3503+1.164·z+99.93λ+36.10·θ	0.963	0.927	122.4
Model (1971-2000)	*CDD*=-814.3-0.229·z+17.81·λ+17.74·θ	0.907	0.823	48.1
A1B (2071-2100)	*CDD*=-804.7-0.434·z+26.42·λ+20.64·θ	0.919	0.844	82.3
A2 (2071-2100)	*CDD*=-856.7-0.460·z+27.25·λ+24.62·θ	0.917	0.841	88.1

3.2. Future changes of HDD and CDD

The spatial distribution of *HDD* and *CDD* are presented for the end of the 21st century (2071–2100) under two different emission scenarios (A1B and A2). A1B and A2 scenarios are known as ‘medium’ and ‘high’ forcing scenarios

(*IPCC*, 2007), where CO_2 concentration at the end of the 21st century is about 1.8 and 2.2 times higher than the present value (*Nakićenović* and *Swart*, 2000). *HDD* and *CDD* values are calculated as 30-year averages for the future period and compared with model projection for the period 1971 to 2000. Based on the estimated regression model (*Table 1*), *HDD* and *CDD* were calculated in relation to the altitude, longitude, and latitude for each point of coordinates by using a geographical information system (GIS) environment (*QGIS*, 2014) and appropriate digital elevation model (DEM). The lower values of the coefficient of determination for *CDD* reveals a weaker correlation between *CDD* and geographical parameters. This could be influenced by some other factors such as humidity, urban heat island effects, and predominant winds from northwest and west during the warmer part of the year (*Kržić et al.*, 2011; *Smailagić et al.*, 2013).

The spatial distribution of *HDD* is presented in *Fig. 2* for the future (2071–2100) and the reference period (1971–2000) under the A1B and A2 scenarios. The figure shows the values of *HDD* in 30 points derived from the bias corrected data of the RCM EBU-POM. The rest of Serbia is mapped using the regression analysis technique and correlation between *HDD* and geographical parameters with residual corrections. A decrease of *HDD* is expected all over Serbia.

The largest change of *HDD* is expected in the mountainous (southern) Serbia with a reduction of more than 1000 °D. According to the A1B and A2 scenarios by the end of the 21th century, Kopaonik will suffer a record reduction of *HDD*, 1366 and 1533 °D, respectively. Minimum reduction of *HDD*, 752 and 884 °D are expected at Veliko Gradište according to A1B and A2 scenarios, respectively. The population weighted regional average of *HDD* for the reference period (1971–2000) is 2675 °D, while for the future period (2071–2100), under the A1B scenario it is 1877 °D. A2 scenario projects even larger reduction of *HDD* with regional average of 1743 °D. We assumed that the ratio between the settlements population will not change, so that the future population decline in Serbia will not affect the population weighted regional average of *HDD* and *CDD*.

The spatial distribution of *CDD* is presented in *Fig. 3* for the future (2071-2100) and the reference period (1971-2000) under the A1B and A2 scenarios. Figures show the values of *CDD* in 30 points derived from the bias corrected data of the RCM EBU-POM. The rest of Serbia is mapped using the regression analysis technique and correlation between *CDD* and geographical parameters with residual corrections. An increase of *CDD* is expected all over Serbia. Unlike for *HDD*, the largest change of *CDD* is expected in northern (lowland) Serbia with an increase of more than 500 °D. According to the A1B and A2 scenarios by the end of the 21st century, Belgrade will suffer a record increase of *CDD*, 505 and 584 ^{0}D, respectively. Minimum reduction of *CDD*, 105 and 129 ^{0}D are expected for Kopaonik according to the A1B and A2 scenarios, respectively. Population weighted regional average of *CDD* for the reference period (1971–2000) is 365 ^{0}D, while for the future period (2071-2100) under the A1B scenario, it is 823 ^{0}D. A2 scenario projects even larger *CDD* increase with a regional average of 894 ^{0}D.

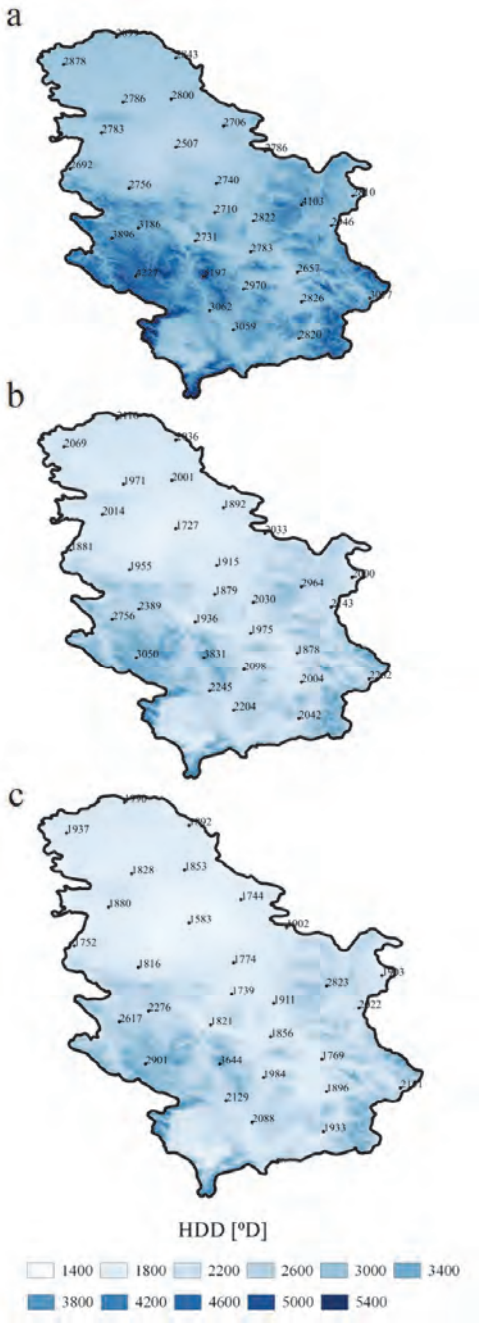

Fig. 2. Spatial distribution of *HDD* (a) for the reference period (1971–2000), (b) for the future period (2071–2100) under the A1B scenario, and (c) for the future period (2071 to 2100) under the A2 scenario.

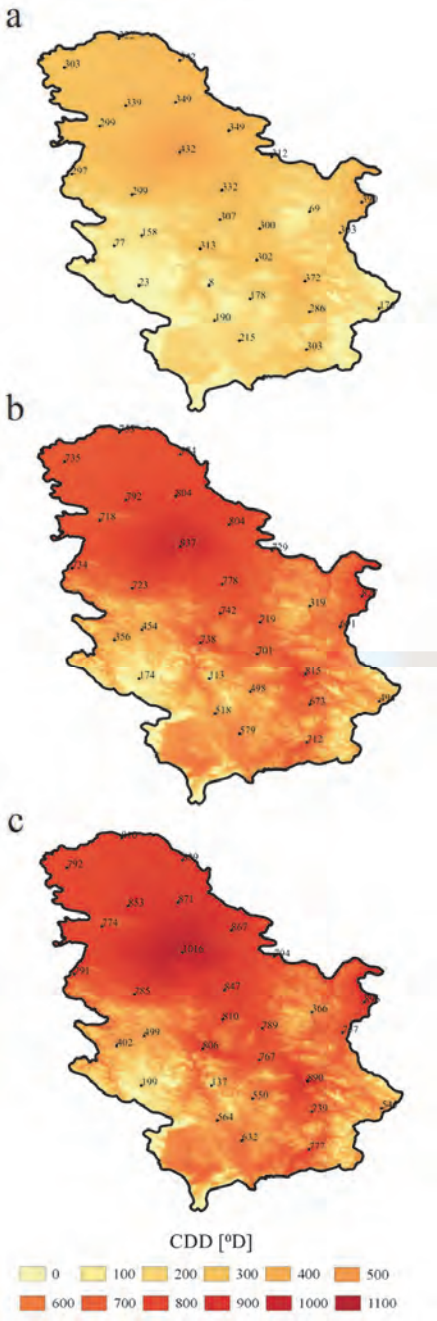

Fig. 3. Spatial distribution of *CDD* (a) for the reference period (1971–2000), (b) for the future period (2071–2100) under the A1B scenario, and (c) for the future period (2071 to 2100) under the A2 scenario.

According to the population weighted regional average, the ratio between *CDD* and *HDD* for the reference period (1971–2000) is 1:7.3. By the end of the 21st century, the ratio between *CDD* and *HDD* could be reduced to 1:2.3 according to the A1B scenario and 1:2.0 according to the A2 scenario, which leads us to the conclusion that climate change will alter the balance between the energy demands for cooling and heating. Compared to the present-day energy demand, much more energy will be required for cooling the buildings by the end of the 21st century. The sum of *HDD* and *CDD* (*HDD*+*CDD*) can be considered as an indicator of the total energy required for heating and cooling, although we have to be quite cautious with this assumption, because there is no general agreement in the scientific community on the definition of *CDD* for Serbia. Relative to the reference period (1971–2000), the population weighted *HDD*+*CDD* averaged over Serbia will decrease by the end of the 21st century (2071–2100) up to 11.2% and 13.3% according to the A1B and A2 scenarios, respectively. Although this means a reduction in the total required energy for heating and cooling, the increased electricity demand for cooling will probably lead to higher costs, because electricity is more expensive than the central heating by natural gas, heating oil, or biomass (*Jaglom et al.*, 2014).

The temporal evolution of the population weighted *HDD* and *CDD* averaged over Serbia under the A1B and A2 scenarios are presented in *Fig. 4*. Until 2035, no significant downward/upward trend in *HDD* / *CDD* is expected, respectively. More pronounced changes are expected during the second half of the 21st century, where the decrease in *HDD* is almost twice larger (–670 and –915 °D according to the A1B and A2 scenarios, respectively) than the increase in *CDD* (385 and 565 °D according to A1B and A2 scenario, respectively). During this period, an almost linear increase of *CDD* is expected by both scenarios (64 and 94 °D per decade according to the A1B and A2 scenarios, respectively), while *HDD* according to the A1B scenario is expected to stabilize after 2085 at ~1700 °D.

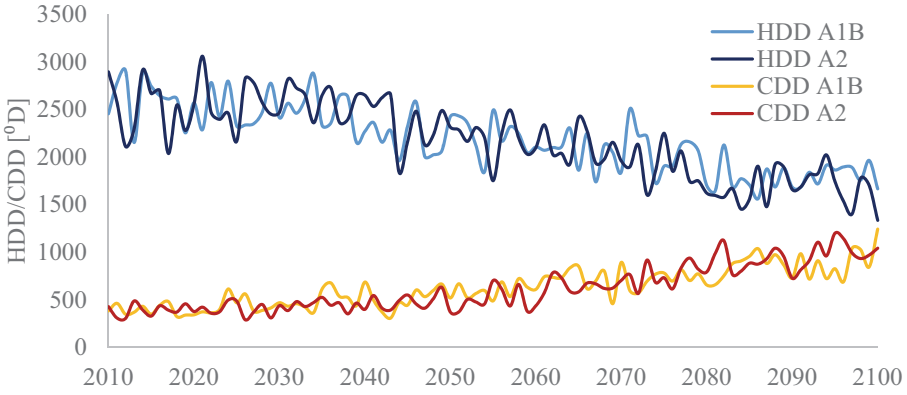

Fig. 4. Temporal evolution of the population weighted *HDD* and *CDD* averaged over Serbia in the 21st century (2011-2100) under the A1B and A2 scenarios.

Annual cycles of the population weighted *HDD* and *CDD* averaged over Serbia in the future compared to the reference period are shown in *Fig. 5*. The population weighted regional mean monthly values averaged for three future periods (2011–2040, 2041–2070, 2071–2100) under the A1B and A2 scenarios are compared with the corresponding values from the reference period (1971–2000). According to both scenarios, transition from the reference period to the first future period (2011–2040) does not bring significant changes of *HDD* / *CDD* in the first six months, while in the later part of the year, the changes in these quantities are more pronounced. For the other two periods in the future (2041–2070, 2071–2100), *HDD* reduction and *CDD* increase are expected in all months under both scenarios. Compared to the reference period, the peak of *HDD* in winter becomes less intensive in the future, while the peak of *CDD* in summer becomes more pronounced and sharpen, with this change being more prominent in the A2 scenario than in the A1B. Also there is a monthly shift, where the January at the end of the 21st century is more similar to the February at the end of the 20th century, February is like March, and so on. During the last future period (2071–2100), *CDD* becomes dominant over *HDD* in May, and the number of *CDD* in July exceeds the number of *HDD* in April by both scenarios. Although global warming is expected to reduce *HDD* and increase *CDD*, Serbia will remain the country where *HDD* dominates *CDD*, although this ratio will change considerably.

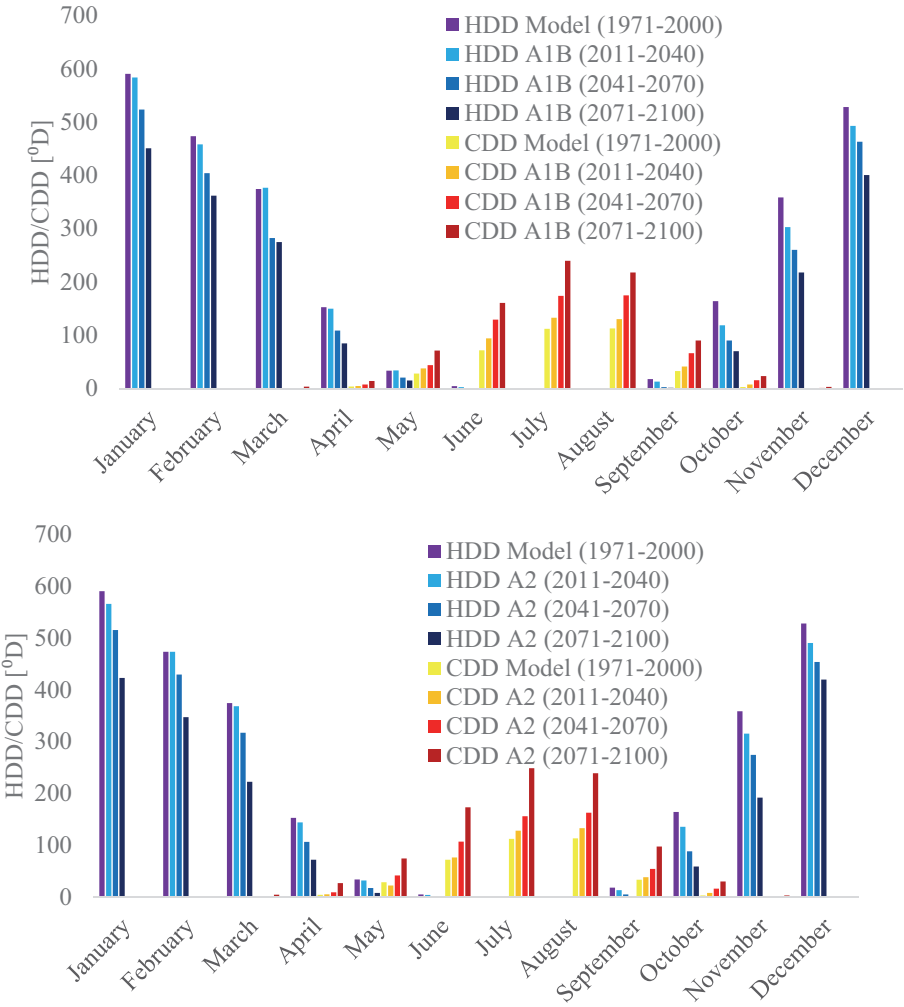

Fig. 5. Annual cycle of the population weighted *HDD* and *CDD* averaged over Serbia for the reference (1971–2000) and the future periods (2011–2040, 2041–2070, 2071–2100) according to the (a) A1B and (b) A2 scenario.

Regionally averaged length and temperature of the heating and cooling season of the four different considered periods are shown in *Table 3*. Both quantities are population weighted in order to more accurately reflect temperature-related energy demand at the country level. By the end of the 21st century, the reduction in the number of days of the heating season is somewhat less than 40 days according to the A1B scenario. A2 scenario projects even larger

reduction of about 50 days or 25.7% relative to the reference period (1971–2000). Both scenarios projects an increase of the mean temperature of the heating season for about 2 °C. This could be a consequence of that the model expects almost the same temperature rise in winter (DJF) according to both scenarios (3.2–3.8 °C for A1B and 3.0–3.8 °C for A2 scenario) (*Second National Communication of the Republic of Serbia under the United Nations Framework Convention on Climate Change*, 2017). The cooling season extension is somewhat greater than the heating season shortening with a difference in the sign of a change. At the end of the 21st century, the cooling season length will be almost twice longer than at the end of the 20th century (44.7 and 51.8% relative change according to the A1B and A2 scenarios, respectively) According to both scenarios, the increase of the mean temperature of the cooling season is slightly lower than the increase of the mean temperature of the heating season. Considering the projected decrease of *HDD*, the temperature of the heating season, and its length, it is expected that the residential heating energy demand will decrease also on national and per capita levels. This assumption is even more probable according to the predicted decline in the population of Serbia (*World Population Prospects,* 2017) and the improvement of the energy efficiency of residential buildings (*Novikova et. al.,* 2015). On the other hand, although the *CDD*, the mean temperature of the cooling season, and its length is projected to increase, we can not reasonably claim that the residential cooling energy demand will increase too on the national and per capita levels, because of the expected improvement of the energy efficiency of the residential buildings and population decline. A more accurate assessment can be made taking into account the demographic and economic factors, which will be the subject of the following research.

Table 3. Population weighted regional mean temperature and length of the heating and cooling season of the four different considered periods.

Period	Heating season				Cooling season			
	Length [days]		Temperature [°C]		Length [days]		Temperature [°C]	
	A1B	A2	A1B	A2	A1B	A2	A1B	A2
1971–2000	180		4.1		99		21.9	
2011–2040	170	171	4.2	4.3	107	103	22.0	21.9
2041–2070	154	156	5.1	5.0	125	121	22.7	22.4
2071–2100	143	133	6.0	6.1	143	150	23.6	23.8

4. Conclusions and discussion

In this paper, future changes of *HDD* and *CDD* for Serbia are investigated using RCM EBU-POM under two different forcing scenarios (A1B and A2). Our main conclusions and findings can be summarized as follows:

(1) RCM has proven to produce spatial variability and annual cycles of *HDD* and *CDD* very well.

(2) A decrease of *HDD* is expected all over Serbia. It is expected that population weighted regional average of *HDD* will decrease from 2675 °D (1971–2000) to 1877 °D (2071–2100) under the A1B scenario. A2 scenario projects even larger reduction with regional average of 1743 °D. The largest change is expected in southern (mountainous) Serbia with a reduction of more than 1000 °D. An increase of *CDD* is expected all over Serbia. It is expected that the population weighted regional average of *CDD* will increase from 365 °D (1971–2000) to 823 °D (2071–2100) under the A1B scenario. A2 scenario projects even larger increase with regional average of 894 °D. Unlike for *HDD*, the largest change of *CDD* is expected in northern (lowland) Serbia with an increase of more than 500 °D.

(3) By the end of the 21st century, the existing ratio between the population weighted *HDD* and *CDD* averaged over Serbia of 1:7.3 could be reduced to 1:2.3 according to the A1B scenario and 1:2.0 according to the A2 scenario. Although global warming is expected to reduce *HDD* and increase *CDD*, Serbia will remain the country where *HDD* dominates *CDD*, although this ratio will change considerably. Population weighted regional mean *HDD*+*CDD* will decrease by the end of the 21st century. Until 2035, no significant downward/upward trend in population weighted regional mean *HDD* / *CDD* is expected, respectively. More pronounced changes are expected in the last two thirds of the 21st century, where the decrease in *HDD* is almost twice larger than the increase in *CDD*.

(4) Annual cycles of the population weighted *HDD* and *CDD* averaged over Serbia in the future (2041–2070, 2071–2100) compared to the reference period (1971–2000) shows *HDD* reduction and *CDD* increase in all months under both scenarios. During the last future period (2071–2100), *CDD* becomes dominant over *HDD* in May, and the number of *CDD* in July exceeds the number of *HDD* in April by both scenarios.

(5) The population weighted regional mean length of the cooling season will be twice longer at the end of the 21st century than at the end of the 20th century, while the population weighted regional mean length of the cooling season will be reduced by 25%. Both scenarios predict an increase of the population weighted regional mean temperature of heating and cooling season for a slightly less than 2 °C.

(6) The results of the research unambiguously show that at the end of the 21st century, the residential heating energy demand will be lower both at national and per capita levels. The expected improvement of the energy efficiency of residential buildings and decline of the population of Serbia contribute to this assumption. For the assessment of change in residential cooling energy demand at national and per capita levels, the influence of other factors should be taken into account (population decline, overall heat insulation quality of future residential buildings, floor area per capita, etc.)

This study provides high spatial resolution analysis over the territory of Serbia under the future climate change. The presented analysis should help the policy of energy management and planning in Serbia through the provided indications of future spatial and seasonal changes of *HDD* and *CDD* within Serbia. In light of the projected increase of *CDD*, the published results should encourage the necessity for introduction of legal frameworks and the energy classification of buildings based on the maximum allowable energy required for cooling. According to the current legislation in Serbia, the categorization is done on the basis of the maximum allowable annual final energy required for heating. Future work will go in the direction of the direct assessment of energy demand for heating and cooling at national and per capita levels based on the characteristics of the building, the accumulated temperature difference, and other climatic factors.

References

Al-Hadhrami, L.M., 2013: Comprehensive review of cooling and heating degree days characteristics over Kingdom of Saudi Arabia. *Renew. Sustain. Energ. Rev. 27*, 305–314. https://doi.org/10.1016/j.rser.2013.04.034

ASHRAE, 2005: Handbook – Fundamentals (SI). American Society of Heating, Refrigerating and Air-Conditioning Engineers, Atlanta.

Boermans, T. and *Petersdorff, C.,* 2007: U-values for better energy performance of buildings. Eurima/Ecofys, Brussels.

Christenson, M., Manz, H., and *Gyalistras, D.,* 2006: Climate warming impact on degree-days and building energy demand in Switzerland. *Energy Convers. Manage. 47*, 671−686. https://doi.org/10.1016/j.enconman.2005.06.009

Day, A.R. and *Karayiannis, T.G.,* 1998: Degree-days: comparison of calculation methods. *Build. Serv. Engin. Res. Technol. 19*, 1757–1764. https://doi.org/10.1177/014362449801900102

Djurdjevic, V. and *Rajković, B.,* 2008: Verification of a coupled atmosphere–ocean model using satellite observations over the Adriatic Sea. *Ann. Geophys. 26*, 1935–1954. https://doi.org/10.5194/angeo-26-1935-2008

Djurdjevic,V. and *Rajković, B.,* 2010: Development of the EBU-POM Coupled Regional Climate Model and Results from Climate Change Experiments. In (Eds: *Mihailović, D.T., Lalić, B.*,) Advances in Environmental Modeling and Measurements. Nova Science, New York, 23–32.

European standard EN ISO 15927-6, 2007: Hygrothermal performance of buildings — Calculation and presentation of climatic data — Part 6: Accumulated temperature differences (degree-days). European committee for standardization, Brussels.

Hitchen, E.R., 1981: Degree days in Britain. *Building Serv. Engin. Res. Technol. 2,* 73–82. https://doi.org/10.1177/014362448100200202

Idchabania, R., Garouma, M., and *Khaldounb, A.,* 2013: Analysis and mapping of the heating and cooling degree-days for Morocco at variable base temperatures. *Int. J. Ambient Energ. 36*, 190–198. https://doi.org/10.1080/01430750.2013.842497

IPCC (Intergovernmental Panel on Climate Change), 2007: *The physical science basis*. In (eds: *Solomon, S., Qin, D., Manning, M., Chen, Z., Marquis, M., Averyt, K.B., Tignor, M., Miller, H.M.*) Contribution of Working Group I to the Fourth Assessment Report of the Intergovernmental Panel on Climate Change. Cambridge University Press, Cambridge.

IPCC (Intergovernmental Panel on Climate Change), 2013: *The physical science basis.* In (eds: *Stocker, T.F., Qin, D., Plattner, G-K., Tignor, M., Allen, S.K., Boschung, J., Nauels, A., Xia, Y., Bex, V., Midgley, P.M.,*) Contribution of Working Group I to the Fifth Assessment Report of the Intergovernmental Panel on Climate Change. Cambridge University Press, Cambridge.

Isaac, M. and *van Vuuren, D.P.,* 2009: Modelling global residential sector energy demand for heating and air conditioning in the context of climate change. *Energy Policy 37*, 507−521. https://doi.org/10.1016/j.enpol.2008.09.051

Jaglom, W.S., McFarland, J.R., Colley, M.F., Mack, C.B., Venkatesh, B., Miller, R.L., Juanita, H., Schultz, P.A., Perkins, B., Casola, J.H., Martinich, J.A., Cross, P., Kolian, M.J., and *Kayin, S.,* 2014: Assessment of projected temperature impacts from climate change on the U.S. electric power sector using the Integrated Planning Model®. *Energy Policy 73*, 524–539. https://doi.org/10.1016/j.enpol.2014.04.032

Krese, G., Matjaž, P., and *Butala, V.,* 2011: Incorporation of latent loads into the cooling degree days concept. *Energy Buildings 43,* 507−521. https://doi.org/10.1016/j.enbuild.2011.03.042

Krzić, A., Tosić, I., Djurdjevic, V., and *Rajković, B.* 2012: Some indicators of the present and future climate of Serbia acording to the SRES-A1B scenario. In (eds: *Berger A, Mesinger F, Šijački Đ*) Climate Change. Springer-Verlag, Wien. https://doi.org/10.1007/978-3-7091-0973-1_17

Kržić, A., Tošić, I., Djurdjevic, V., Veljović, K., and *Rajković, B.,* 2011: Changes in climate indices for Serbia according to the SRES-A1B and SRES-A2 scenarios. *Climate Res. 49*, 73–86. https://doi.org/10.3354/cr01008

Lindelöf, D., 2017: Bayesian estimation of a building's base temperature for the calculation of heating degree-days. *Energy Buildings 134*, 154–161. https://doi.org/10.1016/j.enbuild.2016.10.038

Martinaitis, V., 1998: Analytic calculation of degree-days for the regulated heating season. *Energy Buildings 28*, 185–189. https://doi.org/10.1016/S0378-7788(98)00015-2

Matzarakis, A. and *Balafoutis, C.,* 2004: Heating degree days as an index of energy consumption. *Int.J. Climatol. 24,* 1817–1828. https://doi.org/10.1002/joc.1107

Nakićenović, N. and *Swart, R.,* 2000: Special report of the Intergovernmental Panel on Climate Change. Cambridge University Press, Cambridge.

National Renewable Energy Action Plan of the Republic of Serbia, 2013. Ministry of Energy, Development and Environmental Protection, Belgrade

Novikova, A., Csoknyai, T., Jovanović Popović, M., Stanković, B., Živković, B., Ignjatović, D., Sretenović, A., and *Szalay, Z.* 2015: The typology of the residential building stock in Serbia and modelling its low-carbon transformation. The Regional Environmental Center for Central and Eastern Europe (REC), Szentendre.

Petri, Y. and *Caldeira, K.,* 2015: Impacts of global warming on residential heating and cooling degree-days in the United States. *Sci. Rep. 5*, 12427. https://doi.org/10.1038/srep12427

Piani, C., Haerter, J.O., and *Coppola, E.,* 2010: Statistical bias correction for daily precipitation in regional climate models over Europe. *Theor. Appl. Climatol. 99*, 187–192. https://doi.org/10.1007/s00704-009-0134-9

QGIS Development Team, 2014: *QGIS* Geographic Information System. Open Source Geospatial Foundation Project. https://qgis.org/

Quayle, R.G. and *Diaz, H.F.,* 1980: Heating degree day data applied to residential heating energy consumption. *J.Appl. Meteorol. 19*, 241–246. https://doi.org/10.1175/1520-0450(1980)019<0241:HDDDAT>2.0.CO;2

Raisanen, J. and *Raty, O.,* 2013: Projections of daily mean temperature variability in the future: cross-validation tests with ENSEM- BLES regional climate simulations. *Climate Dynam. 41*, 1553–1568. https://doi.org/10.1007/s00382-012-1515-9

Roeckner, E., Bäuml, G., Bonaventura, L., Brokopf, R., Esch, M., Giorgetta, M., Hagemann, S., Kornblueh, L., Schlese, U., Schulzweida, U., Kirchner, I., Manzini, E., Rhodin, A., and *Tompkins, A.,* 2003: The atmospheric general circulation model ECHAM5. Part I: model description. Report 349. Max-Planck-Institute, Hamburg.

Rule Book on energy efficiency of buildings, 2011. Ministry of Energy, Development and Environmental Protection, Belgrade.

Ruml M., Vuković A., Vujadinović M., Djurdjevic V., Ranković-Vasić Z., Atancaković Z., Sivčev B., Marković N., Matijašević S., and *Petrović N.,* 2012: On the use of regional climate models: Implications of climate change for viticulture in Serbia*, Agricult. Forest Meteorol. 158,* 53–62. https://doi.org/10.1016/j.agrformet.2012.02.004

Second National Communication of the Republic of Serbia under the United Nations Framework Convention on Climate Change, 2017. Ministry of Environmental Protection, Belgrade.

Shen, X. and *Binhui, L.,* 2016: Changes in the timing, length and heating degree days of the heating season in central heating zone of China. *Scientific Rep. 6*, 33384. https://doi.org/10.1038/srep33384

Shi, Y., Gao, X., Xu, Y., Giorgi, F., and *Chen, D.,* 2016: Effects of climate change on heating and cooling degree days and potential energy demand in the household sector of China. *Climate Res. 67*, 135–149. https://doi.org/10.3354/cr01360

Smailagić, J., Savović, A., Marković, D., and *Nešić, D.,* 2013: Climate characteristics of Serbia. Republic Hydrometeorological Service of Serbia, Belgrade.

Spinoni, J., Vogt, J.V., Barbosa, P., Dosio, A., McCormick, N., Biganob, A., and *Füssele, H-M.,* 2018: Changes of heating and cooling degree-days in Europe from 1981 to 2100. *Int. J. Climatol. 38*, e191-e208. https://doi.org/10.1002/joc.5362

U.S. Geological Survey, 2017: https://earthexplorer.usgs.gov/ (accessed 7 December 2017).

United Nations, Department of Economic and Social Affairs, Population Division, 2017: *World Population Prospects: The 2017 Revision, Key Findings and Advance Tables*. Working Paper No. ESA/P/WP/248.

Vizi, L., Hlasny, T., Farda, A., Štepanek, P., Skalak, P., and *Siktova, Z.,* 2011: Geostatistical modeling of high resolution climate change scenario data. *Időjárás 115,* 71–85.

Živković, B. and *Novoselec, A.,* 1998: Kriterijumi za izračunavanje broja stepen dana. *KGH – Klimatizacija, grejanje, hlađenje 4*, 45-48. (In Serbian)

DOI:10.28974/idojaras.2019.3.7

IDŐJÁRÁS

Quarterly Journal of the Hungarian Meteorological Service
Vol. 123, No. 3, July – September, 2019, pp. 371–390

Modeling of urban heat island using adjusted static database

Gergely Molnár*, **András Zénó Gyöngyösi**, and **Tamás Gál**

Department of Climatology and Landscape Ecology,
University of Szeged,
H-6722 Szeged, Egyetem u. 2., Hungary

**Corresponding author E-mail: molnarge@geo.u-szeged.hu*

(Manuscript received in final form June 26, 2018)

Abstract— In this study, the Weather Research and Forecasting (WRF) model was applied to examine the spatial and temporal formation of urban heat island (UHI) phenomenon in Szeged, Hungary. In order to achieve a more accurate representation of complex urban surface properties in WRF, a modified static database (consists of land use and urban canopy parameters) had been developed using satellite images and building information. In the new database, the number of urban grids increased by 76% related to the default case. The urban landscape in WRF has become more complex after employing two urban land use classes instead of only one. The modification of the default parameters of a single layer urban scheme (i.e., Single Layer Urban Canopy Model – SLUCM) revealed that urban fractions decreased in all urban categories, while street widths increased resulting in narrower urban canyons. For testing the impact of the modifications on near-surface temperature estimation, a four-day heatwave period was selected from 2015. The model outputs had been evaluated against the observations of the local urban climate monitoring system (UCMS). WRF with the modified parameters simulated most of the features of UHI reasonably well. In most cases, biases with the simulations of the adjusted static database tended to be significantly lower than with the default parameters. Additionally, we picked out a longer time period (i.e., the summer of 2015) when the extreme values of near-surface air temperature and maxima of UHI intensities were evaluated on the basis of an urban and a rural site of UCMS. It was concluded that the maxima and minima of observed near-surface air temperature were underestimated (overestimated) by about 1–3 °C at the urban (rural) site. The maxima of UHI intensities indicated cold biases on 86 of 91 days.

Key-words: Weather Research and Forecasting model, Single Layer Urban Canopy Model, adjusted static database, urban heat island, Szeged (Hungary)

1. Introduction

Because of rapid urbanization since the 1850s, more than the half of Earth's population live in cities nowadays, and estimations (*UN*, 2014) states that this ratio will likely to increase to 70% by the 2050s. The growing amount of artificial land cover alters the surface-atmosphere interaction of heat, moist, and momentum (*Oke*, 1973). Urban areas can be characterized by the urban heat island (UHI) phenomenon, which is a heat surplus related to rural regions (*Oke*, 1982). UHI has been widely investigating recently, because climate change exacerbates this temperature anomaly (as a positive feedback) and also modifies urban bioclimatic conditions (*Li* and *Bou-Zeid*, 2013, *IPCC*, 2013). In addition to that, anthropogenic heat and pollutant release from industry, transportation, and residents gain energy consumption and medical expenditures (*Crutzen*, 2004, *Kolokotroni et al*., 2015). Monitoring of urban environment is mostly disposed by using in-situ measurements, satellite observations, and numerical meteorological models. Owing to a consecutive development of computer technology, application of numerical models comes with lower computational costs. The other obvious advantage of this method in contrast with in-situ measurements is that models can produce a nearly contiguous, high-resolution, three-dimensional meteorological field (*Hidalgo et al*., 2008). The quality and reliability of satellite products highly depend on atmospheric attenuation, which limits their application during the overpass time (*Streutker*, 2003). Contrarily, numerical simulations are not restricted by time and weather condition.

One of the major modeling challenges is to characterize complex urban surfaces (*Mirzaei*, 2015). It must be determined that whether a given land use grid (or a pixel on satellite images) is urban or non-urban, and if urban to which sub-category should be classified. In practice, the sub-categories consist of aerodynamic, thermodynamic, and geometric properties of the surface. The derivation of these parameters is troublesome, because the process requires a vast and accurate land surface information. In case of lack of such data, default values are used to give a "first guess" for the parameters, but this stipulation increases the uncertainty of simulations. It is also problematic that there is only a limited number of methods regarding the characterization of the complicated urban geometry.

A great effort was made by *Stewart* and *Oke* (2012) to address this issue with the Local Climate Zones (LCZs) scheme. LCZs aimed to define classes with a minimum extension of 200–400 m and analogous parameter-sets of geometric/surface cover (e.g., sky view factor, aspect ratio, building surface fraction, and terrain roughness class) and thermal/radiative/metabolic attributes (e.g., surface albedo and anthropogenic heat output). The categories were designated according to building type (from LCZ 1 to LCZ 10), land cover type (from LCZ A to LCZ G), and various land cover properties (from b to w). The World Urban Database and Portal Tool (WUDAPT) (*Mills et al*., 2015) project

has also been contributing to the global application and spread of urban climate modeling. Within this framework, a global, community land use database had been created utilizing the LCZ classification. Depending on complexity, the database of each city was separated into three levels. The lowest level (Level 0) includes LCZ maps with only a few parameters, while the others contain a more precise and detailed description of the measures. Recently (in April of 2018), the WUDAPT data is available to view for 21 European cities.

The Weather Research and Forecasting (WRF) numerical model has been employed in a wide range of applications, such as the simulation of UHI in specific cities (e.g., *Sarkar* and *De Ridder*, 2011, *Salamanca et al*., 2012, *Giannaros et al*., 2013), heatwave events (e.g., *Li* and *Bou-Zeid*, 2013, *Wang et al.*, 2013, *Chen at al.,* 2014), heavy rainfalls (e.g., *Miao et al.*, 2011, *Zhong* and *Yang*, 2015), the impact of land use change on local climate (e.g., *Pathirana et al*., 2014, *Brousse et al*., 2016). *Miao et al*. (2009) investigated the behavior of urban heat island and boundary layer in Beijing. The results suggested that WRF coupled with the Single Layer Urban Canopy Model (SLUCM) scheme simulated reasonably well the spatial distribution and temporal variability of temperature field. Moreover, the model system captured the magnitude and direction of mountain-valley wind as well. *Bhati* and *Mohat* (2015) analyzed the impact of different land use categories on land surface temperature and near-surface air temperature in Delhi. The simulations were performed with (WRF-SLUCM) and without (WRF) the application of canopy parameterization scheme. By switching the SLUCM scheme on, RMSE of the land surface temperature decreased in urban grids (in non-urban grids) from 1.63 °C to 1.13 °C (from 2.89 °C to 2.75 °C). The hit rate of mean UHI enhanced by coupling WRF with SLUCM from 72% to 75% in urban grids, from 65% to 73% in coastal grids, and from 52% to 71% in vegetation grids.

In Szeged, urban climate investigations have been typically based on in-situ (e.g., *Unger et al.*, 2015) and mobile (e.g., *Unger et al.,* 2001) measurements, but WRF was not used up to now. The study of *Gál et al*. (2016) must be pointed out, who evaluated a one-year long observation of the local urban climate monitoring system established in the spring of 2014. On average, UHI released around sunset and decreased to 0 °C after a few hours after sunrise. The maximum values of UHI arose generally three hours after sunset. The highest intensities culminated in LCZ 2, LCZ 3, and LCZ 5 in summer, with around 3.5 °C. The springtime means were just a little below 3 °C. On the other hand, the wintertime mean intensities remained only around 2 °C.

The specific aims of this study is i) to modify the default land use database and urban canopy parameter to allow a better representation for the surface geometry of Szeged, ii) to compare the spatial and temporal behavior of UHI with the default and adjusted dataset under anticyclonic weather condition, and iii) to evaluate the model performance during a longer time period using the observations of our local urban climate monitoring system.

2. Material and methods

2.1. Study area and urban climate monitoring system

Szeged (46.26° N; 20.15° E) lies in the middle of the Hungarian Great Plain, at an elevation of 78–82 m AMSL, between sandy (to the west) and loamy (to the east) soil covered flat terrains. The Tisza River crosses the city, and several small-sized lakes are located to the northwest (*Fig. 1*), that may influence the local climate through evaporation cooling.

According to the Köppen-Geiger's classification, Szeged is on the border of Cfb (marine temperate) and Dfb (humid continental) climates (*Kottek et al.*, 2006), with an annual mean temperature of 10–12 °C and total precipitation of 500–600 mm. The dominance of high-pressure synoptic situation and local hot, dry wind blowing from the south in summer results in a high amount of annual sunshine duration (around 2000 hours).

With the population of 162,000, Szeged is the third largest city in Hungary. Szeged has a concentric structure with radial avenues and several boulevards. The inner city accommodates offices, administrative and educational buildings, apartment houses. Towards outer parts, blocks of flats (mostly in the north-western part), family and gardening houses are found. At the outermost areas of Szeged, industrials, logistics, railway and highway junctions are located.

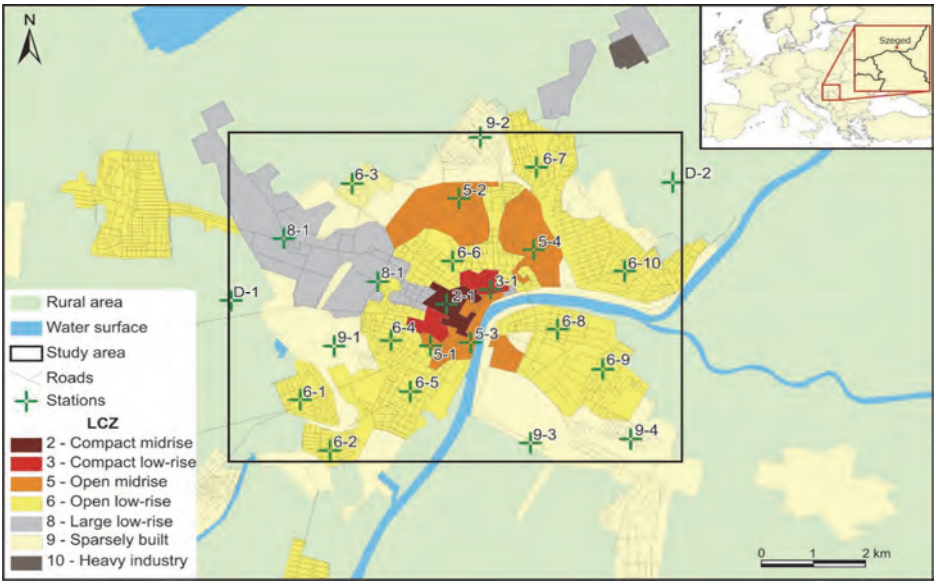

Fig. 1. Study area with the corresponding LCZs and urban climate monitoring sites.

An urban climate monitoring system (UCMS) has been established in the spring of 2014 within the framework of an EU project (*URBAN-PATH Project*, 2014, Lelovics et al., 2014). UCMS consists of 22 urban and two rural stations (*Fig. 1*.) and measures near-surface air temperature (with 0.2 °C accuracy between 10 °C and 60 °C) and humidity (with 1.8% accuracy between 10% and 90%) at the height of 4 m (*Unger et al.,* 2015). Since urban canopy layer is well-mixed close to the surface, temperature measurements at this height are representative for lower layers as well (*Nakamura* and *Oke*, 1988). Until April of 2018, almost a four-year-long observation data is accessible for the evaluation of urban climate simulations, the model system, and further parameter fine-tuning purposes.

2.2. Modification of the land use database and specification of the SLUCM parameters

For accounting urban environment in numerical models, several urban canopy schemes have been created (*Masson*, 2000, *Kusaka et al*., 2001, *Kusaka* and *Kimura*, 2004, *Martilli et al.,* 2002, *Best et al.,* 2006, *Oleson et al*., 2008, *Salamanca et al.*, 2010, *Salamanca* and *Martilli*, 2010). Here, we focused on the Single Layer Urban Canopy Model (SLUCM) of *Kusaka et al*. (2001), because other schemes (e.g., Building Energy Model (BEM) of *Salamanca* and *Martilli* (2010) require more complex parameters of anthropogenic activity in buildings (e.g., peak heat and heating profile generated by indoor equipment, etc.). SLUCM describes a 'default' city with a series of infinitely-long urban canyons where the effects of shadowing, reflection, and building orientation on short- and long-wave radiation are considered. Prognostic variables are skin temperature of wall, road and canopy, wind speed and direction at canopy level.

In order to achieve the best performance of a numerical weather prediction model, high-quality meteorological input, precise surface information (land use or soil data), physically consistent parameterization is needed. For representing the land use/land cover (LULC) of a given area, WRF offers the USGS (US Geological Survey) database (*Homer et al.,* 2004) with a horizontal resolution of 30 m as an option. Over Europe, the CORINE (Coordination of Information on the Environment) data (*Bossard et al*., 2000) provides an alternate source of input static data with a horizontal resolution of 25 m. For the total study area, both databases largely underestimate the complexity of urban geometry, with only one urban category (*Fig. 2*). Therefore, we carried out a new LULC classification, based on the spectral features of urban grids, using eight Landsat 8 images. For non-urban grids, CORINE data was considered.

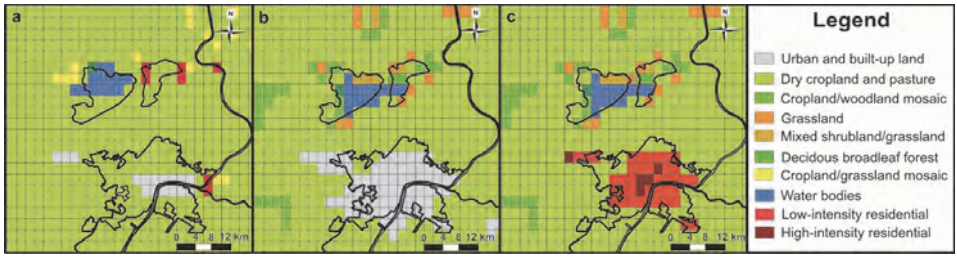

Fig. 2. USGS (a), CORINE (b), and modified (c) land use database at a model grid spacing of 2 km.

The Landsat 8 images (with a cloud fraction less than 3% for the entire scene) were merged into one false color composite to execute a maximum likelihood classification (*Fig. 3*). During the supervised classification, such small areas/clusters (region of interests; ROIs) were assigned (*Fig. 3*), that includes information about the size, location, and statistics of a given ROI representing LULC classes (i.e., commercial/industrial/transportation (CIT), low-intensity (LIR), and high-intensity residential (HIR)) in WRF.

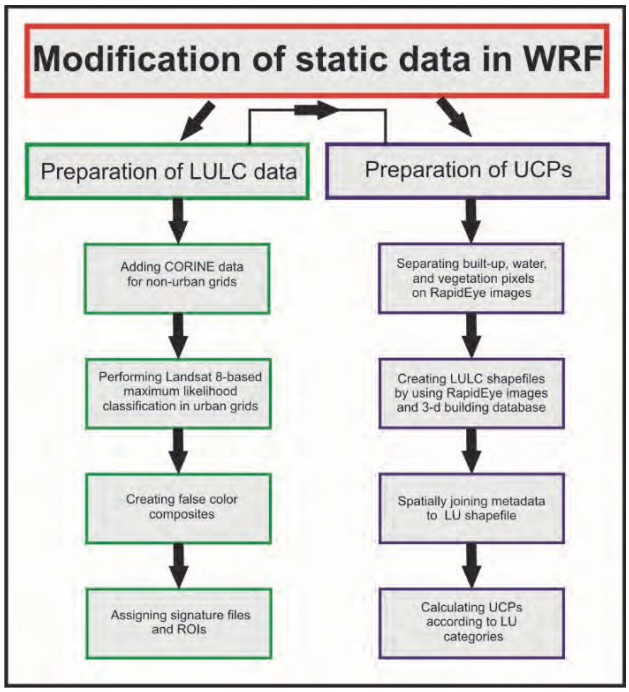

Fig. 3. Methods utilized along the modification of land use (left panel) and SLUCM (right panel) databases.

After the classification, it is concluded that 19% of the total urban (313) grids were categorized to LIR, 4% to HIR, and 0% to CIT, at a horizontal resolution of 2 km (*Table 1* and *Fig. 2*).

Table 1. Number of urban grids in the default and the modified database according to LULC category

LULC category	Number of grids [default LULC]	Number of grids [modified LULC]
Urban built-up and land	178	240
Low-intensity residential	0	59
High-intensity residential	0	14
Commercial/Industrial/Transportation	0	0

WRF-SLUCM parameters (*Kusaka et al*., 2001; *Kusaka* and *Kimura*, 2004) tend to describe thermodynamic (e.g., wall, road, and roof albedo, heat capacities, and heat conductivities) and geometric (e.g., wall, road, and roof widths and heights, urban fraction) properties of an idealized urban canyon. Since default SLUCM values are not always suitable for any type of urban area, it is worth to modify these parameters if adequate surface information is available. In order to give a better representation of the surface elements in Szeged, we calculated some of the SLUCM parameters utilizing RapidEye satellite images and three-dimensional building database (containing building and roof height, building area and volume). First, the NDVI (normalized difference vegetation index) distribution of the satellite images was computed to separate water (NDVI < 0.0), built-up (0.0 ≤ NDVI ≤ 0.2), and vegetated (NDVI > 0.2) surfaces (*Sobrino et al.*, 2004). In the following step, the building and NDVI databases were spatially joined to the three urban categories (*Fig. 3*). Assuming square-shaped urban canyons (on top-view), the road (R_x) and roof widths (r_x) was predicted as follows:

$$r_x = \frac{T_{bx}}{M_x},$$

$$R_x = \frac{1}{N_x}\frac{T_{ox}}{M_x},$$

where T_{bx} is the total building area, T_{ox} is the total open area (difference of total area and total building area), M_x is the mean building height, and N_x is the number

of buildings (*x* refers to the corresponding urban LULC class). Aggregating and averaging the given parameters by urban categories, four new canopy parameters were achieved per LIR/HIR/CIT (*Table 2*).

Table 2. Modified and default (in parenthesis) urban canopy parameters applied to the study

LULC category/canopy parameter	Low-intensity residential	High-intensity residential	Commercial/Industrial/ Transportation
Building height [m]	6 (5)	6 (7.5)	6 (10)
Roof width [m]	5.5 (8.3)	5.5 (9.4)	6.2 (10)
Road width [m]	5.5 (8.3)	5.5 (9.4)	6.2 (10)
Urban fraction [-]	0.4 (0.5)	0.6 (0.9)	0.7 (0.95)

It was concluded that building height decreased (increased) to 6 m in HIR and CIT (LIR). Lower road and roof width (and building height) in each class resulted in a narrower urban canyon compared to the default case (in LIR the urban canyon is higher but also narrower), which may limit the shadowing effect (more energy on the surface) and enhance the reflection (trapping) of daytime incoming shortwave radiation and nocturnal outgoing long-wave radiation in the urban canyon. Consequently, simulated near-surface air temperatures may be higher in the daytime and lower in the nighttime as a result of the modification of canopy parameters. Urban fraction also decreased with an order between 10% and 30% (*Table 2*). Elevated evapotranspiration by lower urban fraction (and higher vegetation fraction) may counteract the potential warming during the daytime and strengthen the nocturnal cooling in the simulations. The rest of the default parameters have not been changed, because they fit to the local conditions or more suitable information were not obtained for further modifications.

3. Model setup

For testing the influence of the aforementioned modifications on near-surface air temperature (T_a) prediction over Szeged, we performed two types of model experiment with common grid and physical configurations but different static databases. Hereafter, simulations with the default (updated) land use and canopy parameters will be referred to as WRF-DEF (WRF-MOD) (*Table 3*).

WRF version 3.8. (*Skamarock et al*., 2008) had been used for each modeling purpose. Initial and boundary conditions were generated from the 0.25°×0.25° resolution outputs of the Global Forecasting System (GFS) model at a three-hour interval. Parent domain (d01) employed a 10-km grid spacing, hosting a telescopic nest at 1:5 grid ratio resulting in a child domain (d02) with a final horizontal resolution of 2 km, with 96×96 grids centered over Szeged. 44 vertical sigma

levels were applied between the surface and 20 hPa. Physical parameterizations were chosen according to the applied urban scheme and above domain setup: WSM 5-class scheme for microphysics (*Hong et al.,* 2004), RRTMG scheme for long- and shortwave radiation (*Iacono et al*., 2008), MM5 Similarity scheme for surface layer (*Jimenez et al*., 2012), Unified Noah LSM (*Tewari et al*., 2004), BouLac scheme for boundary layer (*Bougeault* and *Lacarrere*, 1989), and Kain–Fritsch scheme for cumulus convection (*Kain*, 2004), applied only for the parent domain.

Table 3. Model configuration and physical schemes applied to the modeling experiments

WRF-DEF	**Configurations**	**WRF-MOD**
General information		
WRF v3.8	Model version	WRF v3.8
24 h and 48 h	Spin-up and simulation time	24 h and 48 h
GFS 0.25°×0.25° with 3-h interval	Initial and boundary condition	GFS 0.25°×0.25° with 3-h interval
Grid information		
2 km	Grid spacing of finest domain	2 km
2 and 1:5	Number of domains and grid ratio	2 and 1:5
44 (sigma)	Number of vertical levels	44 (sigma)
Physical parameterization		
Noah LSM	Land surface model	Noah LSM
Revised MM5	Surface layer	Revised MM5
BouLac	Boundary layer	BouLac
RRTMG	Short- and long-wave radiation	RRTMG
WSM5	Microphysics	WSM5
Kain-Fritsch	Cumulus convection	Kain-Fritsch
Static parameters		
SLUCM	Urban physics	SLUCM
Default	Urban table	Modified
FAO	Soil	DKSIS

For representing soil texture in WRF-DEF, we employed the 16-category FAO (Food and Agriculture Organization) global database. To give a better characterization for the soil distribution in WRF-MOD, FAO was replaced to the DKSIS (Digital Kreybig Soil Information System) database (*Pásztor et al*., 2012) for those grids that located within the administrative border of Hungary (*Fig 4*).

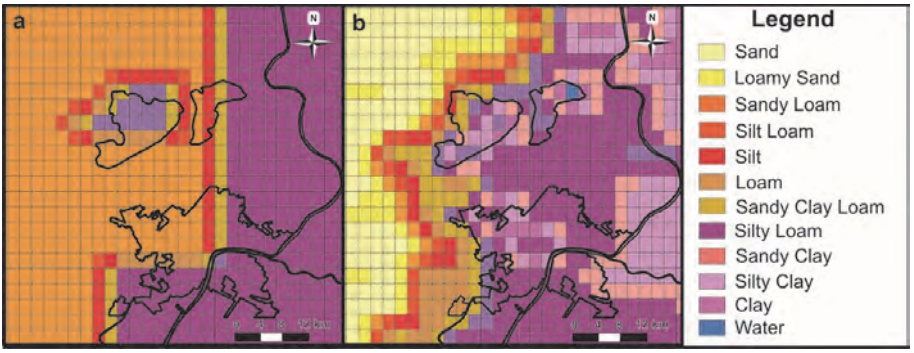

Fig. 4. FAO (a) and DKSIS (b) soil databases at a model grid spacing of 2 km.

The integration of each day was initialized at 00 UTC and lasted for 48 hours. The first 24 hours were dropped as spin-up, only the second half of the results (from 00 UTC to the next day's midnight) were considered and compared to the measurements under the verification process. The time-series of T_a at urban locations during their cooling stages showed a high-frequency noise of up to 3 °C amplitude. One-minute moving averages, however, induced pretty much reliable and low-biased results compared to the observations. For the reasons above, we performed a one-minute rolling average to the time-series of T_a.

The model output had been analyzed trough the UHI intensity parameter, which was defined as follows:

$$\Delta T_{OBS} = T_{OBS\,x} - T_{OBS\,D-1},$$

$$\Delta T_{WRF} = T_{WRF\,x} - T_{WRF\,D-1},$$

where ΔT_{OBS} is the observed UHI intensity, $T_{OBS\,x}$ is the observed T_a at a given monitoring site, $T_{OBS\,D\text{-}1}$ is the observed T_a at the D-1 reference rural station, ΔT_{WRF} is the modelled UHI intensity, $T_{WRF\,x}$ is the modeled T_a in the grid that located closest to the interested monitoring site, and $T_{WRF\,D\text{-}1}$ is the modeled T_a in the grid that located closest to theD-1 reference rural station. For the evaluation, we selected time periods when urban effects were observed to be very well pronounced ($\Delta T_{OBS\,MAX} > 4.5$ °C). Based upon the above criterion, four consecutive days between August 11 and August 14, 2015 was selected for the evaluation process of the two static datasets.

Once the standard model setup (WRF-MOD) was established, a series of background model integration was carried out for the whole period of the summer of 2015. On 48 days, the daily means of T_a ranged between 25–30 ºC, or even above 30 ºC on nine days in July and early August. Maxima were over 35 °C in 18 days in July and August. These heatwaves were characterized by high evening T_a and large

differences between urban and rural T_a. On the other hand, on 18 days daily means were under 20 ºC. Urban effect was completely missing or very weak during these periods. Otherwise, ΔT_{OBS} were in most cases (on 56 nights) over 5 °C.

4. Results and discussion

4.1. Evaluation of the default and adjusted static dataset

Both static databases had been verified against ΔT_{OBS} of UCMS during the 4-day heatwave period. *Fig. 5* represents the spatial distribution of ΔT_{WRF} on each day at 03 UTC and 23 UTC, when this variable, on average, was observed to be the most intense. It is concluded that ΔT_{MAX} with WRF-DEF was simulated to be 1–2 °C at 03 UTC and 2–3 °C at 23 UTC. Spatially, ΔT_{WRF} correlated well with the distribution of USGS LULC data, and so it was limited to a small part of the city, with highest magnitudes over the northeast.

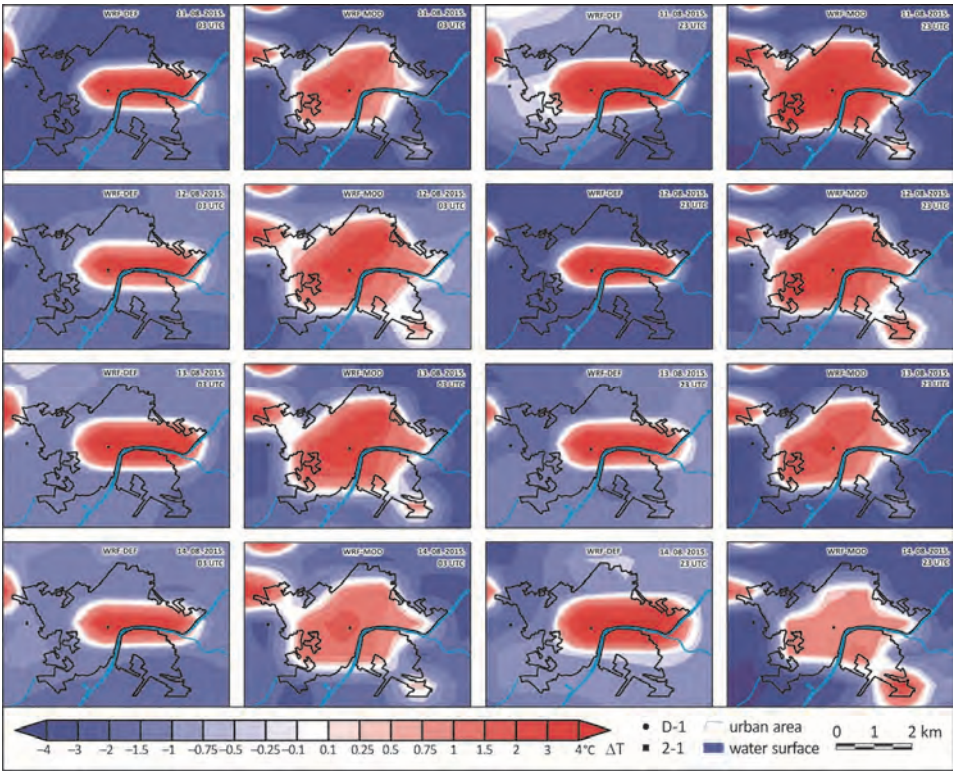

Fig. 5. Spatial distributions of ΔT_{WRF} with WRF-DEF (A) and WRF-MOD (B) over Szeged between August 11 and 14, 2015 at 03 UTC (left side) and 23 UTC (right side). The black dots indicate the location of the monitoring sites D-1 (rural) and 2–1 (urban).

ΔT_{WRF} with WRF-MOD extended towards the outer areas, with peaks ranged from 2.5 °C to 4.5 °C. The tendency in $\Delta T_{WRF\ MAX}$ between the two hours was not such straightforward in this case as previously: on the last two days, ΔT_{WRF} was generally stronger at 03 UTC than at 23 UTC, by around 0.5 °C. $\Delta T_{WRF\ MAX}$ was culminated along a southwest-northeast axis being reflected to the location of HIR classes (building fraction is 0.6). A more significant spatial variability of ΔT_{WRF}, induced by the updated database, stemmed from the distinction of two urban categories (and two sets of canopy parameters) instead of using only the 'urban built-up and land' class to typify the sophisticated urban geometry.

Another remarkable peak (around 3 °C) was predicted over the south-eastern periphery of Szeged, particularly around 03 UTC. This obvious overestimation of ΔT_{OBS} was the consequence of the horizontal resolution applied during the integration. Family houses and blocks of flats exist nearby, thus this area was classified to LIR. Those transition areas that lying near to the border of a given city are always difficult to threat on urban climate modeling, because they are characterized by urban and rural land cover features as well. Enhancing the horizontal resolution and introducing further LULC classes (e.g., LCZs) can be a potential way to avoid such inaccuracies.

The mean diurnal variation of ΔT_{OBS} and ΔT_{WRF} averaged according to LULC classes was illustrated in *Fig. 6*. The highest $\Delta T_{OBS\ MAX}$ occurred in HIR on August 12 (around 5.5 °C), while the lowest was in LIR on August 14 (around 4 °C). Overall, it was confirmed that the model, with WRF-MOD in particular, had the ability to estimate the daily fluctuation of ΔT_{OBS} and to distinguish the evolution of ΔT_{OBS} in different LULC. Regardless of the day of the simulation period, ΔT_{OBS} was approximated with lower accuracy in LIR, especially with WRF-DEF. On the other hand, biases with both parameter-sets decreased in HIR.

In the nighttime, ΔT_{OBS} was mostly underestimated by the simulations of all datasets. With WRF-DEF, ΔT_{WRF} remained around a constant value of 0.5–1 °C in LIR and showed only a moderate variability during the entire day. In HIR, the underestimation of ΔT_{OBS} with WRF-DEF clearly decreased, especially in a couple of hours after sunset. The introduction of the new dataset decreased the uncertainties of nocturnal ΔT_{WRF} with an order of 1–1.5 °C in LIR and 0.5 °C in LIR. In both urban categories, the underestimations simulated by WRF-MOD was shifted by an overestimation of 0.5–1 °C around sunset. The transition of nighttime to daytime ΔT_{OBS} around sunrise (04 UTC) was captured properly in LIR and HIR as well. However, a slight time lag and faster balance of urban and rural T_a (i.e., faster decrease of ΔT_{WRF} to 0 °C) existed.

The lower ΔT_{WRF} in the nighttime could be the result of higher T_{WRF} in the rural reference grid or lower T_{WRF} in urban grids. In the next subsection it will be seen, that WRF generally underestimated T_{OBS} over the urban area, thus ΔT was not being intensified by the simulation as by the observations. The substantial overestimations of ΔT_{OBS} in WRF-MOD after sunset might be the consequence of an excessive energy income by the release of the formerly stored heat from artificial materials.

In the daytime, ΔT_{WRF} with each of the two databases tended to be around 0 °C being in line with ΔT_{OBS} of -0.5–0 °C. Therefore, no significant difference was given between WRF-DEF and WRF-MOD in neither LULC class at that time of the days. Otherwise, the magnitude of ΔT_{WRF} was almost independent on the selection of the static parameters during the day.

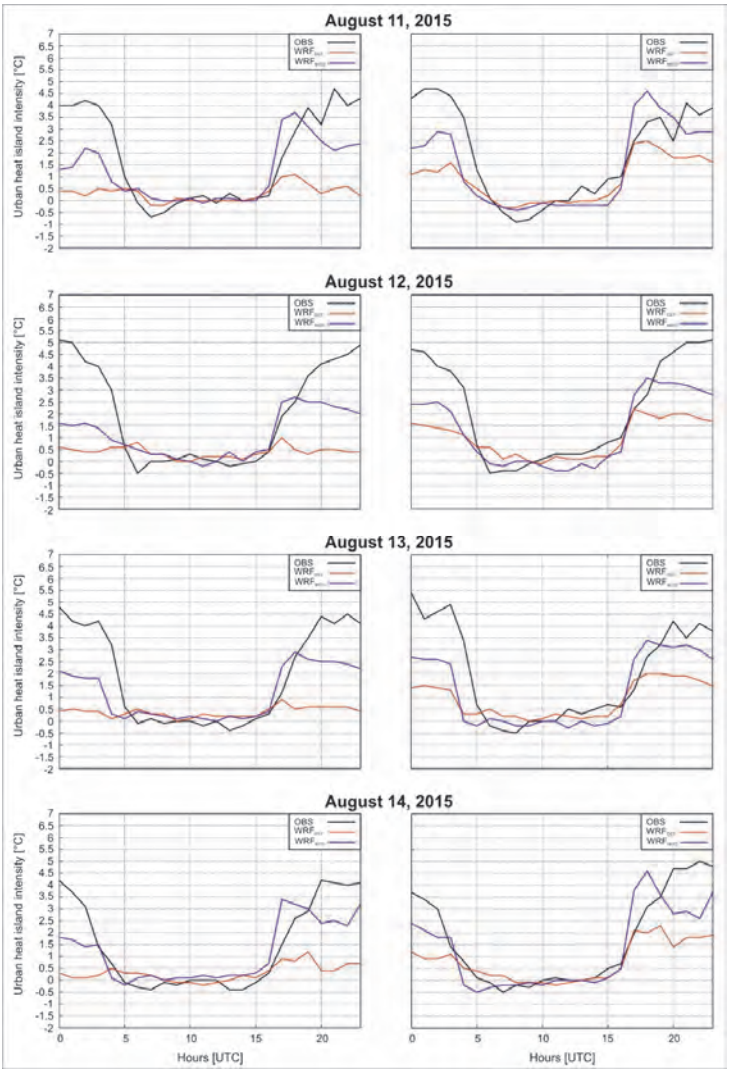

Fig. 6. Mean diurnal variations of ΔT_{OBS} and ΔT_{WRF} with WRF-DEF and WRF-MOD in LIR (diagrams on the left) and HIR (diagrams on the right) LULC categories.

To analyze the accuracy of ΔT_{WRF} with the different datasets on a statistic approach, the model outputs were compared with the observations through the daily means of bias, absolute error (AE), root mean squared error (RMSE), index of agreement (IOA), and spatial correlation coefficient (SCC) measures (*Table 4*). Additionally, with the independent two-sample t-test, we investigated whether or not WRF-MOD was significantly enhanced the quality of the simulations.

As it was pointed out earlier, a robust underestimation of ΔT_{OBS} occurred in each urban category. The biases (ΔT_{WRF}-ΔT_{OBS}) ranged from –1.60 °C to –0.26 °C. The outputs of WRF decreased the corresponding errors, with around 0.8°C in LIR and 0.4 °C in HIR. AEs of ΔT_{WRF} with WRF-MOD stayed below 1.18 °C, with the best performance on August 14 (around 0.75 °C). Even though WRF with each dataset performed similarly over the four days, some uncertainties still emerged on August 12 because of the less accurate initial field of GFS. In the future, it would be important to determine a threshold below which the erroneous data should be filtered out. *Emery et al.* (2001 employed a desired model accuracy of 0.8–1.0 for IOA. While WRF-DEF did not manage to exceed that limit, WRF-MOD, except on August 12 and 13 in LIR, fulfilled the expectations.

We performed the independent two-sample t-test at a confidence level of 0.95 and 0.99. The results suggested that ΔT_{WRF} with WRF-MOD was estimated significantly better either in LIR or in HIR LULC categories, at a confidence of 95%. By increasing the confidence to 99%, the significance still persisted in LIR but not in HIR. Indeed, in HIR only a mean difference of 0.4 °C in ΔT_{WRF} existed between the two datasets. In other words, the selection of the default static data does not generate larger uncertainties in a little part of the city (four HIR grids at 2 km horizontal resolution) under such conditions, although in the vast majority of the grids, the introduction of new parameters can contribute to a more efficient simulation of ΔT.

Table 4. Daily means of statistics of ΔT_{OBS} and ΔT_{WRF} (averaged for each day) with WRF-DEF and WRF-MOD in LIR and HIR LULC categories

Statistics/Date	**August 11, 2015**		**August 12, 2015**		**August 13, 2015**		**August 14, 2015**	
LIR	**WRF_{DEF}**	**WRF_{MOD}**	**WRF_{DEF}**	**WRF_{MOD}**	**WRF_{DEF}**	**WRF_{MOD}**	**WRF_{DEF}**	**WRF_{MOD}**
Bias [°C]	-1.55	-0.65	-1.60	-0.88	-1.50	-0.73	-1.15	-0.26
AE [°C]	1.70	1.07	1.85	1.18	1.77	1.06	1.40	0.80
RMSE [°C]	2.34	1.40	2.55	1.66	2.42	1.43	2.01	1.08
IOA	0.55	0.80	0.50	0.73	0.51	0.71	0.52	0.86
SCC	0.57	0.77	0.35	0.80	0.48	0.85	0.52	0.83
HIR								
Bias [°C]	-1.07	-0.52	-1.18	-0.83	-1.08	-0.71	-0.90	-0.40
AE [°C]	1.22	1.00	1.38	1.03	1.33	0.96	1.05	0.76
RMSE [°C]	1.68	1.22	1.86	1.26	1.82	1.31	1.56	1.04
IOA	0.72	0.88	0.68	0.88	0.65	0.86	0.71	0.91
SCC	0.82	0.83	0.88	0.92	0.78	0.83	0.86	0.87

4.2. Analysis of the model performance with WRF-MOD

Through the detailed analysis of the measured data at all urban and rural locations (not shown here), it was found that the typical time variation of T_a at the 2–1 station represents the urban thermal conditions properly: compared to other time-series, this site was among the warmest ones at nights. Additionally, the station D-1 was still considered as rural station during the analysis. In this sub-section, we examined ΔT_{OBS} and Δ_{TWRF} based solely on T_{OBS} and T_{WRF} at these two stations. The simulations were executed with the WRF-MOD configuration under a longer, 91-day period from June 1 to August 31, 2015. In order to validate the model results, we compared the mean and extreme values of $T_{OBS\ 2\text{-}1}$, $T_{OBS\ D\text{-}1}$, and ΔT_{OBS} to the corresponding $T_{WRF\ 2\text{-}1}$, $T_{WRF\ D\text{-}1}$, and ΔT_{WRF}.

It can be seen in *Fig 7* that the daily averages of T_{OBS}, on average, were underestimated (overestimated) at the urban (rural) site by about 1.5 °C. Same can be stated for the $T_{OBS\ MAX}$ with slightly higher biases (around 2 °C). For $T_{OBS\ MIN}$, a negative bias evolved at station 2–1 and a slight positive bias at station D-1. It must be noted that the underestimation of nocturnal T_{OBS} over urban grids were also reported, for example, in the study of *Bhati* and *Mohan* (2015) and *Kim et al.* (2013).

The daily $\Delta T_{OBS\ MAX}$ was systematically underestimated on most of the days. $\Delta T_{WRF\ MAX}$ was higher than $\Delta T_{OBS\ MAX}$ only in five cases. Negative biases in ΔT_{WRF} were even higher during the nights with a minimum of $T_{OBS\ 2\text{-}1} > 20$ °C (warm nights in climate definition). It must be emphasized again that even if the magnitude of the $\Delta T_{WRF\ MAX}$ had a systematic negative bias compared to the observations, the temporal variation was captured reasonably well.

If we concentrate on those days when both $\Delta T_{OBS\ MAX}$ and $\Delta T_{WRF\ MAX}$ (i.e., for example, around August 20) are low (i.e., less than 2.5 °C), it can be discovered that the minima of $T_{2\text{-}1}$ and $T_{D\text{-}1}$ was modeled with lower biases. On the other hand, large underestimations occurred in $T_{OBS\ MAX}$ at each station. At this time of the simulation period, a cut-off low pressure system dominated the Carpathian Basin causing a high degree of instability. This synoptic situation favored for daytime convective precipitation, which was not forecasted adequately by the model. Therefore, we intend to perform a data assimilation using the UCMS measurements and local radio sounding data of the Hungarian Meteorological Service. This time-consuming technique has been proven to be an efficient tool to predict most of the urban climate indicators (*Liu et al.*, 2006 *Tan et al.*, 2015).

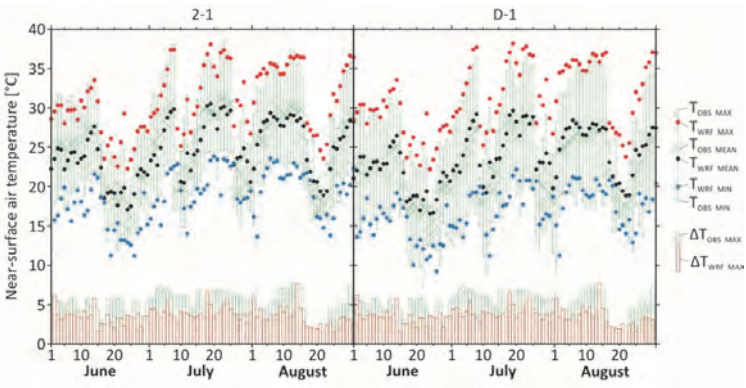

Fig. 7. Maxima, means, and minima of ΔT_{OBS} and ΔT_{WRF} at a representative urban (station 2-1) and rural (station D-1) site of UCMS during the summer of 2015.

5. Conclusions and further plans

Using detailed city-specific built-up information and remote sensing data of Landsat 8 and RapidEye satellites, an adjusted static database (in terms of land use and urban canopy parameters; UCPs) had been created in order to better represent the physical characteristics of the urban forms in Szeged related to the default WRF dataset (WRF-DEF). In contrast with WRF-DEF, the modified land use dataset (WRF-MOD) consists of 76% more urban grids in the study area and employs two urban classes instead of only one at a model horizontal resolution of 2 km. After the calculation of canopy parameters, it was revealed that the urban canyons have become narrower, i.e., the parameters of building height, roof, and road width decreased related to WRF-DEF. Additionally, the building fraction also decreased from 90% (50%) to 60% (40%) in HIR (LIR). In turn, the vegetation fraction increased in both categories.

Following a predefined criterion ($\Delta T_{OBS\ MAX} > 4.5$ °C), four days were selected to evaluate WRF with the above databases in simulating T_a. The model with WRF-MOD was able to capture the spatiotemporal variation of ΔT_{OBS} properly. On the other hand, the simulations with WRF-DEF contained large uncertainties. ΔT_{WRF} with WRF-DEF restricted only to the downtown of Szeged, with maxima of around 2–3 °C. In WRF-MOD, ΔT_{WRF} covered a much wider area of Szeged, with maxima (of around 4–4.5 °C) along a southwest-northeast axis located over the HIR LULC category. Some overestimations occurred near to the borders of the city, where a gradual transition of urban to rural surface is typical, that is really difficult to handle at such model resolution.

According to the observations of the local urban climate monitoring system, the highest ΔT_{OBS} formed in HIR in a couple hours after sunset (18 UTC), with values of up to 5–5.5 °C. The nocturnal ΔT_{OBS} was systematically underestimated, particularly in LIR. The biases decreased in HIR with the simulations of both static datasets. With WRF-MOD, slight overestimations occurred around sunset caused by the inaccurate timing of the nighttime heat release from artificial surface elements. ΔT_{WRF} with WRF-DEF remained almost identical (0.5–1 °C) in LIR during the entire day. In the daytime, only a weak (0.5 °C) or even a negative (cool) (heat) island formed. Then ΔT_{WRF} with either WRF-DEF or WRF-MOD was in line with the measurements in LIR and HIR as well.

Statistic scores of AE less than 1.18 °C with WRF-MOD indicated a good overall performance on ΔT_{OBS} estimation. Moreover, the desired model accuracy of ΔT (IOA between 0.8 and 1.0) was mostly overachieved with ΔT_{WRF} of WRF-MOD, except on August 12 and 13, in LIR. On the other hand, IOAs of WRF-DEF stayed always below 0.8. An independent two-sample t-test at a confidence level of 0.95 and 0.99 was performed to decide how much the introduction of the modified static database contributed to a better estimation of ΔT_{OBS} during the 4-day heatwave event. It was concluded that ΔT with WRF-MOD was modeled significantly better (at both 95% and 99% confidence) in LIR than with WRF-DEF. In HIR, however, the significance was only valid at 95% confidence.

We analyzed the extreme values of T_{OBS}, T_{WRF}, $\Delta T_{OBS\,MAX}$, and $\Delta T_{WRF\,MAX}$ based upon the observations and simulations (solely with WRF-MOD) of an urban (station 2–1) and rural (station D-1) site during the whole summer of 2015. $T_{OBS\,MAX}$ was underestimated (overestimated) by about 2 °C at the urban (rural) site. Similar tendencies were drawn out for $T_{OBS\,MIN}$ at both sites, with lower warm biases (around 1.5 °C), however, at station D-1. During this longer simulation period, $\Delta T_{OBS\,MAX}$ was still underestimated (86 of 91 nights). If we considered those days when $T_{OBS\,2\text{-}1} >$ 20 °C, the biases of $\Delta T_{OBS\,MAX}$ increased further on. Nonetheless, as we have seen earlier, the biases were generally within the acceptance limit, which implied an adequate quality of the simulations with WRF-MOD.

In order to improve our results and take the three-dimensionality of urban canopy into consideration even more accurately, we intend to test other urban parameterizations of WRF (i.e., BEM and BEP), with different parametrization schemes (for example, changing radiation, PBL, or LSM schemes) and domain setups (e.g., higher resolution). Inclusion of anthropogenic heat in the calculation and definition of further urban categories based on the LCZs may also contribute to better simulations. Furthermore, based on the high amount of measurements yielded by the unique urban temperature measurement network, we plan to assimilate the measured temperature data using three-dimensional variational technique.

Acknowledgements: This work was granted by the Hungarian Scientific Research Fund (OTKA K-111768). The third author was supported by the ÚNKP-18-4 New National Excellence Program of the Ministry of Human Capacities.

References

Best, M.J., Grimmond, C.S.B., and *Villani, M.G.,* 2006: Evaluation of the urban tile in MOSES using surface energy balance observations. *Bound.-Layer Meteorol. 118*, 503–525. http://dx.doi.org/10.1007/s10546-005-9025-5

Bhati, S. and *Mohan, M.,* 2015: WRF model evaluation for the urban heat island assessment under varying land use/land cover and reference site conditions. *Theor. Appl. Climatol. 126*, 385–400. http://dx.doi.org/10.1007/s00704-015-1589-5

Bougeault, P. and *Lacarrere, P.,* 1989: Parameterization of Orography–Induced Turbulence in a Mesobeta—Scale Model. *Mon. Weather Rev. 117,* 1872–1890. http://dx.doi.org/10.1175/1520-0493(1989)117%3C1872:POOITI%3E2.0.CO;2

Bossard, M., Feranec, J., and *Otahel, J.,* 2000: CORINE land cover technical guide. Addendum 2000. Technical Report No. 40. Copenhagen: European Environmental Agency.

Brousse, O., Martilli, A., Foley, M., Mills, G., and *Bechtel, B.,* 2016: WUDAPT, an efficient land use producing tool for mesoscale models? Integration of urban LCZ WRF over Madrid. *Urb. Clim. 17,* 116–134. http://dx.doi.org/10.1016/j.uclim.2016.04.001

Chen, F., Yang, X., and *Zhu, W.,* 2014: WRF simulations of urban heat island under hot-weather synoptic conditions: The case study of Hangzhou City, China. *Atmos. Res. 138*, 364–377. http://dx.doi.org/10.1016/j.atmosres.2013.12.005

Crutzen, P.J., 2004: New directions: The growing urban heat and pollution "island" effect-impact on chemistry and climate. *Atmos. Environ. 38*, 3539–3540. http://dx.doi.org/10.1016/j.atmosenv.2004.03.032

Emery, C., Tai E., and *Yardwood, G.,* 2001: Enhanced meteorological modeling and performance evaluation for two Texas ozone episodes. Environ. International Corporation.

Gál, T., Skarbit, N., and *Unger, J.,* 2016: Urban heat island patterns and their dynamics based on an urban climate measurement network. *Hun. Geo. Bull. 65*, 105–116. http://dx.doi.org/10.15201/hungeobull.65.2.2

Giannaros, T.M., Melas, D., Daglis, I.A., Keramitsoglou, I., and *Kourtidis, K.,* 2013: Numerical study of the urban heat island over Athens (Greece) with the WRF model. *Atmos. Environ. 73,* 103–111. http://dx.doi.org/10.1016/j.atmosenv.2013.02.055

Hidalgo, J., Masson, V., Baklanov, A., and *Gimeno, L.,* 2008: Advances in urban climate modeling. *Ann. NY. Acad. Sci. 1146*, 354–374. http://dx.doi.org/10.1196/annals.1446.015

Homer, C., Huang, C., Yang, L., Wylie, B., and *Coan, M.,* 2004: Development of a 2001 national land cover database for the United States. *Photogram. Eng. Rem. S. 70*, 829–840. http://dx.doi.org/10.14358/PERS.70.7.829

Hong, S.Y., Dudhia, J., and *0Chen, S.H.,* 2004: A revised approach to ice microphysical processes for the bulk parameterization of clouds and precipitation. *Mon. Weather Rev. 132*, 103–120. http://dx.doi.org/10.1175/1520-0493(2004)132%3C0103:ARATIM%3E2.0.CO;2

Iacono, M.J., Delamere, J.S., Mlawer, E.J., Shephard, M.W., Clough, S.A., and *Collins, W.D.,* 2008: Radiative forcing by long- lived greenhouse gases: Calculations with the AER radiative transfer models. *J. Geophys. Res. 113*, D13103. http://dx.doi.org/10.1029/2008JD009944

IPCC, 2013: Climate Change 2013: The Physical Science Basis. Contribution of Working Group I to the Fifth Assessment Report of the Intergovernmental Panel on Climate Change (eds. *Stocker, T.F., Qin, D., Plattner, G.K., Tignor, M., Allen, S.K., Boschung, J., Nauels, A., Xia, Y., Bex, V., Midgley, P.M.*) Cambridge University Press, Cambridge, United Kingdom and New York, NY, USA.

Jimenez, P.A., Dudhia, J., Gonzalez–Rouco, J.F., Navarro, J., Montavez, J.P., and *Garcia–Bustamante, E.,* 2012: A revised scheme for the WRF surface layer formulation. *Mon. Weather Rev. 140,* 898–918. http://dx.doi.org/10.1175/MWR-D-11-00056.1

Kain, J.S., 2004: The Kain–Fritsch convective parameterization: An update. *J. Appl. Meteor. 43,* 170–181. http://dx.doi.org/10.1175/1520-0450(2004)043%3C0170:TKCPAU%3E2.0.CO;2

Kim, Y., Sartelet, K., Raut, J.C., and *Chazette, P.,* 2013: Evaluation of the Weather Research and Forecasting/Urban Model Over Greater Paris. *Bound.-Layer Meteorol. 149*, 105–132. http://dx.doi.org/10.1007/s10546-013-9838-6

Kolokotroni, M., Ren, X., Davies, M., and *Mavrogianni, A.,* 2015: London's urban heat island: Impact on current and future energy consumption in office buildings. *Energ. Buildings 47*, 302–311. http://dx.doi.org/10.1016/j.enbuild.2011.12.019

Kottek, M., Grieser, J., Beck, C., Rudolf, B., and *Rubel, F.,* 2006: World map of the Köppen-Geiger climate classification update. *Meteorol. Z. 15*, 259–263.

Kusaka, H., Kondo, H., Kikegawa, Y., and *Kimura, F.,* 2001: A simple single-layer urban canopy model for atmospheric models: Comparison with multi-layer and slab models. *Bound.-Layer Meteorol. 101*, 329–358. http://dx.doi.org/10.1023/A:1019207923078

Kusaka, H. and *Kimura, F.,* 2004: Coupling a Single-Layer Urban Canopy Model with a Simple Atmospheric Model: Impact on Urban Heat Island Simulation for an Idealized Case. *J. Meteorol. Soc. Jpn. 82*, 67–80. http://dx.doi.org/10.2151/jmsj.82.67

Lelovics, E., Unger, J., Gál, T., and *Gál, C.V.,* 2014: Design of an urban monitoring network based on Local Climate Zone mapping and temperature pattern modelling. *Clim. Res. 60*, 51–62. http://dx.doi.org/10.3354/cr01220

Li, D. and *Bou-Zeid, E.,* 2013: Synergistic interactions between urban heat islands and heat waves: The impact in cities is larger than the sum of its parts. *J. Appl. Meteorol. Clim. 52*, 2051–2064. http://dx.doi.org/10.1175/JAMC-D-13-02.1

Liu, Y., Chen, F., Warner, T., and *Basara, J.,* 2006: Verification of a Mesoscale Data-Assimilation and Forecasting System for the Oklahoma City Area during the Joint Urban 2003 Field Project. *J. Appl. Meteor. Climatol. 45*, 912–929. http://dx.doi.org/10.1175/JAM2383.1

Martilli, A., Clappier, A., and *Rotach, M.W.,* 2002: An urban surface exchange parameterisation for mesoscale models. *Bound.-Layer Meteorol. 104*, 261–304. http://dx.doi.org/10.1023/A:1016099921195

Masson, V., 2000: A Physically-Based Scheme For The Urban Energy Budget In Atmospheric Models. *Bound.-Layer Meteorol. 94*, 357–397. http://dx.doi.org/10.1023/A:1002463829265

Miao, S., Chen, F., LeMone, M.A., Tewari, M., Li, Q., and *Wang, Y.,* 2009: An observational and modeling study of characteristics of urban heat island and boundary layer structures in Beijing. *J. Appl. Meteor. Climatol. 48*, 484–501. http://dx.doi.org/10.1175/2008JAMC1909.1

Miao, S., Chen, F., Li, Q., and *Fan, S.,* 2011: Impacts of urban processes and urbanization on summer precipitation: A case study of heavy rainfall in Beijing on 1 August 2006. *J. Appl. Meteorol. Climatol. 50*, 806–825. http://dx.doi.org/10.1175/2010JAMC2513.1

Mills, G., Bechtel, B., Ching, J., See, L., Feddema, J., Foley, M., Alexander, P., and *O'Connor, M.,* 2015: An introduction to the WUDAPT project. Proceedings of the ICUC9. Meteo France, Toulouse, France.

Mirzaei, P.A., 2015: Recent challenges in modeling of urban environment. *Sust. Cit. Soc. 19*, 200–206. https://doi.org/10.1016/j.scs.2015.04.001

Nakamura, Y. and *Oke, T.R.,* 1988: Wind, temperature and stability conditions in an east-west oriented urban canyon. *Atmos. Environ. 22,* 2691–2700. http://dx.doi.org/10.1016/0004-6981(88)90437-4

Oke, T.R., 1973: City size and the urban heat island. *Atmos. Environ. 7,* 769–779. http://dx.doi.org/10.1016/0004-6981(73)90140-6

Oke, T.R., 1982: The energetic basis of urban heat island. *Q. J. Roy. Meteor. Soc. 108*, 1–24. http://dx.doi.org/10.1002/qj.49710845502

Oleson, K.W., Bonan, G.B., Feddema, J., Vertenstein, M., and *Grimmond, C.S.B.,* 2008: An urban parameterization for a global climate model. Part 1: Formulation and evaluation for two cities. *J. Appl. Meteor. Climat. 47*, 1038–1060. http://dx.doi.org/10.1175/2007JAMC1597.1

Pathirana, A., Denekew, H.B., Veerbeek, W., Zevenbergen, C., and *Banda, A.T.,* 2014: Impact of urban growth-driven landuse change on microclimate and extreme precipitation – A sensitivity study. *Atmos. Res. 138*, 59–72. http://dx.doi.org/10.1016/j.atmosres.2013.10.005

Pásztor, L., Szabó, J., Bakacsi, Zs., Matus, J., and *Laborczi, A.,* 2012: Compilation of 1:50,000 scale digital soil maps for Hungary based on the digital Kreybig soil information system. *J. Maps 8,* 215–219. https://doi.org/10.1080/17445647.2012.705517

Salamanca, F., Krpo, A., Martilli, A., and *Clappier, A.,* 2010: A new building energy model coupled with an urban canopy parameterization for urban climate simulations–part I. formulation, verification, and sensitivity analysis of the model. *Theor. Appl. Climatol. 99,* 331–344. http://dx.doi.org/10.1007/s00704-009-0142-9

Salamanca, F. and *Martilli, A.,* 2010: A new building energy model coupled with an urban canopy parameterization for urban climate simulations–part II. Validation with one dimension offline simulations. *Theor. Appl. Climatol. 99*, 345–356. http://dx.doi.org/10.1007/s00704-009-0143-8

Salamanca, F., Martilli, A., and *Yagüe, C.,* 2012: A numerical study of the Urban Heat Island over Madrid during the DESIREX (2008) campaign with WRF and an evaluation of simple mitigation strategies. *Int. J. Climatol. 32*, 2372–2386. http://dx.doi.org/10.1002/joc.3398

Sarkar, A. and *De Ridder, K.,* 2011: The urban heat island intensity of Paris: A case study based on a simple urban surface parametrization. *Bound. Lay. Meteorol. 138*, 511–520. http://dx.doi.org/10.1007/s10546-010-9568-y

Skamarock, W.C., Klemp, J.B., Dudhia, J., Gill, D.O., Barker, D.M., Duda, M.G., Huang, X.Y., Wang, W., and *Powers, J.G.,* 2008: A Description of the Advanced Research WRF Version 3. *NCAR Tech. Note NCAR/TN-475+STR,* 113 p. http://dx.doi.org/10.5065/D68S4MVH.

Sobrino, J.A., Jimenez-Munoz, J.C., and *Paolini, L.,* 2004: Land surface retrieval from Landsat 5 TM. *Rem. S. Environ. 90*, 434–440. https://doi.org/10.1016/j.rse.2004.02.003

Stewart, I.D. and *Oke, T.R.,* 2012: Local Climate Zones for urban temperature studies. *Bull. Amer. Meteor. Soc. 93*, 1879−1900. http://dx.doi.org/10.1175/BAMS-D-11-00019.1

Streutker, D.R., 2003: Satellite-measured growth of the urban heat island of Houston. Texas. *Rem. Sens. Environ. 85,* 282–289. http://dx.doi.org/10.1016/S0034-4257(03)00007-5

Tan, J., Yang, L., Grimmond, C.S., Shi, J., Gu, W., Chang, Y., Hu, P., Sun, J., Ao, X., and *Han, Z.,* 2015: Urban Integrated Meteorological Observations: Practice and Experience in Shanghai, China. *Bull. Amer. Meteor. Soc. 96*, 85–102. https://doi.org/10.1175/BAMS-D-13-00216.1

Tewari, M., Chen, F., Wang, W., Dudhia, J., LeMone, M.A., Mitchell, K., Ek, M., Gayno, G., Wegiel, J., and *Cuenca, R.H.,* 2004: Implementation and verification of the unified NOAH land surface model in the WRF model. 20th conference on weather analysis and forecasting/16th conference on numerical weather prediction, 11–15.

Unger, J., Sümeghy, Z., Gulyás, Á., Bottyán, Zs., and *Mucsi, L.,* 2001: Land-use and meteorological aspects of the urban heat island. *Meteorol. Appl. 8*, 189–194. http://dx.doi.org/10.1017/S1350482701002067

Unger, J., Gál, T., Csépe, Z., Lelovics, E., and *Gulyás, Á.,* 2015: Development, data processing and preliminary results of an urban human comfort monitoring and information system. *Időjárás 119*, 337–354.

United Nations, 2014: World Urbanization Prospects: The 2014 Revision. Department of Economic and Social Affairs, Population Division, 32 p.

URBAN-PATH Project, 2014: Evaluations and public display of urban patterns of human thermal conditions. http://urban-path.hu/

Wang, M., Yan, X., Liu, J., and *Zhang, X.,* 2013: The contribution of urbanization to recent extreme heat events and potential mitigation strategy in the Beijing–Tianjin–Hebei metropolitan area. *Theor. Appl. Climatol. 114*, 407–416. http://dx.doi.org/10.1007/s00704-013-0852-x

Zhong, S. and *Yang, X.Q.,* 2015: Ensemble simulations of the urban effect on a summer rainfall event in the Great Beijing Metropolitan Area. *Atmos. Res. 153*, 318–334. http://dx.doi.org/10.1016/j.atmosres.2014.09.005

DOI:10.28974/idojaras.2019.3.8

IDŐJÁRÁS

Quarterly Journal of the Hungarian Meteorological Service
Vol. 123, No. 3, July – September, 2019, pp. 391–408

Anomalies in the length of the growing season in Poland in the period 1966–2015

Katarzyna Szyga-Pluta* and **Arkadiusz M. Tomczyk**

Department of Climatology
Institute of Physical Geography and Environmental Planning
Adam Mickiewicz University in Poznań
Krygowskiego 10, 61-680 Poznań, Poland

**Corresponding author E-mail: pluta@amu.edu.pl*

(Manuscript received in final form July 17, 2018)

Abstract—The purpose of the study was to determine the anomalous length of growing seasons, the frequency of their occurrence, and to determine the temporal and spatial changes of their frequency in Poland in the period 1966–2015. The analyses used daily average air temperature values for 30 stations located in Poland from years 1966–2015 (*Fig. 1*). The data was provided by the Institute of Meteorology and Water Management - National Research Institute. The growing season was defined as the period with average daily air temperature ≥5 °C. The start and end dates of the growing season were determined using the mathematical formulas proposed by *R. Gumiński* (1948). In the period 1966–2015 in Poland, anomalously short growing seasons occurred sporadically and covered the largest area of Poland in 1997. Short growing seasons were more frequent in the first three decades of the analyzed multi-year period, and long growing seasons were characterized by higher frequency in the second half of the surveyed period. Anomalously long growing seasons before 1990 occurred sporadically and only in individual stations. Anomalously short growing seasons occurred only in the middle eastern part of Poland, while anomalously long ones covered most of the country.

Key words: growing season, typical and anomalous length, climate change, Poland

1. Introduction

In the Northern Hemisphere, the 1983–2012 period was probably the warmest 30-year-long period in the last 1400 years (*IPCC,* 2013). In most surface temperature data sets, the years 2014, 2015, and again 2016 set new global heat records since the start of regular measurements (*Rahmstorf at al.* 2017). According to the NOAA (2018), in the period 1880–2017, 9 out of 10 warmest years are those after 2000, and the warmest year was 2016. The forecast increase in the growing season length is a consequence of the increase in the average global air temperature observed in recent years. *Nieróbca et al.,* (2013) indicated that in the perspective of 2030, the growing season in central Poland may increase by 10–14 days in comparison to the reference period of 1971–2000, and in the perspective of 2050 by 18–27 days, while in south-western Poland, respectively, by 11–17 days and 22–30 days. Also in the long term, a longer growing season in Poland can be expected, which will be a consequence of the increasing air temperature, even by 3.8 °C in 2071–2100 (*Piniewski et al.,* 2017). A similar trend is forecasted by *Skaugen* and *Tveito* (2004) for Norway in the perspective of 2050. This affects the modification of phenological phases of individual plants (*Menzel* and *Fabian,* 1999; *Chmielewski* and *Rötzer,* 2001; *Chmielewski et al.,* 2004).

Changes in thermal conditions may also have adverse effects on agriculture (*Nieróbca,* 2009), causing a decrease in the productivity of some crops, the development of thermophilic weeds, pests, or the emergence of new plant diseases. Changes in the start and end dates as well as the length of the growing season, in addition to the consequences for ecosystems, may lead to long-term changes in the carbon dioxide cycle, and changes in vegetation will affect the climate system (*Linderholm*, 2006). Changes of different meteorological elements in recent decades have exceeded the limits of the typical cyclical nature of weather conditions, manifested by the intensification of extreme phenomena (*Miętus,* 2005; *Christidis et al.,* 2007; *Tomczyk* and *Bednorz*, 2016; *Czernecki* and *Miętus,* 2017; *Wibig*, 2018).

The subject of the research was the anomalous growing seasons in Poland. The purpose of the study was to determine the anomalous length of growing seasons, the frequency of their occurrence, and to determine the temporal and spatial changes of their frequency in Poland in 1966–2015.

2. Data and methods

The analyses used daily average air temperature values for 30 stations located in Poland, excluding the mountain regions, from years 1966–2015 (*Fig. 1*). The data was provided by the Institute of Meteorology and Water Management - National Research Institute.

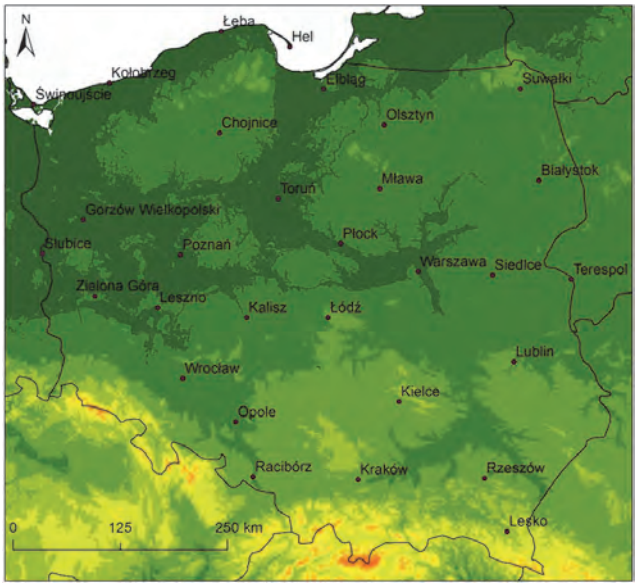

Fig. 1. Locations of meteorological stations.

First, the start and end dates of the growing season were determined, and the season itself was defined as the period with average daily air temperature ≥5 °C. The above definition was previously accepted in numerous studies (*Carter*, 1998; *Skaugen* and *Tveito*, 2004; *Linderholm*, *et al.,* 2008; *Żmudzka,* 2012; *Radzka*, 2013). The start and end dates of the aforementioned period were determined using the mathematical formulas proposed by *Gumiński* (1948).

This method is based on the following assumptions: the monthly average temperature falls on the 15th day of a month, each month has 30 days, and monthly temperature changes are evenly distributed. The formulas used:

$$x = 30\ [(td\text{-}t1)/(t2\text{-}t1)],$$
$$x = 30\ [(t1\text{-}td)/(t1\text{-}t2)], \quad (1)$$

where *td* is the threshold temperature of the growing season (5 °C); *t1* is the average temperature in the month preceding the threshold temperature; *t2* is the average temperature in the month following the threshold temperature; *x* is the number of days between the day with the threshold temperature and the 15th day of the preceding month.

The number of days calculated on the basis of the aforesaid formulas is added to the 15th day of the month preceding the threshold temperature. If the

sought number is greater than 15, when adding, one should consider the actual number of days in a given month. The obtained date is the beginning of the separated period in time of the temperature increase and the end of the separated period in time of the decreasing temperature. The above-mentioned method is widely adopted in determining the growing and thermal seasons for both the multi-year period and individual years (*Skowera* and *Kopeć*, 2008; *Szyga-Pluta*, 2011; *Kępińska-Kasprzak* and *Mager*, 2015; *Czernecki* and *Miętus* 2017; *Tomczyk* and *Szyga-Pluta*, 2019). *Kępińska-Kasprzak* and *Mager* (2015) compared the thermal vegetation period determined by the method of Gumiński with those determined by the method of Huculak and Makowiec (the latter consists in calculating the accumulated series of deviations of average daily air temperature values from appropriate threshold values) for the period 1966–2005, and stated that in long-term datasets, both methods lead to similar results. The comparison of the results based on the phenological observations, and these obtained with the Gumiński method proved the compatibility of them (*Siłuch et al.,* 2016).

Subsequently, changes in the beginning and end as well as the length of the growing season in the analyzed multi-year period were determined. To this end, the non-parametric Mann-Kendall test was used to detect the trend in the time series. The strength of the trends of characteristics in the multi-year period was determined by Sen's non-parametric method (*Salmi et al.,* 2002).

In the next stage, the classification of the determined growing seasons was made based on the value of the standard deviation. On this basis, the following classes were established (*Węgrzyn*, 2008):

A - anomalously short: $GSL \leq GSL_{AV} - 2\delta$;

B - short: $GSL_{AV} - 2\delta < GSL \leq GSL_{AV} - 1\delta$;

C - normal (average): $GSL_{AV} - 1\delta < GSL < GSL_{AV} + 1\delta$;

D - long: $GSL_{AV} + 1\delta \leq GSL < GSL_{AV} + 2\delta$;

E - anomalously long: $GSL \geq GSL_{AV} + 2\delta$,

where GSL is the growing season length, GSL_{AV} is the average growing season length, δ is the standard deviation.

The above classification was carried out for each station individually. Next, the frequency of occurrence of growing seasons in individual classes was determined.

3. Results

In the years 1966–2015 in Poland, the growing season started the earliest in the western and south-western regions, and the latest in the north-eastern regions. The average date of the beginning of the growing season was March 26, and it

changed from March 18 in Słubice to April 7 in Suwałki (*Fig. 2A*). In most stations, the earliest beginning of the period occurred in 1990, while the latest in 1997, 1970, and 1980. Extreme dates of the beginning of the growing season fluctuated from January 29 (1990) in Słubice to May 5 (1970) in Kołobrzeg. The aforementioned data shows that the range of the variability of the beginning of the growing season was 97 days in the study area.

The growing season ended the earliest in the north-eastern regions and the latest in the northern and western regions. On average, the end of the period was recorded on November 7, although this date changed from October 25 in Suwałki to November 16 in Hel and Łeba (*Fig. 2B*). In the majority of stations, the earliest end of the growing season was recorded in 1993, 1973, and 1998, while the latest in 2015, 2000, and 2006. Extreme dates of the end of the growing season ranged from October 8 (1977) in Terespol to January 19 (2007) in Słubice. It follows that the range of the variability in the ending time of the growing season was 104 days in the study area.

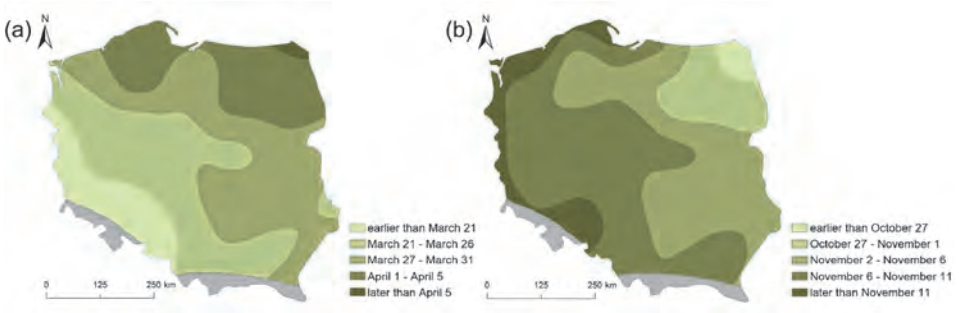

Fig. 2. Average growing season start date (A), end date (B) in Poland in the years 1966–2015.

In the analyzed multi-year period, the growing season started increasingly early. The strongest and statistically significant changes were recorded in northern and north-eastern Poland. In Łeba and Kołobrzeg, the rate of these changes was –4.2 days/10 years and –4.1 days/10 years, respectively (*Figs. 3A* and *4*). On the other hand, the end of the growing season was increasingly late. Statistically significant changes were found on the east coast, in central and southern Poland, and the most intensive changes occurred in Hel (2.6 days/10 years) and Wrocław (2.5 days/10 years) (*Figs. 3B* and *4*).

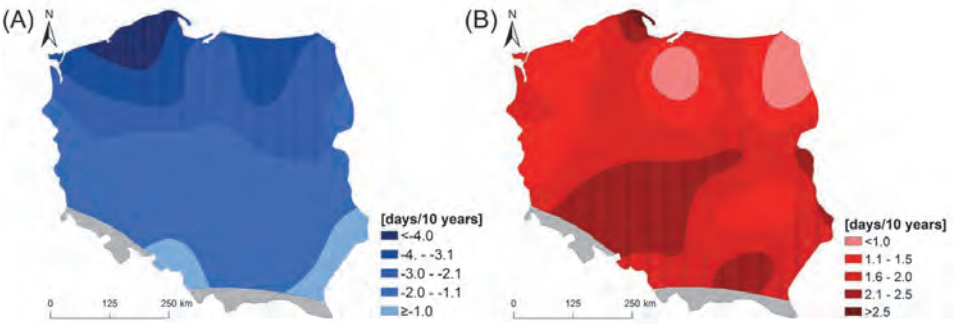

Fig. 3. Changes in the beginning (A) and end (B) dates of the growing season in Poland in years 1966-2015 (vertical lines indicate statistically significant changes).

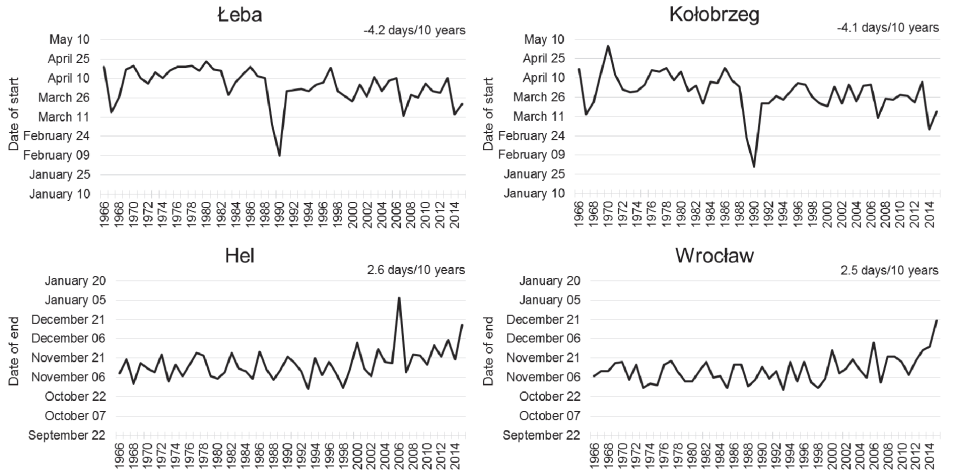

Fig. 4. Changes in the beginning and end dates of the growing season in selected stations in the years 1966–2015.

The average length of the growing season was 227 days in Poland. The increase in the growing season length took place from the northeast to the southwest. In Suwałki, the average length of the period was 202 days, while in Słubice, 242 days (*Fig. 5A*). The variability of length in the majority of the

country was similar, as evidenced by the values of standard deviation, which, apart from seaside stations, fluctuated at a similar level, 13–15 days. In the considered multi-year period, the shortest growing season lasted 179 days in 1992 (Suwałki), while the longest lasted 297 days in 2006 (Słubice). The conducted research showed an increase in the length of the growing season, which was statistically significant, except for two stations in the southern part of the country (*Fig. 5B*). The largest increase in the length of the growing season was recorded in northern Poland, in particular in seaside stations, i.e., in Łeba (6.9 days/10 years) and Hel (6.8 days/10 years).

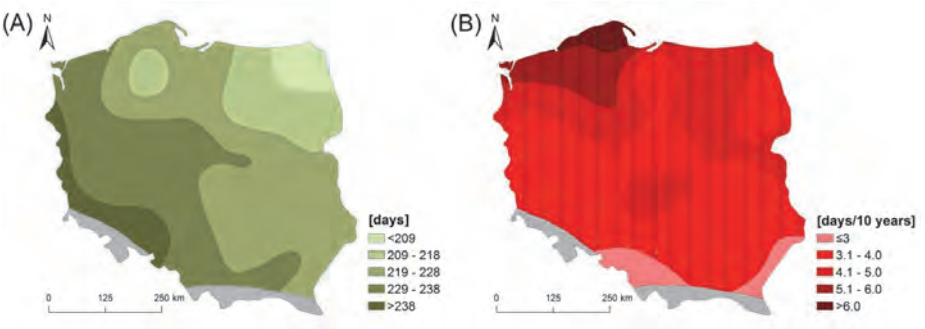

Fig. 5. Average length of the growing season (A) and its changes (B) in Poland in the years 1966–2015 (vertical lines indicate statistically significant changes).

As already indicated above, in the majority of stations (in 56% of stations) the shortest growing season occurred in 1997, and according to the accepted classification, in 9 stations it was classified as anomalously short and in 17 as short. Its length varied from 180 days in Mława to 227 days in Świnoujście. The period in each station was shorter than the average by 9 days in Świnoujście to 35 days in Łódź and Mława. The largest deviations were recorded mainly in the central and southeastern parts of Poland (>30 days). The shortening of the growing season was due to its later start time (except for Świnoujście) and a faster ending (*Fig. 6*). The beginning of the period was recorded from March 23 in Świnoujście to April 21 in Lesko. The average delay was approximately 14 days, while in individual stations it ranged from 4 days in Gorzów Wielkopolski to 23 days in Lesko. The largest deviations were recorded primarily in the central and south-eastern regions. In turn, the end of the period ranged from October 13 in Mława to November 9 in Hel. On average, it

occurred earlier by 10 days in the research area. In individual stations, the advance of the ending changed from 5 days in Kraków to 18 days in Mława. The largest deviations were noted above all in central Poland.

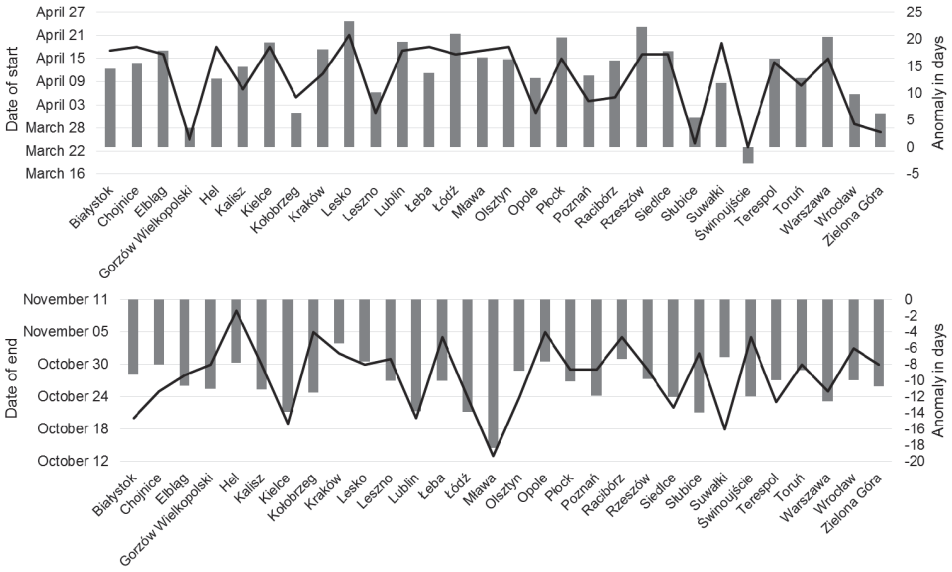

Fig. 6. The beginning and end dates of the growing season in the year 1997 (line) and the deviation from the multi-year average of its length (columns) in Poland.

In turn, in 63% of stations, the longest growing season occurred in 1990 and, according to the adopted classification, in 27 stations it was classified as anomalously long and in 3 as long. This period lasted from 229 days in Suwałki to 295 days in Kołobrzeg. In the entire research area, the period was longer than the average for the multi-year period from 27 days in Kielce and Suwałki to 62 days in Kołobrzeg. The largest deviations were recorded in the northern and western parts of Poland. The prolongation of the growing season was caused by its earlier start and later ending (except for Świnoujście), although the change of the beginning date was decisive (*Fig. 7*). On average, this period began 35 days earlier, and in individual stations these deviations ranged from 3 days in Świnoujście to 58 days in Kołobrzeg. In turn, the end of the period ranged from November 1 in Suwałki to November 22 in Hel. The delay of the end of the

growing season was relatively short and amounted to a maximum of 10 days in Kraków. The largest deviations were recorded mainly in the southern and eastern parts of Poland.

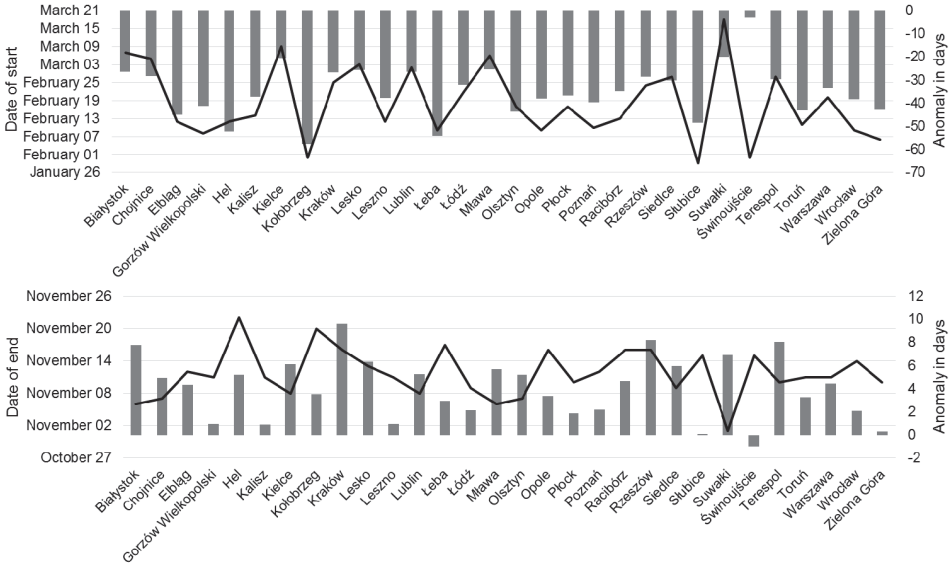

Fig. 7. The beginning and end dates of the growing season in the year 1990 (line) and the deviation from the multi-year average of its length (columns) in Poland.

In Poland in the years 1966–2015, the normal growing season (C in *Table 1*) lasted on average from 213 to 241 days (*Table 1*). The length of the normal growing season varied from 188–216 days in Suwałki to 223–279 days in Słubice. The short period (B) lasted on average 199–213 days, and the season lasting less than 199 days was considered to be anomalously short (A) for Poland. The anomalously short growing season lasted less than 174 days, while in Opole the length of anomalously short growing season was below 208 days. The duration of the long growing season (D) in Poland was on average 241–255 days, and it varied from 216–230 days in Suwałki to 260–279 days in Słubice. The anomalously long growing season (E) in Poland lasted on average over 255 days, changing from >230 days in Suwałki to >279 days in Słubice.

Table 1 The growing season duration classes in Poland with examples of the shortest and longest seasons in days, in the years 1966–2015

Growing season		Poland	The shortest		The longest	
			Suwałki	Mława	Opole	Słubice
A	anomalously short	<199	<174	<188	<208	<204
B	short	199–213	174–188	188–201	208–223	204–223
C	normal	213–241	188–216	201–229	223–254	223–260
D	long	241–255	216–230	229–242	254–270	260–279
E	anomalously long	>255	>230	>242	>270	>279

The classification of the growing season length for the area of Poland showed that in the analyzed years, the normal length of the growing season was dominant (*Table 2*). On average in Poland, normal seasons constituted 70% of all seasons, from 64% in Suwałki to 78% in Kołobrzeg, Zielona Góra, and Słubice, which corresponds to the number of years from 32 to 39. Both short and long seasons occurred with similar frequency (15% each). Anomalously short seasons appeared sporadically. In the first part of the analyzed period, the occurrence of short seasons was observed, i.e., in 1971, 1973, 1979, 1980, 1985, 1988, 1993, and 1997. However, there were no long seasons. In Poland, long seasons occurred four times: in 1989, 2000, 2006, and 2012. On the other hand, anomalously long growing seasons occurred in 1990, 2014, and 2015.

Table 2. Classification of the growing season length in the years 1966–2015 in Poland

Year	GPL	Year	GPL	Year	GPL	Year	GPL	Year	GPL
1966	221	1976	214	1986	228	1996	225	2006	247
1967	240	1977	236	1987	216	1997	202	2007	235
1968	229	1978	225	1988	208	1998	214	2008	238
1969	221	1979	207	1989	241	1999	229	2009	238
1970	216	1980	205	1990	267	2000	249	2010	230
1971	212	1981	223	1991	230	2001	223	2011	227
1972	225	1982	226	1992	218	2002	235	2012	243
1973	210	1983	227	1993	212	2003	226	2013	228
1974	226	1984	219	1994	230	2004	230	2014	258
1975	217	1985	212	1995	218	2005	220	2015	259

GPL – growing period length (in days)

The growing season length varied in individual stations (*Figs. 8* and *9*). Anomalously short periods occurred in stations located in the southeastern and central parts of Poland, and in the remaining area, they did not occur at all. The area in the belt extending from the south, through central Poland to the northeast is characterized by a higher frequency of growing seasons that are shorter than the average. Most often, short seasons were observed in Suwałki, Białystok, Olsztyn, and Racibórz (18%), while the least often in Słubice (8%) and Elbląg (10%). Long growing seasons occurred more often than on average in the eastern regions, and most often in Suwałki and Lublin (16%). The northwestern region of the country was characterized by the smallest frequency of these seasons. In Zielona Góra and Kołobrzeg it was only 4%, and in Hel and Słubice 6%. In Western Poland, anomalously long seasons were the most frequent (Słubice 8%). Their lowest frequency was observed in the northeastern and central-eastern parts of the country (2%).

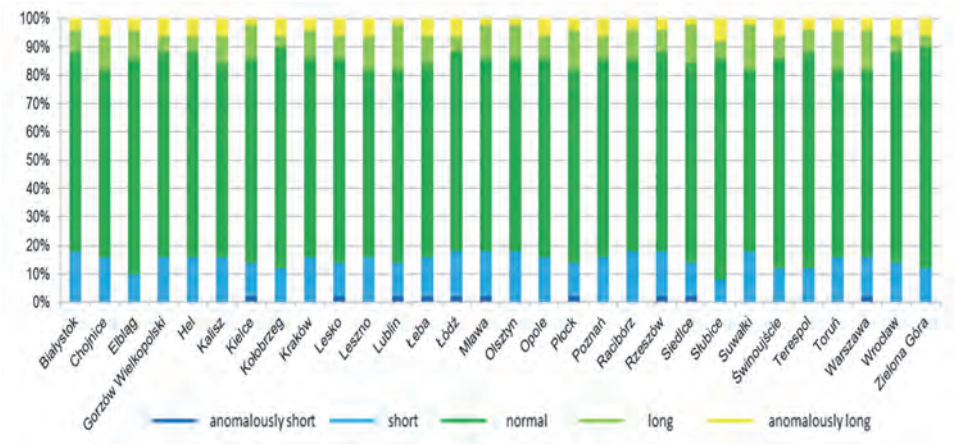

Fig. 8. Frequency (%) of occurrence of particular classes of the growing season length in Poland (1966–2015).

Analysis of the growing season length in individual stations showed that periods longer than the average occurred in several stations in 1967, 1977, and 1989. However, exceptionally long seasons did not occur in any of the stations until 1990 *(Fig. 9*) it was mentioned earlier, in most of the country the growing season of 1990 was classified as anomalously long. In the last 20 years of the analyzed period in individual stations, there were anomalously long seasons. On the other hand, in 2014 and 2015, these seasons occurred in most of Poland.

Short seasons were more frequent than on average in many stations in 1979, 1980, 1988, 1993, and in 1997, which was also the year with the highest number of stations with an anomalously short season.

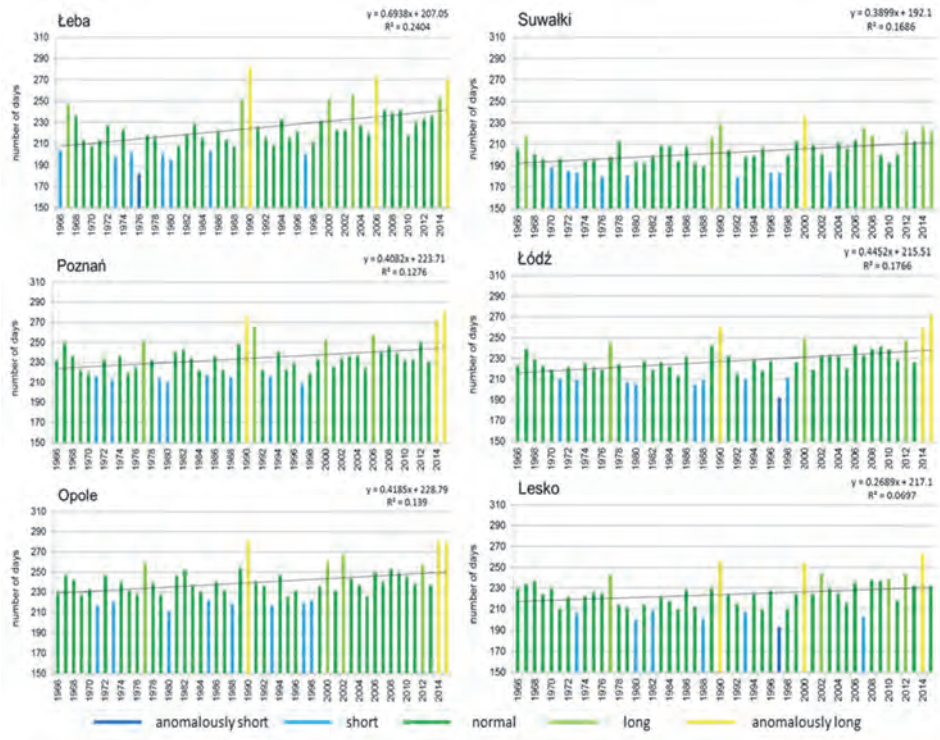

Fig. 9. Classification of the growing season length in selected stations in Poland (1966–2015) along with the trend line.

The occurrence of seasons belonging to particular length classes is reflected in deviations from the average of the growing season length in the years 1966–2015 (*Fig. 10*). Negative deviations were observed more often at the beginning of the analyzed period, especially in stations located in the northern and eastern parts of Poland. For stations in Western Poland, greater variations in deviations from the average are characteristic. The highest negative deviation occurred in Łeba in 1976 (–43 days), and the largest positive deviation occurred in Kołobrzeg in 1990 (+62 days). In the last 10 years, the domination of positive

deviations in the growing season length has been clearly visible in most stations, with particularly high values in the western part of the country. The last two seasons, during which deviations in many stations exceeded 40 days, were especially distinguishing.

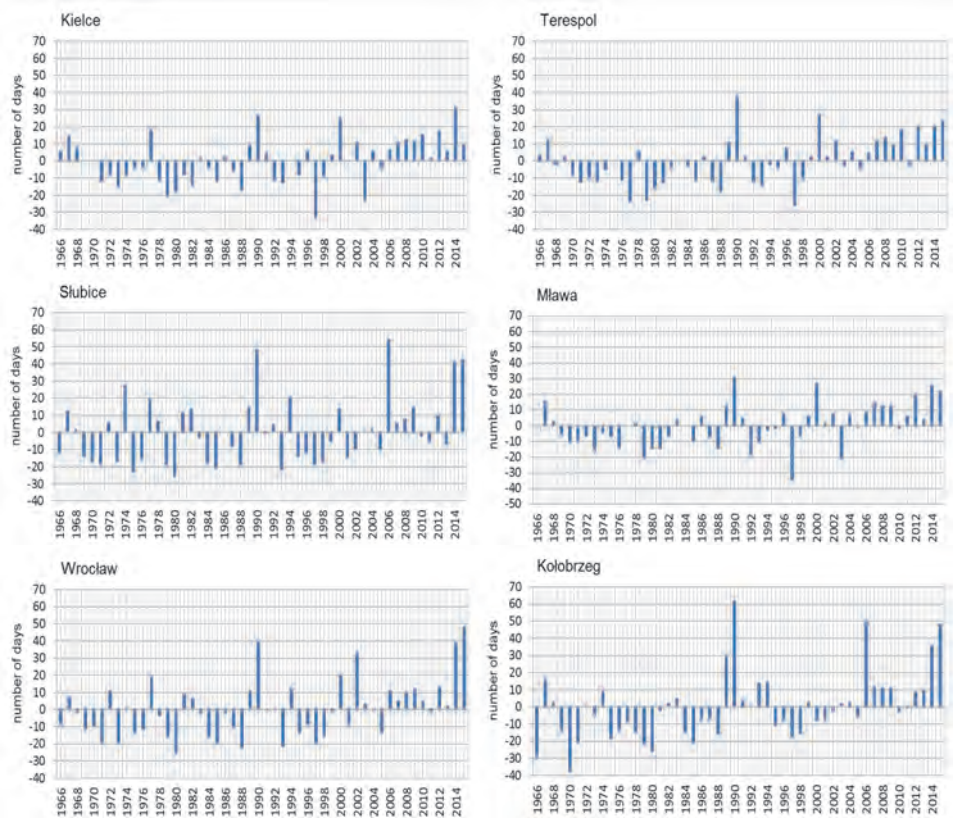

Fig. 10. Deviations from the average growing season length in selected stations in Poland (1966–2015).

4. Discussion and summary

In the years 1966–2015 in Poland, the growing season started the earliest in the western and southwestern regions, and the latest in the northeastern regions. By contrast, the end of the growing season followed the opposite, i.e., it was the earliest in the northeastern regions, and the latest in the northern and western regions. In the analyzed period, the growing season started increasingly early and ended increasingly late. The greatest advance of the beginning was recorded on the coast – in Łeba and Kołobrzeg. The rate of these changes was –4.2 days/10 years and –4.1 days/10 years, respectively. In turn, the delay of the end of the growing season was the greatest in Hel (2.6 days/10 years) and Wrocław (2.5 days/10 years). The start and end dates' shifting contributed to the extension of the growing season in Poland in the analyzed period. The largest increase in the growing season length was recorded in the northern part of Poland, in particular in seaside stations, i.e., in Łeba (6.9 days/10 years) and Hel (6.8 days/10 years), which is in line with the results obtained for the Baltic region, where the duration of this season increased by approximately 7 days in the second half of the twentieth century (*Linderholm et al.,* 2008). The increase in the length of the growing season in Poland in 1966–2015 was mainly due to its earlier beginning, which was confirmed by the results obtained for Poland by *Olszewski* and *Żmudzka* (1997), as well as *Bochenek et al*. (2013) for the southeastern area of Poland in 2001–2011. According to *Nieróbca et al.* (2013), the increasingly late ending of the meteorological growing season was the reason for extending its duration in 2001–2009 in relation to 1971–2000. On the other hand, *Krużel et al.* (2015) stated that the average four-day increase in the duration of this period in Poland between 1981 and 2010 is the result of both its starting two days earlier and ending two days later. Research conducted by *Węgrzyn* (2008) showed that in the southeastern region of Poland in 1991–2006, the average duration of the growing season did not get longer; however, the range of its variability increased significantly. The increase in the length of the growing season in different regions of Poland was also confirmed by other authors, among others, *Skowera* and *Kopeć* (2008), *Żmudzka* and *Dobrowolska* (2001), *Olechnowicz-Bobrowska* and *Wojkowski* (2006), *Tylkowski* (2015), *Graczyk* and *Kundzewicz* (2016). A similar trend was observed in other regions of Europe (*Carter*, 1998; *Menzel et al.,* 2003; *Jaguus,* 2006; *Linderholm et al.,* 2008; *Irannezhad* and *Kløve*, 2015; *Potopova et al.,* 2015) and in China (*Dong et al.,* 2013). The increase in the length of the growing season in Europe by 10.8 days from the 1960s was found by *Menzel* and *Fabian* (1999) on the basis of 30-year-long observations, which has been confirmed by later phenological observations (*Menzel*, 2000; *Stenseth et al.,* 2002). *Christidis et al.* (2007) proved that now the increase in the length of the growing season is mainly due to its earlier beginning, however, in the future both shifting the start and end

dates will contribute to extending its duration. According to *Song et al.* (2010), these changes are occurring faster and faster.

The cause of vegetation lengthening was spatially diverse in Poland. This variation was also present in Finland: in the north it was the ending delay, and the earlier beginning in the center. On the other hand, on the southwest coast of Finland, both the start and the end of the growing season were equally shifted (*Irannezhad* and *Kløve*, 2015). *Song et al.* (2010) showed that the growing season was prolonged mainly due to an earlier beginning by 1.7 days/10 years in northern China, and in the southern part, the reason was an even shifting of the start and end dates. In northern and central Europe, more significant changes occurring in spring were observed on the basis of phenological phases (*Menzel,* 2000).

The growing season in Poland in the analyzed period lasted on average 227 days. The increase in the growing season length took place from the northeast to the southwest. In Suwałki, the average length of the period was 202 days, while in Słubice, 242 days. There are also specific significant fluctuations in the length of the growing season year by year. The shortest period in Poland lasted, on average, 267 days in 1990, and the longest period with 202 days occurred in 1997. For reference, in Finland the average duration of the growing season was 116 days in the years 1961–2011, fluctuating from 98 days in 1977 to 146 days in 2011 (*Irannezhad* and *Kløve*, 2015).

The classification of the growing season length for the area of Poland showed that in the analyzed years, the normal length of the growing season was dominant (70%). Short periods occurred with a frequency of 14%, and for long periods it was 10%. Periods of anomalous length in Poland are rare: anomalously long periods occurred with a frequency 5%, and for anomalously short periods it was 1%. Anomalously short periods occurred in stations located in the southeastern and central parts of Poland, and in the remaining area, they did not occur at all. In Western Poland, anomalously long seasons were the most frequent. Their lowest frequency was observed in the northeastern and central-eastern parts. In the years 1951–1990 in the southeastern part of Poland, normal growing seasons occurred by 71.7%, long periods by 11.1%, and short periods by 11.4%, according to *Węgrzyn* (2008). Sporadically there were anomalously long and anomalously short seasons. However, the higher frequency of anomalously short periods (3.3%) and the lower frequency of anomalously long ones (2.5%) clearly marked in this area, which confirms the results obtained in this study. It can be noticed, that there is a tendency of smaller and smaller frequency of short and anomalously short seasons, and more and more often occurring of long and anomalously long seasons in Poland in the analyzed period. Also, *Bartoszek* and *Banasiewicz* (2007) stated that the tendency of the occurrence of warmer than normal growing seasons, which was clearly visible in Central Europe in the decade of 1991–2000, persists.

5. Conclusions

In summary, it should be noted that in the years 1966–2015 in Poland:

- Statistically significant changes of the growing season length were found on the east coast, in the central and southern parts of Poland, and the most intensive changes occurred in Hel (2.6 days/10 years) and Wrocław (2.5 days/10 years);
- Anomalously short growing seasons occurred sporadically and covered the largest area of Poland in 1997;
- Short growing seasons were more frequent in the first three decades of the analyzed multi-year period;
- Long growing seasons were characterized by higher frequency in the second half of the surveyed period;
- Anomalously long growing seasons occurred sporadically before 1990 and only in individual stations;
- Anomalously short growing seasons occurred only in the middle eastern part of Poland, while anomalously long ones covered most of the country.

References

Bochenek, W., Dedo, J., and *Marczewski, W.,* 2013: Zróżnicowanie długości i warunków termicznych okresu wegetacyjnego na obszarze Beskidów i Pogórzy w latach 2001-2011 na podstawie danych zgromadzonych w bazie GLDAS. [Differentiation of duration and thermal conditions of the vegetation season in the Beskid Mts. and Carpathian Foothill in years 2001-2011 on the GLDAS database]. *Monitoring Środowiska Przyrodniczego 14*, 79–85. (In Polish).

Carter, T.R., 1998: Changes in the thermal growing season in Nordic countries during the past century and prospects for the future. *Agric. Food Sci.7,* 161–179. https://doi.org/10.23986/afsci.72857

Chmielewski, F.M., Muller, A., and *Bruns, E.,* 2004: Climate changes and trends in phenology of fruit trees and field crops in Germany, 1961–2000. *Agric. Forest Meteorol. 121,* 69–78. https://doi.org/10.1016/S0168-1923(03)00161-8

Chmielewski, F.M. and *Rötzer, T.,* 2001: Response of tree phenology to climate change across Europe. *Agric. Forest Meteorol. 108*, 101–112. https://doi.org/10.1016/S0168-1923(01)00233-7

Christidis, N., Stott, P.A., and *Brown, S.,* 2007: Human contribution to the lengthening of the growing season during 1950-99. *J. Climate 20*, 5441–5454. https://doi.org/10.1175/2007JCLI1568.1

Czernecki, B. and *Miętus, M.,* 2017: The thermal seasons variability in Poland, 1951–2010. *Theor. Appl. Climatol. 127,* 481–493. https://doi.org/10.1007/s00704-015-1647-z

Dong, M.Y., Jiang, Y., Zhang, D.Y., and *Wu, Z.F.,* 2013: Spatiotemporal change in the climatic growing season in Northeast China during 1960–2009. *Theor. Appl. Climatol. 111*, 693–701. https://doi.org/10.1007/s00704-012-0706-y

Graczyk, D. and *Kundzewicz, Z.W.,* 2016: Changes of temperature-related agroclimatic indices in Poland. *Theor. Appl. Climatol. 124*, 401–410. https://doi.org/10.1007/s00704-015-1429-7

Gumiński, R., 1948: Próba wydzielenia dzielnic rolniczo-klimatycznych w Polsce. [Attempt to separate agricultural and climatic districts in Poland]. *Przegląd Meteorologiczno-Hydrologiczny 1,* 7–20. (In Polish).

IPCC, 2013: Climate change: The physical science basis. Contribution of Working Group I to the Fifth Assessment Report of the Intergovernmental Panel in Climate Change, Cambridge University Press, Cambridge, pp. 33.

Irannezhad, M. and *Kløve, B.,* 2015: Do atmospheric teleconnection patterns explain variations and trends in thermal growing season parameters in Finland? *Int. J. Climatol. 35,* 4619–4630. https://doi.org/10.1002/joc.4311

Jaguus, J., 2006: Climatic changes in Estonia during the second half of the 20th century in relationship with changes in large-scale atmospheric circulation. *Theor. Appl. Climatol. 83*, 77–88. https://doi.org/10.1007/s00704-005-0161-0

Kępińska-Kasprzak, M. and *Mager, P.,* 2015: Thermal growing season in Poland calculated by two different methods, *Annals of Warsaw University of Life Sciences-SGGW Land Reclamation 47*, 261–273. https://doi.org/10.1515/sggw-2015-0030

Krużel, J., Ziernicka-Wojtaszek, A., Borek, Ł., and *Ostrowski, K.,* 2015: Zmiany czasu trwania meteorologicznego okresu wegetacyjnego w Polsce w latach 1971-2000 oraz 1981-2010. [The changes in the duration of the meteorological vegetation period in Poland in the years 1971–2000 and 1981–2010]. *Inżynieria Ekologiczna 44*, 47–52. (In Polish). https://doi.org/10.12912/23920629/60024

Linderholm, H.W., 2006: Growing season changes in the last century. *Agric. Forest Meteorol. 137*, 1–14. https://doi.org/10.1016/j.agrformet.2006.03.006

Linderholm, H.W., Walther, A., and *Chen, D.*, 2008: Twentieth-century trends in the thermal growing season in the Greater Baltic Area. *Climatic Change 87*, 405–419. https://doi.org/10.1007/s10584-007-9327-3

Menzel, A. and *Fabian, P.,* 1999: Growing season extended in Europe. *Nature*, *397*, 659. https://doi.org/10.1038/17709

Menzel, A., 2000: Trends in phenological phases in Europe between 1951 and 1996. *International J.Biometeorol. 44*, 76–81. https://doi.org/10.1007/s004840000054

Menzel, A., 2003: Plant phenological anomalies in Germany and their relation to air temperature and NAO. *Climatic Change 57*, 243–263. https://doi.org/10.1023/A:1022880418362

Menzel, A., Jakobi, G., Ahas, R., Scheifinger, H., and *Estrella, N.,* 2003: Variations of the climatological growing season (1951–2000) in Germany compared with other countries. *Int. J. Climatol. 23*, 793–812.

Miętus, M., 2005: Ekstremalne zjawiska klimatyczne z perspektywy IPPC. [Extreme climate phenomena from the IPPC perspective]. In: (eds. *Bogdanowicz, E., Kossowska-Cezak, U., Szkutnicki, J.*,) Ekstremalne zjawiska hydrologiczne i meteorologiczne. [Extreme hydrological and meteorological phenomena]. PTG, IMGW, Warszawa, 19-31. (In Polish)

Nieróbca, A., 2009: Skutki zmian klimatycznych dla rolnictwa w Polsce - ocena zagrożeń. [The effects of climate change on agriculture in Poland - risk assessment]. In: (eds. *Kozyra, J., Nieróbca, A., Mizak, K.*) Zmiany klimatyczne a rolnictwo w Polsce – ocena zagrożeń i sposoby adaptacji. [Climate change and agriculture in Poland - risk assessment and methods of adaptation]. IUNG-PIB, Puławy. (In Polish).

Nieróbca, A., Kozyra, J., Mizak, K., Wróblewska, E., 2013: Zmiana długości okresu wegetacyjnego w Polsce. [Changing length of the growing season in Poland]. *Woda-Środowisko-Obszary Wiejskie*, *13, 2 (42),* 81–94. (In Polish).

NOAA (2018) https://www.ncdc.noaa.gov/sotc/global/201713

Olechnowicz-Bobrowska, B., and *Wojkowski, J.*, 2006: Okresy termiczne w południowej części Wyżyny Krakowsko-Częstochowskiej (1991–2000). [Thermal periods in the southern part of the Cracow-Częstochowa Upland (1971–2000)]. In: (eds. *Trepińska, J., Olecki, Z.*) Klimatyczne aspekty środowiska geograficznego [Climatic aspects of the geographical environment]. Instytut Geografii i Gospodarki Przestrzennej UJ, Kraków, 51–61.

Olszewski, K. and *Żmudzka*, E. 1997: Zmiany okresu wegetacyjnego w Polsce. [Changes of length of the vegetative period in Poland]. *Prace i Studia Geograficzne 20*, 93–103. (In Polish).

Piniewski, M., Mezghani, A., Szcześniak, M., and *Kundzewicz, Z.*, 2017: Regional projections of temperature and precipitation changes: Robustness and uncertainty aspects. *Meteorol. Zeitschrift 26*, 223–234. https://doi.org/10.1127/metz/2017/0813

Potopova, V., Zahradnicek, P., Turkott, L., Stepanek, P., Soukup, J., 2015: The effects of climate change on variability of the growing seasons in the Elbe River Lowland, Czech Republic. *Adv. Meteorol.* Article ID 546920. https://doi.org/10.1155/2015/546920

Radzka, E., 2013: Okresy termiczne w środkowo-wschodniej Polsce (1971–2005). [Thermal periods in central-eastern Poland (1971-2005)]. *Acta Agrophysica 20,* 679–691. (In Polish).

Rahmstorf, S., Foster G., and *Cahill N.,* 2017: Global temperature evolution: recent trends and some pitfalls. *Environ. Res. Lett. 12*, 054001. https://doi.org/10.1088/1748-9326/aa6825

Salmi, T., Maiittii, A., Anttila, P., Ruoho-Airola, T., and *Amnel, T.,* 2002: Detecting Trends of Annual Values of Atmospheric Pollutants by the Mann-Kendall Test and Sen's Slope Estimates–The Excel Template Application MAKESENS. Publications on Air Quality No. 31; Finnish Meteorological Institute: Helsinki, Finland, 1–35.

Siłuch, M., Dąbrowska, A., and *Bartoszek, K.,* 2016: Początek okresu wegetacyjnego określany na podstawie danych meteorologicznych, teledetekcyjnych i pojawów fenologicznych leszczyny pospolitej. [The onset of growing season based on meteorological and remotely sensed data as well as phenological observations of the common haze]. *Acta Scientarum Polonarum Formatio Circumientus 15(2),* 117–125. (In Polish). https://doi.org/10.15576/ASP.FC.2016.2.117

Skaugen, T.E. and *Tveito, O.E.*, 2004: Growing season and degree-day scenario in Norway for 2021–2050. *Climate Res. 26*, 221–232. https://doi.org/10.3354/cr026221

Skowera, B., and *Kopeć, B.,* 2008: Okresy termiczne w Polsce południowo-wschodniej (1971–2000). [Thermal periods in south-eastern part of Poland (1971-2000)]. *Acta Agrophysica 12(2),* 517–526. (In Polish).

Song, Y., Linderholm, H.W., Chen, D., and *Walther, A.,* 2010: Trends of the thermal growing season in China, 1951–2007. *Int. J. Climatol. 30*, 33–43. https://doi.org/10.1002/joc.1868

Stenseth, N.C., Mysterud, A., Ottersen, G., Hurrel, J.W., Chan, K.S., and *Lima, M.*, 2002: Ecological effects of climate fluctuations. *Science 297*, 1292–1296. https://doi.org/10.1126/science.1071281

Szyga-Pluta, K., 2011: Termiczne pory roku w Poznaniu w latach 2001–2008. [Thermal seasons in Poznań in the period 2001–2008]. *Przegląd Geograficzny 83(1),* 109–119. (In Polish). https://doi.org/10.7163/PrzG.2011.1.6

Tomczyk, A.M., Bednorz, E., 2016: Heat waves in Central Europe and their circulation conditions. *Int. J. Climatol. 36,* 770–782. https://doi.org/10.1002/joc.4381

Tomczyk, A.M. and *Szyga-Pluta, K.,* 2019: Variability of thermal and precipitation conditions in the growing season in Poland in the years1966–2015. *Theor. Appl. Climatol. 135,* 1517-1530. https://doi.org/10.1007/s00704-018-2450-4

Tylkowski, J., 2015: The variability of climatic vegetative seasons and thermal resources at the Polish Baltic Sea coastline in the context of potential composition of coastal forest communities. *Baltic Forestry 21,* 73–82.

Węgrzyn, A., 2008: Typowe i anomalne długości okresu wegetacyjnego na Lubelszczyźnie. [Typical and abnormal duration of vegetation season in the Lublin region]. *Acta Agrophysica 12(2),* 561–573. (In Polish).

Wibig, J., 2018: Heat waves in Poland in the period 1951-2015: trends, patterns and driving factors. *Meteorol. Hydrol. Water Manage. 6,* 37–45. https://doi.org/10.26491/mhwm/78420

Żmudzka, E., 2012: Wieloletnie zmiany zasobów termicznych w okresie wegetacyjnym i aktywnego wzrostu roślin w Polsce. [Long-term changes of thermal resources in the vegetative period and the active growth of plants in Poland]. *Woda-Środowisko-Obszary Wiejskie 12, 2 (38),* 377–389. (In Polish).

Żmudzka, E. and *Dobrowolska, M.,* 2001: Termiczny okres wegetacyjny w Polsce – zróżnicowanie przestrzenne i zmienność czasowa. [Thermal vegetation in Poland – spatial and temporal variability]. *Przegląd Naukowy Wydziału Inżynierii i Kształtowania Środowiska SGGW 21*, 75–80. (In Polish).

INSTRUCTIONS TO AUTHORS OF *IDŐJÁRÁS*

The purpose of the journal is to publish papers in any field of meteorology and atmosphere related scientific areas. These may be

- research papers on new results of scientific investigations,
- critical review articles summarizing the current state of art of a certain topic,
- short contributions dealing with a particular question.

Some issues contain "News" and "Book review", therefore, such contributions are also welcome. The papers must be in American English and should be checked by a native speaker if necessary.

Authors are requested to send their manuscripts to

Editor-in Chief of IDŐJÁRÁS
P.O. Box 38, H-1525 Budapest, Hungary
E-mail: journal.idojaras@met.hu

including all illustrations. MS Word format is preferred in electronic submission. Papers will then be reviewed normally by two independent referees, who remain unidentified for the author(s). The Editor-in-Chief will inform the author(s) whether or not the paper is acceptable for publication, and what modifications, if any, are necessary.

Please, follow the order given below when typing manuscripts.

Title page should consist of the title, the name(s) of the author(s), their affiliation(s) including full postal and e-mail address(es). In case of more than one author, the corresponding author must be identified.

Abstract: should contain the purpose, the applied data and methods as well as the basic conclusion(s) of the paper.

Key-words: must be included (from 5 to 10) to help to classify the topic.

Text: has to be typed in single spacing on an A4 size paper using 14 pt Times New Roman font if possible. Use of S.I. units are expected, and the use of negative exponent is preferred to fractional sign. Mathematical formulae are expected to be as simple as possible and numbered in parentheses at the right margin.

All publications cited in the text should be presented in the *list of references*, arranged in alphabetical order. For an article: name(s) of author(s) in Italics, year, title of article, name of journal, volume, number (the latter two in Italics) and pages. E.g., *Nathan, K.K.,* 1986: A note on the relationship between photosynthetically active radiation and cloud amount. *Időjárás 90,* 10–13. For a book: name(s) of author(s), year, title of the book (all in Italics except the year), publisher and place of publication. E.g., *Junge, C.E.,* 1963: *Air Chemistry and Radioactivity.* Academic Press, New York and London. Reference in the text should contain the name(s) of the author(s) in Italics and year of publication. E.g., in the case of one author: *Miller* (1989); in the case of two authors: *Gamov* and *Cleveland* (1973); and if there are more than two authors: *Smith et al.* (1990). If the name of the author cannot be fitted into the text: *(Miller,* 1989); etc. When referring papers published in the same year by the same author, letters a, b, c, etc. should follow the year of publication. DOI numbers of references should be provided if applicable.

Tables should be marked by Arabic numbers and printed in separate sheets with their numbers and legends given below them. Avoid too lengthy or complicated tables, or tables duplicating results given in other form in the manuscript (e.g., graphs). *Figures* should also be marked with Arabic numbers and printed in black and white or color (under special arrangement) in separate sheets with their numbers and captions given below them. JPG, TIF, GIF, BMP or PNG formats should be used for electronic artwork submission.

More information for authors is available: journal.idojaras@met.hu

Published by the Hungarian Meteorological Service

Budapest, Hungary

INDEX 26 361

HU ISSN 0324-6329